

LYAPUNOV-BASED CONTROL OF LIMIT CYCLE OSCILLATIONS IN UNCERTAIN
AIRCRAFT SYSTEMS

By
BRENDAN BIALY

A DISSERTATION PRESENTED TO THE GRADUATE SCHOOL
OF THE UNIVERSITY OF FLORIDA IN PARTIAL FULFILLMENT
OF THE REQUIREMENTS FOR THE DEGREE OF
DOCTOR OF PHILOSOPHY

UNIVERSITY OF FLORIDA

2014

© 2014 Brendan Bialy

To my parents William and Kelly Bialy for their support and encouragement

ACKNOWLEDGMENTS

I would like to express my gratitude to my advisor, Dr. Warren E. Dixon, for his guidance and motivation during my academic pursuits. His influence was crucial to the successful completion of my doctoral study. I would also like to extend my gratitude to my committee members: Dr. Mrinal Kumar, Dr. Norman G. Fitz-Coy, and Dr. Oscar D. Crisalle, for their time and recommendations. Finally, I would like to thank my family, coworkers, and friends for their support and encouragement.

TABLE OF CONTENTS

	<u>page</u>
ACKNOWLEDGMENTS	4
LIST OF TABLES	7
LIST OF FIGURES	8
LIST OF ABBREVIATIONS	10
ABSTRACT	11
CHAPTER	
1 INTRODUCTION	13
1.1 Motivation and Literature Review	13
1.2 Contributions	19
1.2.1 Chapter 2: Lyapunov-Based Tracking of Store-Induced Limit Cy- cle Oscillations in an Aeroelastic System	19
1.2.2 Chapter 3: Saturated RISE Tracking Control of Store-Induced Limit Cycle Oscillations	19
1.2.3 Chapter 4: Boundary Control of Limit Cycle Oscillations in a Flex- ible Aircraft Wing:	20
1.2.4 Chapter 5: Adaptive Boundary Control of Limit Cycle Oscillations in a Flexible Aircraft Wing	20
2 LYAPUNOV-BASED TRACKING OF STORE-INDUCED LIMIT CYCLE OS- CILLATIONS IN AN AEROELASTIC SYSTEM	21
2.1 Aeroelastic System Model	21
2.2 Control Objective	24
2.3 Control Development	25
2.4 Stability Analysis	29
2.5 Simulation Results	32
2.6 Summary	37
3 SATURATED RISE TRACKING CONTROL OF STORE-INDUCED LIMIT CY- CLE OSCILLATIONS	40
3.1 Control Objective	40
3.2 Control Development	41
3.3 Stability Analysis	43
3.4 Simulation Results	47
3.5 Summary	52

4	BOUNDARY CONTROL OF LIMIT CYCLE OSCILLATIONS IN A FLEXIBLE AIRCRAFT WING	55
4.1	Aircraft Wing Model	55
4.2	Boundary Control of Wing Twist	56
4.3	Boundary Control of Wing Bending	59
4.4	Numerical Simulation	62
4.5	Summary	65
5	ADAPTIVE BOUNDARY CONTROL OF LIMIT CYCLE OSCILLATIONS IN A FLEXIBLE AIRCRAFT WING	69
5.1	Aircraft Wing Model	69
5.2	Boundary Control Development	70
5.3	Stability Analysis	72
5.4	Summary	80
6	CONCLUSION AND FUTURE WORK	81
6.1	Dissertation Summary	81
6.2	Limitations and Future Work	82
APPENDIX		
A	PROOF THAT M IS INVERTIBLE (CH 3)	85
B	PROOF OF $g > 0$ (CH 3)	87
C	GROUPING OF TERMS IN $\dot{\chi}_1$ AND $\dot{\chi}_2$ (CH 3)	88
D	DEVELOPMENT OF THE BOUND ON \tilde{N} (CH 3)	89
E	DETAILS ON THE DEVELOPMENT OF THE CONSTANTS c_{m1} , c_{m2} , AND c_{m3} (CH 4)	91
F	DERIVATION OF THE BENDING AND TWISTING DYNAMICS OF A FLEXIBLE WING (CH 5/6)	92
G	EXPONENTIAL STABILITY OF THE TARGET SYSTEM (CH 5)	98
H	INTEGRATION BY PARTS OF SELECT TERMS IN \dot{E}_c (CH 6)	101
	REFERENCES	103
	BIOGRAPHICAL SKETCH	108

LIST OF TABLES

<u>Table</u>	<u>page</u>
2-1 Aeroelastic Model Parameters	33
2-2 Monte Carlo Simulation Results	37
3-1 Aeroelastic Model Parameters	47
3-2 Monte Carlo Simulation Results	51

LIST OF FIGURES

<u>Figure</u>	<u>page</u>
2-1 Diagram depicting the two degree of freedom airfoil section with attached store based on that in [1].	22
2-2 Aeroelastic system free response without disturbances	34
2-3 Comparison of the controlled aeroelastic system response	35
2-4 Control surface deflections, $\delta(t)$, for the developed controller and the controller from [15]	35
2-5 Aeroelastic system states in the presence of an additive disturbance	36
2-6 Control surface deflection, $\delta(t)$, for the developed controller and the controller from [15]	36
2-7 Monte Carlo AOA trajectories	38
2-8 Monte Carlo vertical position trajectories	38
2-9 Monte Carlo control effort	39
3-1 Aeroelastic system open-loop response without disturbances	49
3-2 State trajectories of the controller developed in [2] with and without an <i>ad hoc</i> saturation.	49
3-3 Commanded control effort for the controller developed in [2] with and without an <i>ad hoc</i> saturation.	50
3-4 Comparison of the closed-loop aeroelastic system response of the controller in [2] with an <i>ad hoc</i> saturation and the developed saturated controller.	51
3-5 Comparison of the control surface deflections for the developed saturated controller and <i>ad hoc</i> saturated controller from [2]	51
3-6 AoA trajectories for all 1500 Monte Carlo samples. The developed saturated controller suppressed the LCO behavior in all samples and the majority of the samples exhibit similar transient performance.	52
3-7 Vertical position trajectories of all 1500 Monte Carlo samples. The vertical position remained bounded for all samples despite being an uncontrolled state.	53
3-8 Control surface deflection for all 1500 Monte Carlo samples. The control effort for all samples remain within the actuation limit and demonstrate similar steady state performance.	53

4-1	Approximation of the modified Bessel function used in the subsequent simulation section.	60
4-2	Open-loop twist deflection of the flexible aircraft wing.	64
4-3	Open-loop bending deflection of the flexible aircraft wing.	64
4-4	Open-loop response at the wing tip of the flexible aircraft wing.	65
4-5	Closed-loop twist deflection of the flexible aircraft wing.	66
4-6	Closed-loop bending deflection of the flexible aircraft wing.	66
4-7	Closed-loop response at the wing tip of the flexible aircraft wing.	67
4-8	Lift and Moment commanded at the wing tip.	67

LIST OF ABBREVIATIONS

a.e.	Almost Everywhere
AoA	Angle of Attack
LCO	Limit Cycle Oscillations
LP	Linear-in-the-Parameters
LPV	Linear Parameter Varying
LQR	Linear-Quadratic Regulator
NN	Neural Network
PDE	Partial Differential Equation
RISE	Robust Integral of the Sign of the Error
ROM	Reduced Order Model
SDRE	State-Dependent Riccati Equation
SMC	Sliding Mode Control
SMRAC	Structured Model Reference Adaptive Control

Abstract of Dissertation Presented to the Graduate School
of the University of Florida in Partial Fulfillment of the
Requirements for the Degree of Doctor of Philosophy

LYAPUNOV-BASED CONTROL OF LIMIT CYCLE OSCILLATIONS IN UNCERTAIN
AIRCRAFT SYSTEMS

By

Brendan Bialy

May 2014

Chair: Warren E. Dixon

Major: Aerospace Engineering

Store-induced limit cycle oscillations (LCO) affect several fighter aircraft and is expected to remain an issue for next generation fighters. LCO arises from the interaction of aerodynamic and structural forces, however the primary contributor to the phenomenon is still unclear. The practical concerns regarding this phenomenon include whether or not ordnance can be safely released and the ability of the aircrew to perform mission-related tasks while in an LCO condition. The focus of this dissertation is the development of control strategies to suppress LCO in aircraft systems.

The first contribution of this work (Chapter 2) is the development of a controller consisting of a continuous Robust Integral of the Sign of the Error (RISE) feedback term with a neural network (NN) feedforward term to suppress LCO behavior in an uncertain airfoil system. The second contribution of this work (Chapter 3) is the extension of the development in Chapter 2 to include actuator saturation. Suppression of LCO behavior is achieved through the implementation of an auxiliary error system that features hyperbolic functions and a saturated RISE feedback control structure.

Due to the lack of clarity regarding the driving mechanism behind LCO, common practice in literature and in Chapters 2 and 3 is to replicate the symptoms of LCO by including nonlinearities in the wing structure, typically a nonlinear torsional stiffness. To improve the accuracy of the system model a partial differential equation (PDE) model of a flexible wing is derived (see Appendix F) using Hamilton's principle. Chapters 4

and 5 are focused on developing boundary control strategies for regulating the bending and twisting deformations of the derived model. The contribution of Chapter 4 is the construction of a backstepping-based boundary control strategy for a linear PDE model of an aircraft wing. The backstepping-based strategy transforms the original system to a exponentially stable system. A Lyapunov-based stability analysis is then used to show boundedness of the wing bending dynamics. A Lyapunov-based boundary control strategy for an uncertain nonlinear PDE model of an aircraft wing is developed in Chapter 5. In this chapter, a proportional feedback term is coupled with an gradient-based adaptive update law to ensure asymptotic regulation of the flexible states.

CHAPTER 1 INTRODUCTION

1.1 Motivation and Literature Review

Store-induced limit cycle oscillations (LCO) commonly occur and remain an issue on high performance fighter aircraft [3]. LCO behavior is characterized by antisymmetric non-divergent periodic motion of the wing and lateral motion of the fuselage. LCO motion can be self-induced or initiated through the control inputs; however the motion is self-sustaining and persists until the flight conditions have been sufficiently altered. LCO behavior related to flutter, except coupling between the unsteady aerodynamic forces and nonlinearities in the aircraft structure results in a limited amplitude motion [4]. In fact, store-induced LCO responses are present on fighter aircraft configurations that have been theoretically predicted to be sensitive to flutter. Classical linear flutter analysis techniques have been shown to accurately predict the oscillation frequency and modal composition of LCO behavior; however, due to unmodeled nonlinearities in the system, they fail to adequately predict its onset velocity or amplitude [5].

The major concern with LCO is the pilot's ability to successfully complete the mission in a safe and effective manner. Specifically, the LCO-induced lateral motion of the fuselage may cause the pilot to have difficulty reading cockpit gauges and heads-up displays and can lead to the termination of the mission or the avoidance of a part of the flight envelope critical to combat survivability. Additionally, questions have been raised about the effects of LCO on ordnance [4]. These questions include whether or not the ordnance can be safely released during LCO, the effects on target acquisition for smart munitions, and the effects on the accuracy of unguided weapons.

Concerns regarding the effects of LCO on mission performance necessitate the development of a control strategy that could suppress LCO behavior in an uncertain nonlinear aircraft system. Several control strategies have been developed in recent years to suppress LCO behavior in aeroelastic systems that require knowledge of the

system dynamics. A linear-quadratic regulator (LQR) controller with a Kalman state estimator was developed in [6] to stabilize a two degree of freedom airfoil section. The unsteady aerodynamics were modeled using an approximation of Theodorsen's theory. The developed controller was shown to be capable of stabilizing the system at velocities over twice the flutter velocity. However, when the control system was employed after the onset of LCO behavior, it was only effective near the flutter velocity. A feedback linearization controller was developed in [7] that uses a quasi-steady aerodynamic model and requires exact cancellation of the nonlinearities in the system. An output feedback LQR controller was designed in [8] using a linear reduced order model for the unsteady transonic aerodynamics. Danowsky et al. [9] developed an active feedback control system based on a linear reduced order model (ROM) of a restrained aeroservoelastic high-speed fighter aircraft. The effectiveness of the designed controller was verified using simulations of the full-order aircraft model. A linear input-to-output ROM of an unrestrained aeroservoelastic high-speed fighter aircraft model was developed in [10] that included rigid body aircraft dynamics. Linear control techniques were proven to stabilize the states of linear vehicle dynamics while suppressing aeroelastic behavior. A control system based on an aerodynamic energy concept was designed for a four control surface forward swept wing in [11]. The aerodynamic energy concept determines the stability of an aeroelastic system by examining the work done per oscillation cycle by the system. The controller is designed to produce positive work per oscillation cycle which corresponds to the dissipation of energy in the system and thus the system will remain stable. Prime et al. [12] developed an LQR controller based on a linear parameter varying (LPV) model based on freestream velocity of a three degree of freedom wing section. The LPV controller auto-schedules with freestream velocity and was shown to suppress LCO behavior over a wide range of velocities. A comparison of State-Dependent Riccati Equation (SDRE) and sliding mode control (SMC) approaches

for LCO suppression in a wing section without an external store was performed in [13]. Both control approaches used linearized dynamics and exact model knowledge.

Multiple adaptive controllers have been developed to compensate for uncertainties only in the torsional stiffness model. An adaptive nonlinear feedback control strategy was designed in [14] for a wing section with structural nonlinearities and a single trailing edge control surface. The design assumes linear-in-the-parameters (LP) structural nonlinearities in the model of the pitch stiffness only, and achieves partial feedback linearization control. Experimental results using the adaptive controller developed in [14] and the multivariable linear controller developed in [6] were presented in [15]. The results showed that the adaptive controller was capable of suppressing the LCO behavior at velocities up to 23% higher than the flutter velocity. A structured model reference adaptive control (SMRAC) strategy was developed in [16] to suppress the LCO behavior of a typical wing section with LP uncertainties in the pitch stiffness model. The SMRAC strategy was compared with an adaptive feedback linearization method and was shown to suppress LCO behavior at higher freestream velocities. A control strategy that uses multiple control surfaces and combines feedback linearization via Lie algebraic methods and model reference adaptive control was developed in [17] to improve the control of LCO behavior on a typical wing section with the same uncertainties as in [14]. The proposed controller showed improved transient performance and was capable of stabilizing the wing section at higher freestream velocities when compared to the control strategy developed in [16].

Previously developed controllers either use linearized system dynamics and are restricted to specific flight regimes, require exact knowledge of the system dynamics, or consider only uncertainties in the dynamics that satisfy the linear-in-the-parameters assumption. When any of these conditions are not met, the previously developed controllers can no longer guarantee stability. Furthermore, these controllers have neglected the fact that the commanded control input may exceed the actuation limits of the system,

which can result in unpredictable closed-loop responses. Chapter 2 proposes a control strategy to suppress LCO in a two degree of freedom airfoil section in the presence of bounded disturbances using the full nonlinear system model. Uncertainties in the system are assumed to be present in the structural and aerodynamic models and are not required to satisfy the LP condition. The developed control strategy consists of a neural network (NN) feedforward term to approximate the uncertain system dynamics while a Robust Integral of the Sign of the Error (RISE) feedback term ensures asymptotic tracking in the presence of unknown bounded disturbances. Chapter 3 extends the result in Chapter 2 to compensate for actuator constraints. While Chapter 3 builds on the work in Chapter 2, the error system, control development, and stability analysis are all redesigned to account for actuator limitations. Asymptotic tracking of a desired angle of attack (AoA) is achieved through the implementation of an auxiliary error system that features hyperbolic functions and a continuous RISE feedback control structure [18].

Previous research, including the development in Chapters 2 and 3, focus on suppressing LCO behavior in an airfoil section, which is described by a set of ordinary differential equations (ODE). However, the airfoil section model is a simplified description of what is happening in reality. To improve the fidelity of the plant model, it is necessary to examine the interactions between the structural dynamics and aerodynamics on a flexible wing. The dynamics of a flexible wing are described by a set of partial differential equations (PDE), which requires a different control method. Typically, the control actuator is located at the spatial boundary of the system (e.g., at the wingtip) and so the control design must use the boundary conditions to exert control over the states of the system across the entire spatial domain. Chapter 4 examines the LCO problem for a flexible wing described by a set of PDEs and associated boundary conditions. Hamilton's principle has been used previously to model the flexible dynamics of

physical systems, including helicopter rotor blades [19–21] and flexible robot manipulators [22–24], and can be applied to obtain the PDE system describing the dynamics of a flexible wing undergoing bending and twisting deformations.

Two control strategies have been developed for systems described by a set of PDEs. The first strategy uses Galerkin or Rayleigh-Ritz methods [25–27], or operator theoretic tools [28–31] to approximate the PDE system by a finite number of ODEs, then a controller is designed using the reduced-order model approximation. The main concern of using a reduced-order model in the control design is the potential for spillover instabilities [32, 33], in which the control strategy excites the higher-order modes that were neglected in the reduced-order model. In special cases, sensor and actuator placement can guarantee the neglected modes are not affected [34]. Specifically, when the zeros of the higher-order modes are known, placing actuators at these locations will mitigate spillover instabilities; however this can conflict with the desire to place actuators away from the zeros of the controlled modes.

The second strategy retains the full PDE system for the controller design and only requires model reduction techniques for implementation. PDE-based control techniques [35, 36] are often developed with the desire to implement boundary control in which the control actuation is applied through the boundary conditions. The PDE backstepping method described in [35] compensates for destabilizing terms that act across the system domain by constructing a state transformation, involving an invertible Volterra integral, that maps the original PDE system to an exponentially stable target PDE system. Since the transformation is invertible, stability of the target system translates directly to stability of the closed-loop system that consists of the original system plus boundary feedback control. While the PDE backstepping method yields elegant solutions to boundary control of PDE systems, it is limited to linear PDEs and nonlinear PDEs in which the nonlinearities are not destabilizing. The boundary control methods described in [36, 37] use Lyapunov-based design and analysis arguments

to control PDE systems. The crux of this method is the assumption that for a physical system, if the energy of the system is bounded, then the states that compose the energy of the system are also bounded. Based on this assumption, the objective of the Lyapunov-based stability analysis is to show that the energy in the closed-loop PDE system remains bounded and decays to zero asymptotically. This method is applicable to both linear and nonlinear PDE systems; however, more complex systems typically require more complex controllers and candidate Lyapunov functions. A notable difference, from an implementation perspective, between the backstepping method in [35] and the Lyapunov-based energy approach in [36, 37] is the signals that are required to be measurable. The backstepping approach typically requires knowledge of the distributed state throughout the spacial domain while the Lyapunov-based energy method only requires measurements at the boundary, however these measurement are typically higher-order spatial derivatives. A PDE-based boundary control approach has been previously used to stabilize fluid flow through a channel [38], maneuver flexible robotic arms [39], control the bending in an Euler beam [40–42], regulate a flexible rotor system [37, 43], and track the net aerodynamic force, or moment, of a flapping wing aircraft [44].

Several PDE and ODE controllers have been previously developed to control the bending in a flexible beam [30, 31, 40, 42]; however this body of work is primarily concerned with structural beams and robotic arms which don't encounter the closed-loop interactions between the flexible dynamics and aerodynamics intrinsic to flexible aircraft wings. Recently, [44] used the PDE-based backstepping control technique from [35] to track the net aerodynamic forces on a flapping wing micro air vehicle using either root-based actuation or tip-based actuation. The control objective in [44] is not concerned with the performance of the distributed state variables, instead the boundary control is designed to track a spatial integral of the distributed state variables. The focus of Chapter 4 is the development of a PDE-based controller to suppress LCO behavior

in a flexible aircraft wing described by a linear PDE via regulation of the distributed state variables. The backstepping technique in [35] is used to ensure the wing twist decays exponentially, and a Lyapunov-based stability analysis of the wing bending dynamics is used to prove that the oscillations in the wing bending dynamics decay asymptotically and the wing bending state reaches a steady-state profile. Chapter 5 uses Lyapunov-based boundary control design and analysis methods motivated by the approaches in [36, 37] to regulate the distributed states of a flexible wing described by a set of uncertain nonlinear PDEs. The considered PDE model has uncertainties that are linear-in-the-parameters and are compensated for using a gradient-based adaptive update law.

1.2 Contributions

The contributions of Chapters 2-5 are as follows:

1.2.1 Chapter 2: Lyapunov-Based Tracking of Store-Induced Limit Cycle Oscillations in an Aeroelastic System

The main contribution of Chapter 2 is the development of a RISE-based control strategy for the suppression of LCO behavior in an uncertain nonlinear aeroelastic system. A NN feedforward term is used to compensate for uncertainties in the structural dynamics and aerodynamics while a continuous RISE feedback term ensures asymptotic tracking of a desired AoA trajectory. Numerical simulations illustrate the performance of the developed controller as well as providing a comparison with a previously developed controller. Furthermore, a Monte-Carlo simulation is provided to demonstrate robustness to variations in the plant dynamics and measurement noise.

1.2.2 Chapter 3: Saturated RISE Tracking Control of Store-Induced Limit Cycle Oscillations

The contribution of Chapter 3 is to extend the result in Chapter 2 to compensate for actuator limits. To account for actuator constraints, the error system and control development are augmented with smooth, bounded hyperbolic functions. A numerical simulation demonstrated the unpredictable closed-loop response of the RISE-based

controller from Chapter 2 when an *ad hoc* saturation is applied to the commanded control effort. Furthermore, the simulations show the developed saturated controller achieves asymptotic tracking of the desired AoA without breaching actuator constraints.

1.2.3 Chapter 4: Boundary Control of Limit Cycle Oscillations in a Flexible Aircraft Wing:

The contribution of Chapter 4 is the development of a boundary control strategy for the suppression of LCO in a flexible aircraft wing described by a set of linear PDEs. The control strategy uses a PDE-based backstepping technique to transform the original system to an exponentially stable system in which the destabilizing terms in the original system are shifted to the boundary conditions. A boundary control is then developed to compensate for the destabilizing terms. The backstepping approach ensures the wing twist decays exponentially while a Lyapunov-based stability analysis proves the oscillations in the wing bending are suppressed and the wing bending achieves a steady-state profile. Numerical simulations demonstrate the performance of the proposed control strategy.

1.2.4 Chapter 5: Adaptive Boundary Control of Limit Cycle Oscillations in a Flexible Aircraft Wing

The contribution of Chapter 5 is the design of a boundary control strategy to suppress LCO motion in an uncertain nonlinear flexible aircraft wing model. The control strategy uses a gradient-based adaptive update law to compensate for the LP uncertainties and a Lyapunov-based analysis is used to show that the energy in the system remains bounded and asymptotically decays to zero. Arguments that relate the energy in the system to the distributed states are used to conclude that the distributed states are regulated asymptotically.

CHAPTER 2
LYAPUNOV-BASED TRACKING OF STORE-INDUCED LIMIT CYCLE OSCILLATIONS
IN AN AEROELASTIC SYSTEM

The focus of this chapter is to develop a controller to suppress LCO behavior in a two degree of freedom airfoil section with an attached store, one control surface, and an additive unknown nonlinear disturbance that does not satisfy the LP assumption. The unknown disturbance represents unsteady nonlinear aerodynamic effects. A NN is used as a feedforward control term to compensate for the unknown nonlinear disturbance and a RISE feedback term [45–47] ensures asymptotic tracking of a desired state trajectory.

2.1 Aeroelastic System Model

The subsequent development and stability analysis is based on an aeroelastic model (see Figure (2-1)), similar to [1], given as

$$M\ddot{q} + C\dot{q} + Kq = F \quad (2-1)$$

where $q \triangleq \begin{bmatrix} h & \alpha \end{bmatrix}^T \in \mathbb{R}^2$ is a composite vector of the vertical position and AoA of the wing-store section, respectively. It is assumed that $\|q\| \leq \kappa_1$, $\|\dot{q}\| \leq \kappa_2$, and $\|\ddot{q}\| \leq \kappa_3$ where $\kappa_1, \kappa_2, \kappa_3 \in \mathbb{R}$ are known positive constants, which is justified by the bounded oscillatory nature of LCO behavior. In (2-1), $M \in \mathbb{R}^{2 \times 2}$, $C \in \mathbb{R}^{2 \times 2}$, $K \in \mathbb{R}^{2 \times 2}$ and $F \in \mathbb{R}^2$ are defined as

$$M \triangleq \begin{bmatrix} m_1 & m_2 \\ m_2 & m_4 \end{bmatrix}, \quad C \triangleq \begin{bmatrix} c_{h1} & c_{h2}\dot{\alpha} \\ 0 & c_\alpha \end{bmatrix} \quad (2-2)$$

$$K \triangleq \begin{bmatrix} k_h & 0 \\ 0 & k_\alpha \end{bmatrix}, \quad F \triangleq \begin{bmatrix} -L \\ P_M \end{bmatrix}. \quad (2-3)$$

In (2-2), the terms $m_1, m_2, m_4 \in \mathbb{R}$ are defined as

$$m_1 \triangleq m_s + m_w \quad (2-4)$$

$$m_2(q) \triangleq (r_x - a) m_w b \cos(\alpha) + (s_x - a) m_s b \cos(\alpha)$$

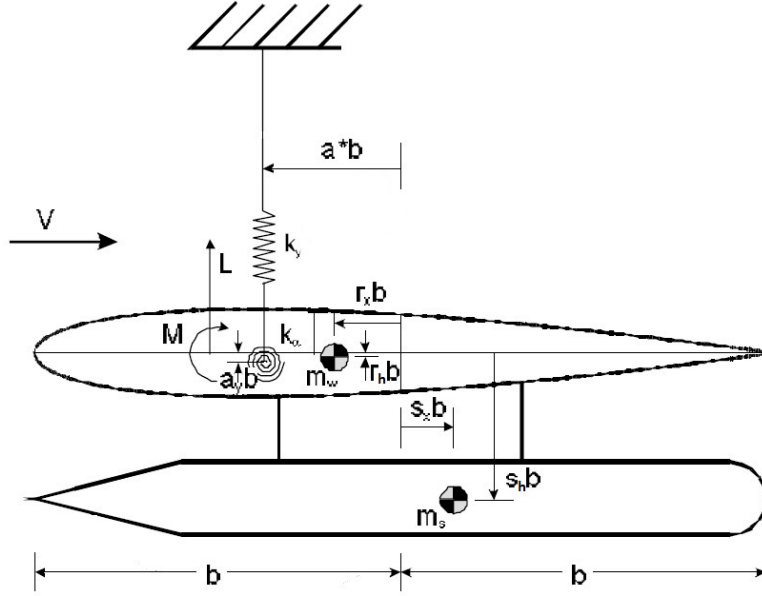


Figure 2-1. Diagram depicting the two degree of freedom airfoil section with attached store based on that in [1].

$$-(r_h - a_h) m_w b \sin(\alpha) - (s_h - a_h) m_s b \sin(\alpha) \quad (2-5)$$

$$m_4 \triangleq [(r_x - a)^2 + (r_h - a_h)^2] b^2 m_w + [(s_x - a)^2 + (s_h - a_h)^2] b^2 m_s + I_w + I_s \quad (2-6)$$

where m_w , m_s , b , r_x , r_h , a , a_h , s_x , s_h , I_w , and $I_s \in \mathbb{R}$ are unknown constants. Specifically, m_w is the mass of the wing section, m_s is the mass of the attached store, b is the semichord length of the wing, r_x , r_h are the distances from the wing center of mass to the wing midchord and the wing chordline in percentage of the wing semichord, respectively, a , a_h are the distances from the elastic axis of the wing to the wing midchord and the wing chordline in percentage of the wing semichord, respectively, s_x , s_h are the distances from the store center of mass to the wing midchord and wing chordline in percentage of the wing semichord, respectively, and I_w , I_s are the wing and store moments of inertia, respectively. In Eqn. (2-2), c_{h1} , $c_\alpha \in \mathbb{R}$ are the unknown constant damping coefficients of the plunge and pitch motion, respectively, and $c_{h2} \in \mathbb{R}$ is defined

as

$$c_{h_2}(q) \triangleq -(r_x - a) m_w b \cos(\alpha) - (s_x - a) m_s b \cos(\alpha) \\ - (s_h - a_h) m_s b \sin(\alpha) - (r_h - a_h) m_w b \sin(\alpha).$$

In (2–3), $k_h \in \mathbb{R}$ is the unknown plunge stiffness coefficient, and $k_\alpha(q) \in \mathbb{R}$ is the unknown nonlinear pitch stiffness coefficient modeled as

$$k_\alpha(q) = k_{\alpha_1} + k_{\alpha_2}\alpha + k_{\alpha_3}\alpha^2 + k_{\alpha_4}\alpha^3 + k_{\alpha_5}\alpha^4$$

where $k_{\alpha_1}, k_{\alpha_2}, k_{\alpha_3}, k_{\alpha_4}$, and $k_{\alpha_5} \in \mathbb{R}$ are constant unknown stiffness parameters. Also in (2–3), L and $P_M \in \mathbb{R}$ are the lift force and pitch moment acting on the wing-store section, respectively, and are modeled as

$$L = \rho U^2 b S C_{l_\alpha} \alpha_{ef} + C_{l_\delta} \delta \quad (2-7)$$

$$P_M = \rho U^2 b^2 S C_{l_\alpha} \left(\frac{1}{2} + a \right) \alpha_{ef} + C_{m_\delta} \delta \quad (2-8)$$

where $\rho, U, S, C_{l_\alpha}, C_{l_\delta}$, and $C_{m_\delta} \in \mathbb{R}$ are unknown constant coefficients. Specifically, ρ is the atmospheric density, U is the freestream velocity, S is the wing span, C_{l_α} is the lift coefficient of the wing, and $C_{l_\delta}, C_{m_\delta}$ are the control effectiveness coefficients for lift and pitching moment, respectively. In Eqns. (2–7) and (2–8), $\delta(t) \in \mathbb{R}$ is the control surface deflection angle, and $\alpha_{ef} \in \mathbb{R}$ is defined as $\alpha_{ef} \triangleq \alpha + \frac{\dot{h}}{U} + \frac{b(\frac{1}{2}-a)\dot{\alpha}}{U}$.

The dynamics in (2–1) can be rewritten as¹

$$\ddot{q} = M^{-1} \left[C_\delta \delta - \tilde{C} \dot{q} - \tilde{K} q \right] + d \quad (2-9)$$

where the auxiliary terms $C_\delta \triangleq \begin{bmatrix} -C_{l_\delta} & C_{m_\delta} \end{bmatrix}^T \in \mathbb{R}^2$, $d \triangleq \begin{bmatrix} d_h & d_\alpha \end{bmatrix}^T \in \mathbb{R}^2$ denotes an unknown, nonlinear disturbance that represents unmodeled, unsteady aerodynamic

¹ See Appendix A for details on the invertibility of $M(\alpha)$.

effects. Moreover, in (2–9), $\tilde{C} \in \mathbb{R}^{2 \times 2}$ and $\tilde{K} \in \mathbb{R}^{2 \times 2}$ are defined as

$$\tilde{C} \triangleq \begin{bmatrix} c_{h_1} + C_L & c_{h_2} \dot{\alpha} + C_L b \left(\frac{1}{2} - a\right) \\ -C_L b \left(\frac{1}{2} + a\right) & c_\alpha - C_L b^2 \left(\frac{1}{4} - a^2\right) \end{bmatrix} = \begin{bmatrix} \tilde{C}_{11} & \tilde{C}_{12} \\ \tilde{C}_{21} & \tilde{C}_{22} \end{bmatrix}$$

$$\tilde{K} \triangleq \begin{bmatrix} k_h & C_L U \\ 0 & k_\alpha - C_L U b \left(\frac{1}{2} + a\right) \end{bmatrix} = \begin{bmatrix} \tilde{K}_{11} & \tilde{K}_{12} \\ 0 & \tilde{K}_{22} \end{bmatrix},$$

and $C_L \triangleq \rho U b S C_{l_\alpha} \in \mathbb{R}$ is an unknown constant. The subsequent control development is based on the assumption that the nonlinear disturbances are bounded as

$$|d_h| \leq \xi_1, \quad \left| \dot{d}_h \right| \leq \xi_2, \quad |d_\alpha| \leq \xi_3, \quad \left| \dot{d}_\alpha \right| \leq \xi_4, \quad (2-10)$$

where $\xi_j \in \mathbb{R}$, ($j = 1, \dots, 4$) are positive, known constants.

2.2 Control Objective

The control objective is to ensure the airfoil section AoA, α , tracks a desired trajectory defined as $\alpha_d \in \mathbb{R}$. The formulation of an AoA tracking problem enables the AoA of the wing to be optimized for a given metric and flight condition. For the extension to the three dimensional case, the control objective provides the ability to alter the wing twist for a given flight condition to optimize a given performance metric, such as aerodynamic efficiency. The subsequent control development and analysis is based on the assumption that $\alpha_d, \dot{\alpha}_d, \ddot{\alpha}_d, \ddot{\alpha}_d \in \mathcal{L}_\infty$. To quantify the control objective and facilitate the control design, a tracking error, $e_1 \in \mathbb{R}$, and two auxiliary tracking errors, $e_2, r \in \mathbb{R}$, are defined as

$$e_1 \triangleq \alpha - \alpha_d \quad (2-11)$$

$$e_2 \triangleq \dot{e}_1 + \gamma_1 e_1 \quad (2-12)$$

$$r \triangleq \dot{e}_2 + \gamma_2 e_2 \quad (2-13)$$

where $\gamma_1, \gamma_2 \in \mathbb{R}$ are positive constants. The subsequent development is based on the assumption that q and \dot{q} are measurable. Hence, the auxiliary tracking error, r , is not

measurable since it depends on \ddot{q} . Substituting the system dynamics from (2–9) into the error dynamics in (2–13) yields the following expression

$$r = f + g\delta + d_\alpha \quad (2-14)$$

where the auxiliary terms $f \in \mathbb{R}$ and $g \in \mathbb{R}$ are defined as

$$f = -\frac{m_2}{\det(M)} \left(-\tilde{C}_{11}\dot{h} - \tilde{C}_{12}\dot{\alpha} - \tilde{K}_{11}h - \tilde{K}_{12}\alpha \right) + \frac{m_1}{\det(M)} \left(-\tilde{C}_{21}\dot{h} - \tilde{C}_{22}\dot{\alpha} - \tilde{K}_{22}\alpha \right) - \ddot{\alpha}_d + \gamma_1\dot{e}_1 + \gamma_2e_2 \quad (2-15)$$

$$g = \frac{m_2}{\det(M)} C_{l_s} + \frac{m_1}{\det(M)} C_{m_s} \quad (2-16)$$

and g is invertible² provided that sufficient conditions on the wing geometry and store location are met.

2.3 Control Development

After some algebraic manipulation, the open-loop error system for $r(t)$ can be obtained as

$$\frac{1}{g}r = \chi + \frac{1}{g_d}f_d + \delta + d_\alpha \quad (2-17)$$

where $g_d \in \mathbb{R}$ and $f_d \in \mathbb{R}$ are defined as

$$f_d = -\frac{m_2(q_d)}{\det(M(q_d))} \left(-\tilde{C}_{11}\dot{h}_d - \tilde{C}_{12}(q_d, \dot{q}_d)\dot{\alpha}_d - \tilde{K}_{11}h_d - \tilde{K}_{12}\alpha_d \right) + \frac{m_1}{\det(M(q_d))} \left(-\tilde{C}_{21}\dot{h}_d - \tilde{C}_{22}\dot{\alpha}_d - \tilde{K}_{22}(q_d)\alpha_d \right) - \ddot{\alpha}_d, \quad (2-18)$$

$$g_d = \frac{m_2(q_d)}{\det(M(q_d))} C_{l_s} + \frac{m_1}{\det(M(q_d))} C_{m_s}, \quad (2-19)$$

where $q_d \triangleq \begin{bmatrix} h_d & \alpha_d \end{bmatrix}^T \in \mathbb{R}^2$, and $h_d \in \mathbb{R}$ is a desired trajectory for the vertical position of the wing. The subsequent development is based on the assumption that the desired trajectories, h_d and \dot{h}_d , are bounded. In (2–17), the auxiliary function $\chi \in \mathbb{R}$ is defined as

² See Appendix B for details.

$\chi = \frac{1}{g}f - \frac{1}{g_d}f_d$. Based on the universal function approximation property, a multi-layer NN is used to approximate the uncertain dynamics $\frac{f_d}{g_d}(h_d, \dot{h}_d, \alpha_d, \dot{\alpha}_d)$ as [45]

$$\frac{f_d}{g_d} = W^T \sigma(V^T x_d) + \varepsilon(x_d) \quad (2-20)$$

where the NN input $x_d \in \mathbb{R}^7$ is defined as $x_d(t) \triangleq \begin{bmatrix} 1 & h_d & \dot{h}_d & \ddot{h}_d & \alpha_d & \dot{\alpha}_d & \ddot{\alpha}_d \end{bmatrix}^T$. In (2-20), $V \in \mathbb{R}^{7 \times n_2}$ is a constant ideal weight matrix for the first-to-second layer of the NN, $W \in \mathbb{R}^{n_2+1}$ is a constant ideal weight matrix for the second-to-third layer of the NN, n_2 is the number of neurons in the hidden layer, $\sigma \in \mathbb{R}^{n_2+1}$ denotes the activation function, and $\varepsilon \in \mathbb{R}$ is the function reconstruction error. Since x_d is defined in terms of desired bounded terms, the inputs to the NN remain on a compact set. Since the desired trajectories are assumed to be bounded, then [45] $|\varepsilon(x_d)| \leq \varepsilon_1$, $|\dot{\varepsilon}(x_d, \dot{x}_d)| \leq \varepsilon_2$, $|\ddot{\varepsilon}(x_d, \dot{x}_d, \ddot{x}_d)| \leq \varepsilon_3$, where $\varepsilon_1, \varepsilon_2, \varepsilon_3 \in \mathbb{R}$ are known positive constants.

Based on the open-loop error system in (2-17) and the subsequent stability analysis, the control surface deflection angle is designed as

$$\delta = -\frac{\widehat{f_d}}{g_d} - \mu \quad (2-21)$$

where $\frac{\widehat{f_d}}{g_d} \in \mathbb{R}$ is defined as

$$\frac{\widehat{f_d}}{g_d} \triangleq \widehat{W}^T \sigma(\widehat{V}^T x_d) \quad (2-22)$$

and $\mu \in \mathbb{R}$ denotes the subsequently defined RISE feedback term. In (2-22), $\widehat{W} \in \mathbb{R}^{n_2+1}$ and $\widehat{V} \in \mathbb{R}^{7 \times n_2}$ denote estimates for the ideal weight matrices whose update laws are defined as

$$\dot{\widehat{W}} \triangleq \text{proj} \left(\Gamma_1 \widehat{\sigma}' \widehat{V}^T \dot{x}_d e_2 \right) \quad (2-23)$$

$$\dot{\widehat{V}} \triangleq \text{proj} \left(\Gamma_2 \dot{x}_d \left(\widehat{\sigma}'^T \widehat{W} e_2 \right)^T \right) \quad (2-24)$$

where $\Gamma_1 \in \mathbb{R}^{(n_2+1) \times (n_2+1)}$, $\Gamma_2 \in \mathbb{R}^{7 \times 7}$ are constant, positive definite control matrices and $\widehat{\sigma}' \triangleq \frac{d\sigma(\widehat{V}^T x_d)}{d(\widehat{V}^T x_d)}$. The smooth projection algorithm in (2-23) and (2-24) is used to ensure

that the ideal NN weight estimates, \hat{W} and \hat{V} , remain bounded [48]. The RISE feedback term in (2-21) is defined as

$$\mu \triangleq (k_{s_1} + k_{s_2}) e_2 - (k_{s_1} + k_{s_2}) e_2(0) + \nu \quad (2-25)$$

where $\nu \in \mathbb{R}$ is the Filippov solution to the following differential equation

$$\dot{\nu} = (k_{s_1} + k_{s_2}) \gamma_2 e_2 + \beta_1 \operatorname{sgn}(e_2), \quad \nu(0) = \nu_0 \quad (2-26)$$

where $k_{s_1}, k_{s_2}, \beta_1 \in \mathbb{R}$ are positive, constant control gains and $\nu_0 \in \mathbb{R}$ is a known initial condition. The existence of solutions for $\dot{\nu} \in K[w_1]$ can be shown using Filippov's theory of differential inclusions [49–52] where $w_1 : \mathbb{R} \rightarrow \mathbb{R}$ is defined as the right-hand side of (2-26) and $K[w_1] \triangleq \bigcap_{\tau > 0} \bigcap_{\mu S_m = 0} \overline{\operatorname{co}} w_1(e_1, B - S_m)$, where $\bigcap_{\mu S_m = 0}$ represents the intersection of all sets S_m of Lebesgue measure zero, $\overline{\operatorname{co}}$ represents convex closure, and $B = \{\xi \in \mathbb{R} \mid |e_2 - \xi| < \tau\}$ [53, 54].

The closed-loop error system is obtained by substituting (2-21) into (2-17) as

$$\frac{1}{g} \dot{r} = \chi + \frac{f_d}{g_d} - \frac{\widehat{f}_d}{g_d} - \mu + d_\alpha. \quad (2-27)$$

To facilitate the subsequent stability analysis, the time derivative of (2-27) is determined as

$$\frac{1}{g} \dot{\dot{r}} = -\frac{d}{dt} \left(\frac{1}{g} \right) r + \dot{\chi} + \frac{d}{dt} \left(\frac{f_d}{g_d} \right) - \frac{d}{dt} \left(\frac{\widehat{f}_d}{g_d} \right) - \dot{\mu} + \dot{d}_\alpha. \quad (2-28)$$

Using (2-20) and (2-22), the closed-loop error system in (2-28) can be rewritten as

$$\begin{aligned} \frac{1}{g} \dot{\dot{r}} = & -\frac{d}{dt} \left(\frac{1}{g} \right) r + \dot{\chi} + W^T \sigma' (V^T x_d) V^T \dot{x}_d - \widehat{W}^T \sigma' (\widehat{V}^T x_d) \dot{\widehat{V}}^T x_d \\ & - \dot{\widehat{W}}^T \sigma (\widehat{V}^T x_d) - \widehat{W}^T \sigma' (\widehat{V}^T x_d) \widehat{V}^T \dot{x}_d + \dot{\varepsilon} - \dot{\mu} + \dot{d}_\alpha. \end{aligned} \quad (2-29)$$

After some algebraic manipulation, (2-29) can be rewritten as

$$\frac{1}{g} \dot{\dot{r}} = -\frac{d}{dt} \left(\frac{1}{g} \right) r + \widehat{W}^T \hat{\sigma}' \widetilde{V}^T \dot{x}_d - \dot{\widehat{W}}^T \hat{\sigma} + \dot{\varepsilon} + \dot{\chi} - \dot{\mu} + \dot{d}_\alpha + \widetilde{W}^T \hat{\sigma}' \widehat{V}^T \dot{x}_d$$

$$-\hat{W}^T \hat{\sigma}' \hat{V}^T x_d - W^T \hat{\sigma}' \hat{V}^T \dot{x}_d + W^T \sigma' V^T \dot{x}_d - \hat{W}^T \hat{\sigma}' \tilde{V}^T \dot{x}_d \quad (2-30)$$

where $\sigma' = \sigma' (V^T x_d) \in \mathbb{R}^{n_2+1 \times n_2}$, $\hat{\sigma} = \hat{\sigma} (\hat{V}^T x_d) \in \mathbb{R}^{n_2+1}$ and the parameter estimation error matrices $\tilde{W} \in \mathbb{R}^{n_2+1}$ and $\tilde{V} \in \mathbb{R}^{7 \times n_2}$ are defined as $\tilde{W} = W - \hat{W}$ and $\tilde{V} = V - \hat{V}$, respectively. Using the NN weight update laws in (2-23) and (2-24) and the time derivative of the RISE feedback term in (2-25), the closed-loop error system in (2-30) can be expressed as

$$\frac{1}{g} \dot{r} = \tilde{N} + N_d + N_B - e_2 - (k_{s_1} + k_{s_2}) r - \beta_1 \text{sgn}(e_2) - \frac{1}{2} \frac{d}{dt} \left(\frac{1}{g} \right) r \quad (2-31)$$

where $\tilde{N} \in \mathbb{R}$, $N_d \in \mathbb{R}$, and $N_B \in \mathbb{R}$ are defined as

$$\begin{aligned} \tilde{N} \triangleq & -\frac{1}{2} \frac{d}{dt} \left(\frac{1}{g} \right) r + \dot{\chi}_1 + e_2 - \text{proj} \left(\Gamma_1 \hat{\sigma}' \hat{V}^T \dot{x}_d e_2 \right)^T \hat{\sigma} \\ & - \hat{W}^T \hat{\sigma}' \text{proj} \left(\Gamma_2 \dot{x}_d \left(\hat{\sigma}'^T \hat{W} e_2 \right)^T \right)^T x_d \end{aligned} \quad (2-32)$$

$$N_d \triangleq W^T \sigma' V^T \dot{x}_d + \dot{\epsilon} + \dot{\chi}_2 + \dot{d}_\alpha \quad (2-33)$$

$$N_B \triangleq N_{B_1} + N_{B_2}. \quad (2-34)$$

In (2-34), the terms $N_{B_1} \in \mathbb{R}$ and $N_{B_2} \in \mathbb{R}$ are defined as

$$N_{B_1} \triangleq -W^T \hat{\sigma}' \hat{V}^T \dot{x}_d - \hat{W}^T \hat{\sigma}' \tilde{V}^T \dot{x}_d \quad (2-35)$$

$$N_{B_2} \triangleq \hat{W}^T \hat{\sigma}' \tilde{V}^T \dot{x}_d + \tilde{W}^T \hat{\sigma}' \hat{V}^T \dot{x}_d. \quad (2-36)$$

The terms in (2-31) are segregated based on their bounds. All the terms in (2-33) are dependent on the desired trajectories, therefore N_d and its derivative can be upper bounded by a constant, which will be rejected by the RISE feedback term in the controller. The terms in (2-34) are segregated into terms that will be rejected by the RISE feedback, N_{B_1} , and terms that will be rejected by a combination of the RISE feedback and NN weight estimate adaptive update laws, N_{B_2} . In (2-32) and (2-34), $\dot{\chi}$ has been segregated into $\dot{\chi}_1$ and $\dot{\chi}_2$ where $\dot{\chi}_1$ denotes the components of $\dot{\chi}$ that are state dependent or can be upper bounded by the norm of the states, and $\dot{\chi}_2$ denotes the

components that can be upper bounded by a constant³. The terms in \tilde{N} can be upper bounded as⁴

$$|\tilde{N}| \leq \eta \|z\| \quad (2-37)$$

where $z \triangleq \begin{bmatrix} e_1 & e_2 & r \end{bmatrix}^T \in \mathbb{R}^3$, and $\eta \in \mathbb{R}$ is a positive bounding constant. Similar to [45], the following inequalities can be developed

$$|N_d| \leq \zeta_1, \quad |\dot{N}_d| \leq \zeta_2, \quad |N_B| \leq \zeta_3, \quad |\dot{N}_B| \leq \zeta_4 + \zeta_5 |e_2| \quad (2-38)$$

where $\zeta_i \in \mathbb{R}$, ($i = 1, 2, \dots, 5$) are positive bounding constants.

2.4 Stability Analysis

To facilitate the subsequent Lyapunov-based stability analysis, let $P \in \mathbb{R}$ be defined as the Filippov solution to the following differential equation

$$\begin{aligned} \dot{P} &= -r(N_{B_1} + N_d - \beta_1 \operatorname{sgn}(e_2)) - \dot{e}_2 N_{B_2} + \beta_2 e_2^2, \\ P(0) &= \beta_1 |e_2(0)| - e_2(0)(N_d(0) + N_B(0)). \end{aligned} \quad (2-39)$$

The existence of solutions for $P(t)$ can be established in a similar manner as in (2-26) by using Filippov's theory of differential inclusions for $\dot{P}(t) \in K[w_2]$, where $w_2 \in \mathbb{R}$ is defined as the right-hand side of (2-39). Provided that β_1 and β_2 are selected based on the sufficient conditions in (2-40), $P(t) \geq 0$ [45]. Furthermore, let $Q \in \mathbb{R}$ be defined as

$$Q \triangleq \frac{\gamma_2}{2} \tilde{W}^T \Gamma_1^{-1} \tilde{W} + \frac{\gamma_2}{2} \operatorname{tr} \left(\tilde{V}^T \Gamma_2^{-1} \tilde{V} \right),$$

where $Q \geq 0$ since Γ_1 and Γ_2 are constant positive definite matrices, and $\gamma_2 \in \mathbb{R}^+$.

³ See Appendix C for details

⁴ See Appendix D for details.

Theorem 2.1. *The controller given in (2–21)-(2–26) ensures that all closed-loop signals are bounded and the tracking error is regulated in the sense that $e_1(t) \rightarrow 0$ as $t \rightarrow \infty$ provided that the control gains are selected as*

$$\beta_1 > \zeta_1 + \zeta_2 + \frac{1}{\gamma_2}\zeta_3 + \frac{1}{\gamma_2}\zeta_4, \quad \beta_2 > \zeta_5, \quad \gamma_1 > \frac{1}{2}, \quad \gamma_2 > \beta_2 + 1. \quad (2-40)$$

Proof. Let $\mathcal{D} \subset \mathbb{R}^5$ be a domain containing $y = 0$, where $y \in \mathbb{R}^5$ and is defined as

$$y \triangleq \begin{bmatrix} e_1 & e_2 & r & \sqrt{P} & \sqrt{Q} \end{bmatrix}^T.$$

Let $V_L(y) : \mathcal{D} \rightarrow \mathbb{R}$ be a positive definite, continuously differentiable function defined as

$$V_L \triangleq e_1^2 + \frac{1}{2}e_2^2 + \frac{1}{2}r^2 + P + Q. \quad (2-41)$$

Equation (2–41) satisfies $U_1 \leq V_L \leq U_2$ provided that β_1 and β_2 are selected based on the sufficient conditions in (2–40). The continuous positive definite functions $U_1, U_2 \in \mathbb{R}$ are defined as $U_1 \triangleq \lambda_1 \|y\|^2$, $U_2 \triangleq \lambda_2 \|y\|^2$ where $\lambda_1, \lambda_2 \in \mathbb{R}$ are defined as $\lambda_1 \triangleq \frac{1}{2} \min \{1, g_l\}$, $\lambda_2 \triangleq \min \{\frac{1}{2}g_m, 1\}$ and $g_l \leq |g| \leq g_m$.

The time derivative of (2–41) exists almost everywhere (a.e), and $\dot{V}_L \in \dot{\tilde{V}}_L$ where $\dot{\tilde{V}}_L = \bigcap_{\Xi \in \partial V_L} \Xi^T K \begin{bmatrix} \dot{e}_1 & \dot{e}_2 & \dot{r} & \frac{P^{-\frac{1}{2}}\dot{P}}{2} & \frac{Q^{-\frac{1}{2}}\dot{Q}}{2} & 1 \end{bmatrix}^T$, where ∂V_L is the generalized gradient of V_L . Since V_L is a continuously differentiable function, $\dot{\tilde{V}}_L$ can be expressed as

$$\dot{\tilde{V}}_L = \nabla V_L^T K \begin{bmatrix} \dot{e}_1 & \dot{e}_2 & \dot{r} & \frac{P^{-\frac{1}{2}}\dot{P}}{2} & \frac{Q^{-\frac{1}{2}}\dot{Q}}{2} & 1 \end{bmatrix}^T, \quad (2-42)$$

where $\nabla V_L = \begin{bmatrix} 2e_1 & e_2 & \frac{1}{g}r & 2P^{\frac{1}{2}} & 2Q^{\frac{1}{2}} & \frac{1}{2}\frac{d}{dt}\left(\frac{1}{g}\right)r^2 \end{bmatrix}$. Using the calculus for K from [54], (2–12), (2–13), (2–31), and (2–39), (2–42) can be expressed as

$$\begin{aligned} \dot{\tilde{V}}_L \subset & 2e_1(e_2 - \gamma_1 e_1) + e_2(r - \gamma_2 e_2) \\ & + r \left(\tilde{N} + N_d + N_B - e_2 - (k_{s_1} + k_{s_2})r - \beta_1 K[\text{sgn}(e_2)] \right) \\ & - r(N_{B_1} + N_d - \beta_1 K[\text{sgn}(e_2)]) - \dot{e}_2 N_{B_2} \\ & + \beta_2 e_2^2 - \gamma_2 \tilde{W}^T \Gamma_1^{-1} \dot{\tilde{W}} - \gamma_2 \text{tr} \left(\tilde{V}^T \Gamma_2^{-1} \dot{\tilde{V}} \right), \end{aligned} \quad (2-43)$$

where $K[\text{sgn}(e_2)] = \text{sgn}(e_2)$ such that $\text{sgn}(e_2) = 1$ if $e_2 > 0$, $[-1, 1]$ if $e_2 = 0$, and -1 if $e_2 < 0$. The set of times $\Lambda \triangleq \{t \in [0, \infty) : r\beta_1 K[\text{sgn}(e_2)] - r\beta_1 K[\text{sgn}(e_2)] \neq \{0\}\} \subset [0, \infty)$ is equal to the set of times $\{t : e_2(t) = 0 \wedge r(t) \neq 0\}$. From Eqn. (2–13), this set can also be expressed as $\{t : e_2(t) = 0 \wedge \dot{e}_2(t) \neq 0\}$. Since e_2 is continuously differentiable, it can be shown using [55], Lemma 2 that the set of time instances $\{t : e_2(t) = 0 \wedge \dot{e}_2(t) \neq 0\}$ is isolated and measure zero; hence Λ is measure zero. Since Λ is measure zero, (2–43) can be reduced to the following scalar inequality

$$\begin{aligned} \dot{V}_L \stackrel{a.e.}{\leq} & 2e_1e_2 - 2\gamma_1e_1^2 - \gamma_2e_2^2 + \beta_2e_2^2 + r\tilde{N} - k_{s_1}r^2 - k_{s_2}r^2 \\ & + \gamma_2e_2 \left[\hat{W}^T \hat{\sigma}' \tilde{V}^T \dot{x}_d + \tilde{W}^T \hat{\sigma}' \hat{V}^T \dot{x}_d \right] - \gamma_2 \tilde{W}^T \Gamma_1^{-1} \dot{W} - \gamma_2 \text{tr} \left(\tilde{V}^T \Gamma_2^{-1} \dot{V} \right), \end{aligned} \quad (2-44)$$

By using Young's inequality and the NN weight update laws in (2–23) and (2–24) along with the upper bound on \tilde{N} given in (2–37), the expression in (2–44) can be rewritten as

$$\dot{V}_L \stackrel{a.e.}{\leq} - (2\gamma_1 - 1)e_1^2 - (\gamma_2 - \beta_2 - 1)e_2^2 - k_{s_1}r^2 + \frac{\eta^2}{4k_{s_2}} \|z\|^2. \quad (2-45)$$

The expression in (2–45) can be further simplified as

$$\dot{V}_L \stackrel{a.e.}{\leq} - \left(\lambda_3 - \frac{\eta^2}{4k_{s_2}} \right) \|z\|^2, \quad (2-46)$$

where $\lambda_3 = \min \{2\gamma_1 - 1, \gamma_2 - \beta_2 - 1, k_{s_1}\}$ is a positive constant provided that γ_1, γ_2 are selected according to (2–40). The expression in (2–46) can be upper bounded as

$$\dot{V}_L \stackrel{a.e.}{\leq} -c \|z\|^2, \quad (2-47)$$

where $c \in \mathbb{R}$ is a positive constant provided that $\lambda_3 > \frac{\eta}{4k_{s_2}}$. The expressions in (2–41) and (2–47) can be used to show that $V_L \in \mathcal{L}_\infty$, and hence, $e_1, e_2, r, P, Q \in \mathcal{L}_\infty$. Given that $e_1, e_2, r \in \mathcal{L}_\infty$, (2–12) and (2–13) indicate that $\dot{e}_1, \dot{e}_2 \in \mathcal{L}_\infty$. Since $e_1, e_2, r \in \mathcal{L}_\infty$ and $\alpha_d, \dot{\alpha}_d, \ddot{\alpha}_d \in \mathcal{L}_\infty$ by assumption, (2–11)-(2–13) can be used to show that $\alpha, \dot{\alpha}, \ddot{\alpha} \in \mathcal{L}_\infty$. If $\alpha, \dot{\alpha} \in \mathcal{L}_\infty$, (2–2) can be used to show that $M, C, K \in \mathcal{L}_\infty$. Given that $M \in \mathcal{L}_\infty$, (2–16) indicates that $g \in \mathcal{L}_\infty$. Since $\alpha(t), \dot{\alpha}(t) \in \mathcal{L}_\infty$ in \mathcal{D} and $\dot{h}(t) \in \mathcal{L}_\infty$ then, (2–2), (2–7),

and (2–8) can be used to show that $F \in \mathcal{L}_\infty$; hence, with the bounds in (2–10) it can be concluded from (2–1) that the control input $\delta \in \mathcal{L}_\infty$. Given that $\tilde{N}, N_d, N_B, r, e_2, g \in \mathcal{L}_\infty$, it can be concluded from (2–31) that $\dot{r} \in \mathcal{L}_\infty$. Since $\dot{e}_1, \dot{e}_2, \dot{r} \in \mathcal{L}_\infty$, the definition of $z(t)$ can be used to show that z is uniformly continuous. Corollary 1 from [56] can be used to show that $\|z\| \rightarrow 0$, and therefore, $e_1 \rightarrow 0$ as $t \rightarrow \infty$. \square

2.5 Simulation Results

A numerical simulation is presented to illustrate the performance of the developed controller and provide a comparison with the controller in [15]. The controller from [15] was selected for comparison because it is one of the few controllers that consider structural uncertainties. However, this is not an equal comparison, since the controller in [15] considers uncertainties in the pitch stiffness only, while the control strategy developed in this paper considers uncertainties in all parameters in the structural and aerodynamic models. For this reason, the structural and aerodynamic parameters that are assumed to be known in [15] are taken to be off by 10% from the actual values. The controller in [15] is given by

$$\delta = \frac{1}{g_4 U^2} \left(-F_L(q, \dot{q}) - \hat{\Theta}^T R(q) - \bar{k}_1 \alpha - \bar{k}_2 \dot{\alpha} \right),$$

where $g_4 \in \mathbb{R}$ is a control effectiveness parameter, $U \in \mathbb{R}$ denotes the freestream velocity, $F_L(q, \dot{q}) \in \mathbb{R}$ is a feedback linearization term that requires exact model knowledge of certain parameters in the structural model and all parameters in the aerodynamic model, $\hat{\Theta} \in \mathbb{R}^i$ denotes a vector of the estimates of the uncertain parameters in the pitch stiffness model, $R(q) \in \mathbb{R}^i$ represents a known regression matrix, and $\bar{k}_1, \bar{k}_2 \in \mathbb{R}$ are positive control gains. The control gains were selected as $\bar{k}_1 = \bar{k}_2 = 60$ based on improving the resulting transient performance of the controller while keeping the control effort within tolerable limits (± 10 deg). The estimate, $\hat{\Theta}$, is

updated via a gradient update law given by

$$\dot{\Theta} = \dot{\alpha} R^T(q).$$

The model parameters for the simulation are shown in Table 2-1 and (2-48)

Table 2-1. Aeroelastic Model Parameters

Parameter		Parameter	
m_w	4.0 kg	I_s	0.0050 kg·m ²
m_s	4.0 kg	c_{h_1}	2.743x10 ¹ kg/s
r_x	0.0	c_α	0.036 kg·m ² /s
r_h	0.0	k_h	2.200x10 ³ N/m
a	-0.6	ρ	1.225 kg/m ³
a_h	0.0	U	1.20x10 ¹ m/s
b	0.14 m	S	1.0 m
s_x	0.098	C_{l_α}	6.8 1/rad
s_h	1.4	C_{l_δ}	9.3x10 ¹ N/rad
I_w	0.043 kg·m ²	C_{m_δ}	2.3 N·m/rad

$$k_\alpha(q) = 0.5 - 11.05\alpha + 657.75\alpha^2 - 4290\alpha^3 + 8644.85\alpha^4. \quad (2-48)$$

The control objective is to regulate the AOA to zero degrees from the initial condition $h(0) = 0$ m, $\dot{h}(0) = 0$ m/s, $\alpha(0) = 3.0$ deg, and $\dot{\alpha}(0) = 0$ deg/s. From Figure (2-2) it is evident that the system, under the above conditions, experiences LCO behavior in the absence of a control strategy and exogenous disturbances. The developed control strategy was applied to the system in the absence of exogenous disturbances with the following gains: $\gamma_1 = 2$, $\gamma_2 = 3$, $k_{s_1} + k_{s_2} = 3$, $\beta_1 = 0.1$, $n_2 = 25$, $\Gamma_1 = 10I_{26}$, and $\Gamma_2 = 10I_7$, where I_m denotes an $m \times m$ identity matrix.

Figures (2-3) and (2-4) show the states of the wing section and the control surface deflection, respectively. The figures indicate that the developed controller suppresses the LCO behavior with control surface deflections that remain within reasonable limits. Furthermore, the developed controller requires a smaller control effort than the controller in [15] and has better transient performance. The two controllers were also applied to the system in the presence of an additive exogenous disturbance selected as $N(t) =$

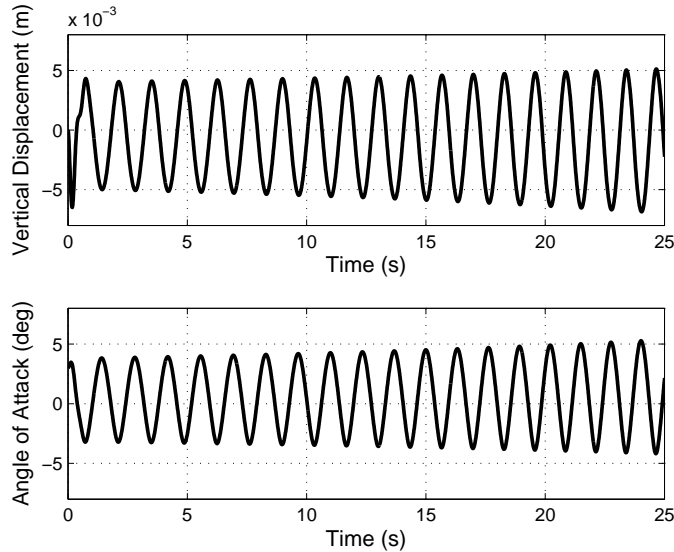


Figure 2-2. Aeroelastic system free response without disturbances

$\begin{bmatrix} 0.25 \cos(t) & 0.25 \sin(t) \end{bmatrix}^T$. Figures (2-5) and (2-6) show the system states and control effort in the presence of the additive disturbance, respectively. The developed controller is capable of regulating the AOA of the wing section in the presence of exogenous disturbances with control surface deflections that remain within tolerable limits. However, the controller in [15] is not capable of eliminating the effects of the disturbance in the wing section vertical position. Due to the coupled nature of the aeroelastic system dynamics and the availability of a single control surface, any disturbance in the AOA will propagate into the vertical position as an unmatched disturbance. One solution to this issue is to include an additional control surface at the leading edge that could be used to suppress unwanted motion in the vertical position.

A 1500 sample Monte Carlo simulation was executed to demonstrate the robustness of the developed controller to plant uncertainties and sensor noise. The uncertain model parameters were uniformly distributed over a range that extended from 80% to 120% of the nominal values found in Table 2-1 and (2-48). A zero mean noise signal uniformly distributed over an interval was added to each measurement. For the vertical

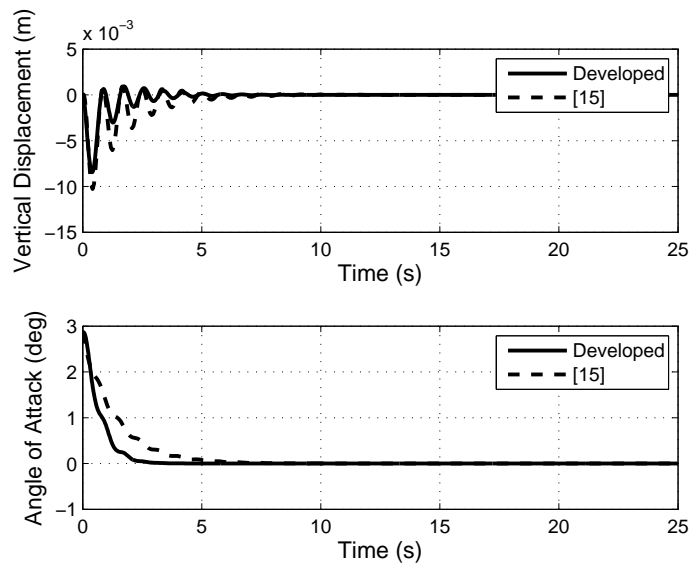


Figure 2-3. Comparison of the controlled aeroelastic system response

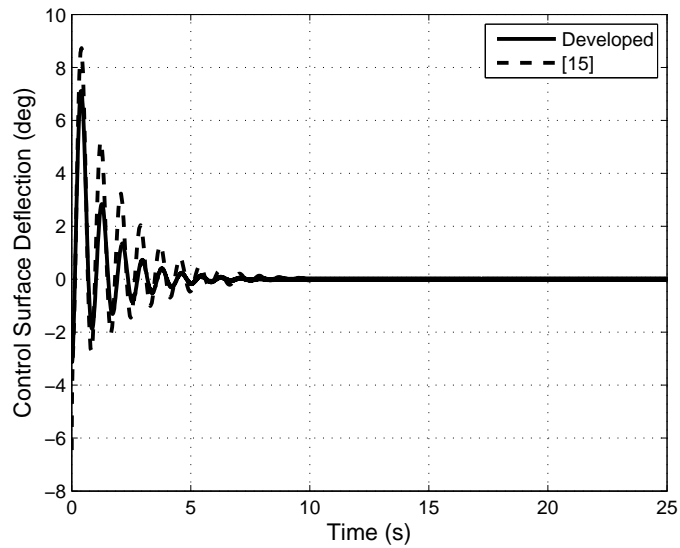


Figure 2-4. Control surface deflections, $\delta(t)$, for the developed controller and the controller from [15]

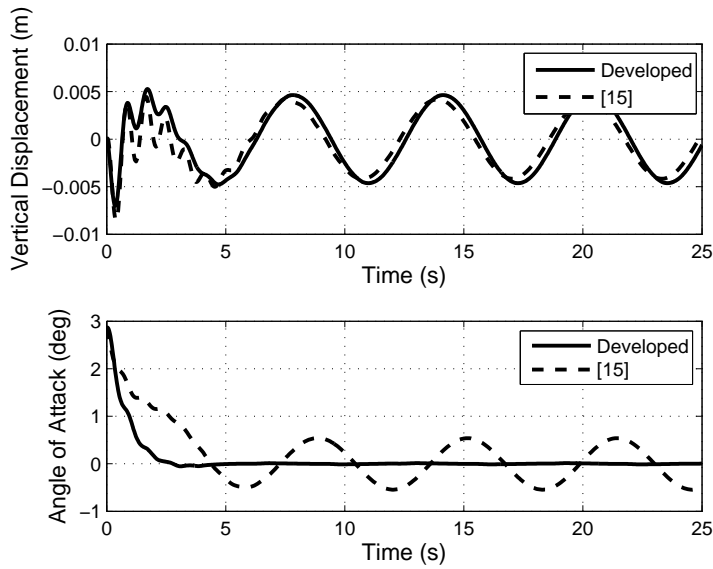


Figure 2-5. Aeroelastic system states in the presence of an additive disturbance

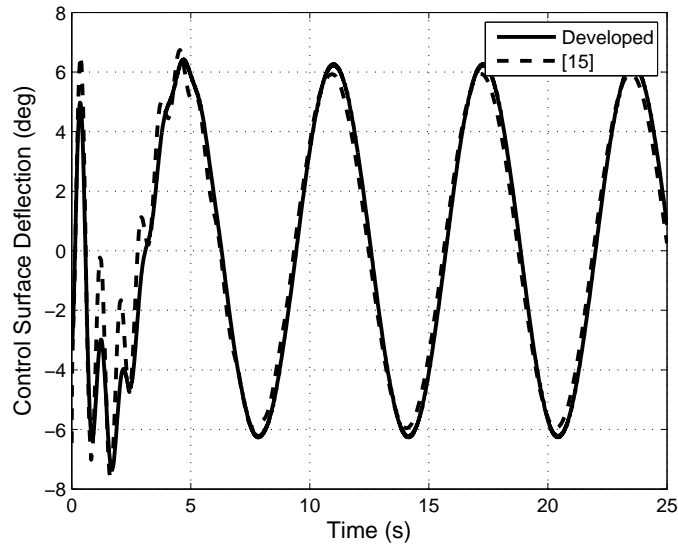


Figure 2-6. Control surface deflection, $\delta(t)$, for the developed controller and the controller from [15]

Table 2-2. Monte Carlo Simulation Results

	Mean	Standard Deviation
Maximum Error	2.9 deg	0.0038 deg
RMS Error	0.97 deg	0.073 deg
Maximum Control Effort	7.5 deg	2.6 deg

displacement and velocity, the interval was $\pm 2.5 \times 10^{-3} m$ and $\pm 2.5 \times 10^{-3} m/s$, respectively. For the AOA and AOA rate, the interval was $\pm 4.5 \times 10^{-3} rad$ and $\pm 1 \times 10^{-2} rad/s$. For each sample, the maximum of the absolute value of the tracking error and control surface deflection, and the RMS value of the tracking error were calculated. The results, presented in Table 2-2, indicate that the maximum error and RMS error of the system do not vary significantly over the range of the uncertainties considered.

Figures (2-7) - (2-9) show the average trajectory and 3σ confidence bounds for the system states and control effort for the 1500 Monte Carlo samples. Figure (2-7) shows that the AOA for all samples converges to zero in approximately 3.5 seconds and the tight confidence bounds indicate that the system performance is not significantly impacted by variations in the uncertain parameters. It is evident from Figure (2-8) that the uncontrolled vertical displacement damps out for all samples. Figure (2-9) shows that the control surface deflection is more sensitive to changes in the system parameters. The 3σ confidence bound for the maximum control effort is approximately three times that of the numerical result shown in Figure (2-6). This sensitivity indicates that in a more severe LCO, variations in the uncertain parameters could lead to a control effort greater than the actuator limits.

2.6 Summary

A robust adaptive control strategy is developed to suppress store-induced LCO behavior of an aeroelastic system. The developed controller uses a NN feedforward term to account for structural and aerodynamic uncertainties and a RISE feedback term to guarantee asymptotic tracking of a desired AOA trajectory. A Lyapunov-based stability analysis is used to prove an asymptotic tracking result. Numerical simulations

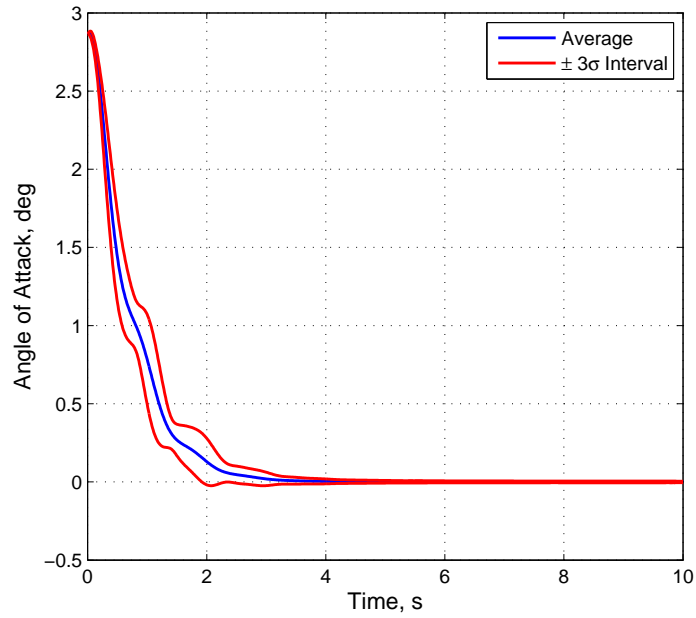


Figure 2-7. Monte Carlo AOA trajectories

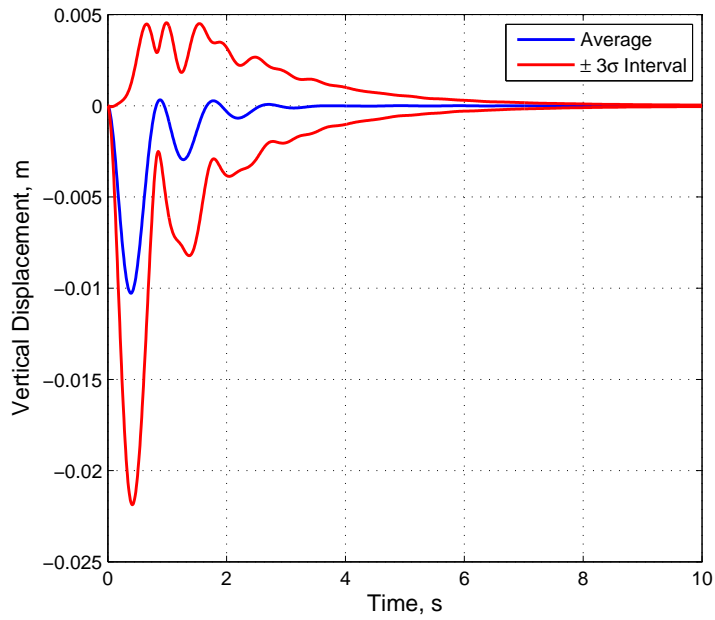


Figure 2-8. Monte Carlo vertical position trajectories

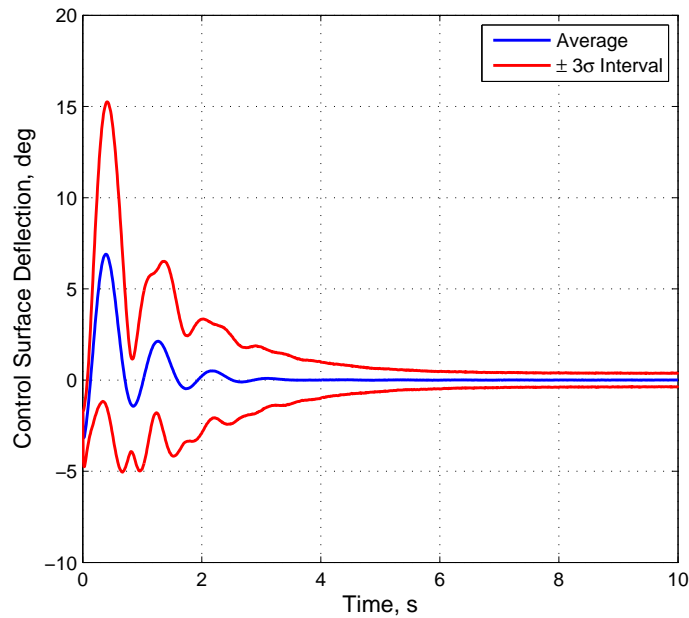


Figure 2-9. Monte Carlo control effort

illustrate LCO suppression and AOA tracking performance over a range of uncertainty. A potential drawback to the developed control strategy is that the control law does not account for actuator limits. As the severity of the LCO behavior increases, the developed controller can demand a large control surface deflection. Additionally, the Monte Carlo simulation results indicated that the maximum control effort is sensitive to variations in the parameter uncertainties, which could lead to unexpected actuator saturation.

CHAPTER 3 SATURATED RISE TRACKING CONTROL OF STORE-INDUCED LIMIT CYCLE OSCILLATIONS

The focus of this chapter is to develop a saturated controller to suppress LCO behavior in a two degree of freedom airfoil section in the presence of structural and aerodynamic uncertainties without breaching actuator limits. A smooth saturation function is included in the closed-loop error system design to ensure the commanded control effort remains within actuator limits and a continuous saturated RISE feedback control structure ensures asymptotic tracking of the AoA [18].

3.1 Control Objective

The subsequent control development and stability analysis is based on the aeroelastic model described in (2–9) (see Figure (2-1)). The control objective is to ensure the airfoil section AoA, α , tracks a desired trajectory defined as $\alpha_d \in \mathbb{R}$ using a limited amplitude, continuous controller. As in Chapter 2, it is assumed that $\alpha_d, \dot{\alpha}_d, \ddot{\alpha}_d, \ddot{\alpha}_d \in \mathcal{L}_\infty$. The control objective is quantified by defining a tracking error $e_1 \in \mathbb{R}$ as

$$e_1 \triangleq \alpha - \alpha_d. \quad (3-1)$$

To facilitate the control design, the auxiliary tracking errors $e_2 \in \mathbb{R}$ and $r \in \mathbb{R}$ are defined as [18]

$$e_2 \triangleq \dot{e}_1 + \gamma_1 \tanh(e_1) + \tanh(e_f), \quad (3-2)$$

$$r \triangleq \dot{e}_2 + \gamma_2 \tanh(e_2) + \gamma_3 e_2, \quad (3-3)$$

where $\gamma_1, \gamma_2, \gamma_3 \in \mathbb{R}$ are positive constant control gains, and the auxiliary signal $e_f \in \mathbb{R}$ is defined as the solution to the following differential equation

$$\dot{e}_f \triangleq \cosh^2(e_f) (-\gamma_4 e_2 + \tanh(e_1) - \gamma_5 \tanh(e_f)), \quad e_f(t_0) = e_{f_0}, \quad (3-4)$$

where $e_{f_0} \in \mathbb{R}$ is a known initial condition and $\gamma_4, \gamma_5 \in \mathbb{R}$ are positive constant control gains. The subsequent development is based on the assumption that q and \dot{q} are measurable. Hence, e_1 and e_2 are measurable, and e_f can be computed from measurable terms, but r is not measurable since it depends on \ddot{q} . The following inequality properties will be used in the subsequent development [57]:

$$|\xi| \geq |\tanh(\xi)|, \quad |\tanh(\xi)|^2 \geq \tanh^2(|\xi|), \quad (3-5)$$

$$\xi \tanh(\xi) \geq \tanh^2(\xi), \quad |\xi|^2 \geq \ln(\cosh(\xi)) \geq \frac{1}{2} \tanh^2(|\xi|). \quad (3-6)$$

3.2 Control Development

Substituting the dynamics from (2-9) into (3-3) and multiplying by $\frac{\det(M)}{g}$ yields

$$\frac{\det(M)}{g} r = \frac{f}{g} + \frac{\det(M)}{g} d_\alpha + \delta, \quad (3-7)$$

where the auxiliary terms $f \in \mathbb{R}$ and $g \in \mathbb{R}$ are defined as

$$\begin{aligned} f &\triangleq -m_1 \left(\tilde{C}_{21} \dot{h} + \tilde{C}_{22} \dot{\alpha} + \tilde{K}_{22} \alpha \right) + m_2 \left(\tilde{C}_{11} \dot{h} + \tilde{C}_{12} \dot{\alpha} + \tilde{K}_{11} h + \tilde{K}_{12} \alpha \right) \\ &\quad - \det(M) \ddot{\alpha}_d + \det(M) \gamma_1 \cosh^{-2}(e_1) (e_2 - \gamma_1 \tanh(e_1) - \tanh(e_f)) \\ &\quad - \det(M) \gamma_5 \tanh(e_f) + \det(M) (\tanh(e_1) + \gamma_2 \tanh(e_2) + \gamma_3 e_2 - \gamma_4 e_2), \\ g &\triangleq m_2 C_{l_\delta} + m_1 C_{m_\delta}. \end{aligned}$$

Based on the open-loop error system in (3-7), the control surface deflection is designed as

$$\delta = -\gamma_4 \tanh(v), \quad (3-8)$$

where $v \in \mathbb{R}$ is the generalized Filippov solution to the differential equation

$$\dot{v} = \beta \cosh^2(v) \operatorname{sgn}(e_2), \quad v(t_0) = v_0, \quad (3-9)$$

where $\beta \in \mathbb{R}$ is a positive constant control gain, and $v_0 \in \mathbb{R}$ is a known initial condition.

The existence of solutions for $\dot{v} \in K[w_1]$ can be shown using differential inclusions as

in Chapter 2, where $w_1 : \mathbb{R} \rightarrow \mathbb{R}$ is defined as the right-hand side of (3–9), $K[w_1] \triangleq \bigcap_{\tau > 0} \bigcap_{\mu S_m = 0} \bar{c} \bar{o} w_1(e_1, B - S_m)$, and $B = \{\varepsilon \in \mathbb{R} \mid |e_2 - \varepsilon| < \tau\}$. The desire to inject a smooth saturation function into the control structure motivates the usage of the hyperbolic tangent function in (3–8). Furthermore, it is clear that the control surface deflection is bounded and will not breach the actuator limits provided that the control gain γ_4 is selected to be less than the limit. The design of the auxiliary term v in (3–9) is motivated by the extra time derivative that will be applied to the closed-loop system obtained by substituting (3–8) into (3–7). The extra derivative introduces a $\cosh^{-2}(v)$ term in the closed-loop dynamics which will be canceled by the $\cosh^{-2}(v)$ term in (3–9).

The closed-loop tracking error dynamics can be obtained by differentiating (3–7) with respect to time and substituting the time derivative of (3–8) to yield

$$\frac{\det(M)}{g} \dot{r} = -\frac{1}{2} \frac{d}{dt} \left(\frac{\det(M)}{g} \right) r + \tilde{N} + N_d + \Omega - \tanh(e_2) - e_2 - \frac{\det(M)}{g} \gamma_4 r - \beta \gamma_4 \operatorname{sgn}(e_2), \quad (3-10)$$

where $\tilde{N} \in \mathbb{R}$, $N_d \in \mathbb{R}$, and $\Omega \in \mathbb{R}$ are defined as

$$\begin{aligned} \tilde{N} \triangleq & -\frac{1}{2} \frac{d}{dt} \left(\frac{\det(M)}{g} \right) r + \frac{d}{dt} \left(\frac{\det(M)}{g} \right) \gamma_1 \cosh^{-2}(e_1) (e_2 - \gamma_1 \tanh(e_1) - \tanh(e_f)) \\ & - \frac{2 \det(M)}{g} \gamma_1 \cosh^{-2}(e_1) \tanh(e_1) \dot{e}_1^2 - \frac{\det(M)}{g} \gamma_1^2 \cosh^{-4}(e_1) \dot{e}_1 + \tanh(e_2) + e_2 \\ & - \frac{\det(M)}{g^2} C_{i_s} \dot{m}_2 (\gamma_1 \cosh^{-2}(e_1) \dot{e}_1 - \gamma_5 \tanh(e_f) + \tanh(e_1) + \gamma_2 \tanh(e_2) + \gamma_3 e_2) \\ & - \frac{d}{dt} \left(\frac{\det(M)}{g} \right) (\gamma_5 \tanh(e_f) - \tanh(e_1) - \gamma_2 \tanh(e_2) - \gamma_3 e_2) \\ & - \frac{\det(M)}{g} (\gamma_5 \tanh(e_1) - \gamma_5^2 \tanh(e_f) - \cosh^{-2}(e_1) \dot{e}_1 - \gamma_2 \cosh^{-2}(e_2) \dot{e}_2 - \gamma_3 \dot{e}_2) \\ & + \frac{\det(M)}{g} \gamma_1 \cosh^{-2}(e_1) (\dot{e}_2 - \tanh(e_1) + \gamma_5 \tanh(e_f)), \end{aligned} \quad (3-11)$$

$$\begin{aligned} N_d \triangleq & \frac{\dot{m}_2}{g} \left(\tilde{C}_{11} \dot{h} + \tilde{C}_{12} \dot{\alpha} + \tilde{K}_{11} h + \tilde{K}_{12} \alpha \right) - \frac{m_1}{g} \left(\tilde{C}_{21} \ddot{h} + \tilde{C}_{22} \ddot{\alpha} + \tilde{K}_{22} \dot{\alpha} + \dot{\tilde{K}}_{22} \alpha \right) \\ & + \frac{m_2}{g} \left(\tilde{C}_{11} \ddot{h} + \tilde{C}_{12} \ddot{\alpha} + \dot{\tilde{C}}_{12} \dot{\alpha} + \tilde{K}_{11} \dot{h} + \tilde{K}_{12} \dot{\alpha} \right) - \frac{d}{dt} \left(\frac{\det(M)}{g} \right) \ddot{\alpha}_d \end{aligned}$$

$$\begin{aligned}
& + \frac{C_{l_\delta} \dot{m}_2}{g^2} \left(m_1 \left(\tilde{C}_{21} \dot{h} + \tilde{C}_{22} \dot{\alpha} + \tilde{K}_{22} \alpha \right) - m_2 \left(\tilde{C}_{11} \dot{h} + \tilde{C}_{12} \dot{\alpha} + \tilde{K}_{11} h + \tilde{K}_{12} \alpha \right) \right) \\
& + \det(M) \ddot{\alpha}_d - \frac{\det(M)}{g} \ddot{\alpha}_d + \frac{\det(M)}{g} \dot{d}_\alpha + \frac{d}{dt} \left(\frac{\det(M)}{g} \right) d_\alpha, \tag{3-12}
\end{aligned}$$

$$\begin{aligned}
\Omega \triangleq & \gamma_4 e_2 \left(\frac{\det(M)}{g} \left(\gamma_1 \cosh^{-2}(e_1) + \gamma_5 + \gamma_3 \right) - \frac{d}{dt} \left(\frac{\det(M)}{g} \right) \right. \\
& \left. + \frac{\dot{m}_2 C_{l_\delta} \det(M)}{g^2} \right) + \frac{\det(M)}{g} \gamma_2 \gamma_4 \tanh(e_2). \tag{3-13}
\end{aligned}$$

Using the assumptions on the desired trajectories and boundedness of the LCO states, upper bounds can be developed for (3-11) and (3-12) as

$$\left| \tilde{N} \right| \leq \zeta_0 \|x\|, \quad |N_d| \leq \zeta_1, \quad \left| \dot{N}_d \right| \leq \zeta_2, \tag{3-14}$$

where $\zeta_0, \zeta_1, \zeta_2 \in \mathbb{R}$ are known bounding constants, and $x \in \mathbb{R}^4$ is defined as

$$x \triangleq \left[\tanh(e_1) \quad e_2 \quad r \quad \tanh(e_f) \right]^T. \tag{3-15}$$

3.3 Stability Analysis

To facilitate the subsequent analysis, let $z \triangleq \left[e_1 \quad e_2 \quad r \quad e_f \right]^T \in \mathbb{R}^4$ and $y \triangleq \left[z^T \quad \sqrt{P} \right] \in \mathbb{R}^5$ where $P \in \mathbb{R}$ is a Filippov solution to the differential equation

$$\dot{P} = -r (N_d - \beta \gamma_4 \operatorname{sgn}(e_2)), \tag{3-16}$$

$$P(t_0) = \beta \gamma_4 |e_2(t_0)| - e_2(t_0) N_d(t_0).$$

Provided $\beta \gamma_4$ is selected such that $\beta \gamma_4 > \zeta_1 + \frac{\zeta_2}{\gamma_3}$, $P(t) \geq 0, \forall t \in [0, \infty)$ [18]. To further facilitate the stability analysis, let the control gain γ_4 be expressed as $\gamma_4 = \gamma_a + \gamma_b$, where γ_a and $\gamma_b \in \mathbb{R}$ are positive constants.

Theorem 3.1. *The controller given in (3-8) and (3-9) yields global asymptotic tracking of the airfoil section AoA in the sense that all Filippov solutions to the differential equations in (3-2)-(3-4), (3-10), and (3-16) are bounded and $e_1 \rightarrow 0$ as $t \rightarrow \infty$,*

provided that the control gains are selected to satisfy the following sufficient conditions

$$\gamma_1 > \frac{1}{2}, \quad \gamma_3 > \gamma_4^2 + 1, \quad \beta\gamma_4 > \zeta_1 + \frac{\zeta_2}{\gamma_3}, \quad \lambda_1\gamma_a > \frac{c_1^2}{2}, \quad \gamma_5 > \frac{\gamma_4^2}{2}, \quad \lambda > \frac{\zeta_0^2}{4\lambda_1\gamma_b}, \quad (3-17)$$

where

$$\lambda \triangleq \min \left\{ \gamma_1 - \frac{1}{2}, 2\gamma_2 + \gamma_3, \gamma_3 - \gamma_4^2 - 1, \lambda_1\gamma_a - \frac{c_1^2}{2}, \gamma_5 - \frac{\gamma_4^2}{2} \right\},$$

where c_1 and $\lambda_1 \in \mathbb{R}$ are positive bounding constants, $\lambda_1 \leq \frac{\det(M)}{g}$, and

$$\begin{aligned} c_1 &\geq \left| \left(\frac{\det(M)}{g} (\gamma_1 + \gamma_3 + \gamma_5) - \frac{\frac{d}{dt}(\det(M))}{g} + \frac{\dot{m}_2 C_{l_\delta} \det(M)}{g^2} \right)^2 \right. \\ &\quad \left. + \left(\gamma_2 \frac{\det(M)}{g} \right)^2 \right|, \\ &\geq (c_{m_1} (\gamma_1 + \gamma_3 + \gamma_5) + c_{m_2} + c_{m_3} C_{l_\delta})^2 + \gamma_2^2 c_{m_1}^2, \end{aligned}$$

where $c_{m_1} > \frac{\det(M)}{g}$, $c_{m_2} > \frac{\frac{d}{dt} \det(M)}{g}$, and $c_{m_3} > \frac{\dot{m}_2 \det(M)}{g^2}$.¹

Remark 3.1. The control gains γ_1 and γ_2 can be selected independently of the remaining control gains and γ_4 is selected less than the actuator limit. After γ_4 is selected, the lower bounds on γ_3 , γ_5 , and β can be calculated. The selection of γ_a depends on the severity of the LCO motion which is captured in the bounding constant c_1 . If the LCO motion is too severe, the gain condition for γ_a can't be satisfied without increasing the saturation limit.

Proof. Let $V_L(y) : \mathbb{R}^5 \rightarrow \mathbb{R}$ be a positive-definite, continuously differentiable function defined as

$$V_L \triangleq \ln(\cosh(e_1)) + \ln(\cosh(e_2)) + \frac{1}{2}e_2^2 + \frac{1}{2} \frac{\det(M)}{g} r^2 + \frac{1}{2} \tanh^2(e_f) + P. \quad (3-18)$$

¹ See Appendix E for details.

From the inequalities in (3–5) and (3–6), V_L satisfies the following inequalities

$$\frac{1}{2} \min(\lambda_1, 1) \tanh^2(\|y\|) \leq V_L(y) \leq \lambda_2 \|y\|^2, \quad (3-19)$$

where $\lambda_2 \in \mathbb{R}$ is a known positive constant. Let y denote a Filippov solution to the closed-loop system described by (3–2)-(3–4), (3–10), and (3–16). The time derivative of (3–18) along the Filippov solution y exists almost everywhere (a.e) and $\dot{V}_L \stackrel{a.e}{\in} \check{V}_L$ where $\check{V}_L \triangleq \bigcap_{\Xi \in \partial V_L} \Xi^T K \left[\begin{array}{cccccc} \dot{e}_1 & \dot{e}_2 & \dot{r} & \dot{e}_f & \frac{\dot{P}}{2\sqrt{P}} & 1 \end{array} \right]^T$ and ∂V_L denotes the generalized gradient of V_L [58]. Since V_L is a continuously differentiable function, \check{V}_L can be expressed as

$$\check{V}_L \subset \nabla V_L^T K \left[\begin{array}{cccccc} \dot{e}_1 & \dot{e}_2 & \dot{r} & \dot{e}_f & \frac{\dot{P}}{2\sqrt{P}} & 1 \end{array} \right]^T, \quad (3-20)$$

where

$$\nabla V_L^T \triangleq \left[\begin{array}{cccccc} \tanh(e_1) & \tanh(e_2) + e_2 & \frac{\det(M)}{g} r & \tanh(e_f) \cosh^{-2}(e_f) & 2\sqrt{P} & \frac{1}{2} \frac{d}{dt} \left(\frac{\det(M)}{g} \right) r^2 \end{array} \right].$$

Using the calculus for K from [54], (3–1)-(3–4), (3–10), and (3–16), the expression in (3–20) can be written as

$$\begin{aligned} \check{V}_L \subset & \tanh(e_1)(e_2 - \gamma_1 \tanh(e_1)) + \tanh(e_2)(-\gamma_2 \tanh(e_2) - \gamma_3 e_2) \\ & + e_2(-\gamma_2 \tanh(e_2) - \gamma_3 e_2) + r \left(\tilde{N} + \Omega - \frac{\det(M)}{g} \gamma_4 r - \beta \gamma_4 K[\text{sgn}(e_2)] \right) \\ & + \tanh(e_f)(-\gamma_4 e_2 - \gamma_5 \tanh(e_f)) + r \beta \gamma_4 K[\text{sgn}(e_2)], \end{aligned} \quad (3-21)$$

As in Chapter 2, (3–21) reduces to a scalar inequality since the right-hand side is continuous except for the Lesbegue negligible set of time instances when $r \beta \gamma_4 K[\text{sgn}(e_2)] - r \beta \gamma_4 K[\text{sgn}(e_2)] \neq \{0\}$. The resulting scalar inequality is expressed as

$$\begin{aligned} \dot{V}_L \stackrel{a.e.}{\leq} & -\gamma_1 \tanh^2(e_1) - \gamma_2 \tanh^2(e_2) - \gamma_3 e_2^2 - \frac{\det(M)}{g} \gamma_4 r^2 - \gamma_5 \tanh^2(e_f) \\ & + r \tilde{N} + r \Omega + \tanh(e_1) e_2 - (\gamma_3 + \gamma_2) \tanh(e_2) e_2 - \gamma_4 \tanh(e_f) e_2. \end{aligned} \quad (3-22)$$

Using Young's Inequality and the bounds on the system states, the term $r\Omega$ can be upper bounded as

$$\begin{aligned}
|r\Omega| &\leq \frac{1}{2} \left(\frac{\det(M)}{g} (\gamma_1 \cosh^{-2}(e_1) + \gamma_5 + \gamma_3) - \frac{\frac{d}{dt}(\det(M))}{g} + \frac{\dot{m}_2 C_{I_\delta} \det(M)}{g^2} \right)^2 r^2 \\
&\quad + \gamma_4^2 e_2^2 + \frac{1}{2} \left(\gamma_2 \frac{\det(M)}{g} \right)^2 r^2 \\
&\leq \frac{c_1^2}{2} r^2 + \gamma_4^2 e_2^2.
\end{aligned} \tag{3-23}$$

By applying Young's Inequality, the inequalities in (3-5) and (3-6), and the upper bounds on \tilde{N} and $r\Omega$ given in (3-11) and (3-23), (3-22) can be upper bounded as

$$\begin{aligned}
\dot{V}_L &\stackrel{a.e.}{\leq} -\gamma_1 \tanh^2(e_1) - \gamma_2 \tanh^2(e_2) - \gamma_3 e_2^2 - \lambda_1 \gamma_4 r^2 - \gamma_5 \tanh^2(e_f) + \zeta_0 \|x\| |r| + \frac{c_1^2}{2} r^2 \\
&\quad + \frac{1}{2} \tanh^2(e_1) + e_2^2 - (\gamma_3 + \gamma_2) \tanh^2(e_2) + \frac{1}{2} \gamma_4^2 \tanh^2(e_f) + \gamma_4^2 e_2^2.
\end{aligned} \tag{3-24}$$

Combining common terms and completing the squares on the term $-(\lambda_1 \gamma_b r^2 - \zeta_0 \|x\| |r|)$ yields

$$\begin{aligned}
\dot{V}_L &\stackrel{a.e.}{\leq} - \left(\gamma_1 - \frac{1}{2} \right) \tanh^2(e_1) - (2\gamma_2 + \gamma_3) \tanh^2(e_2) - (\gamma_3 - 1 - \gamma_4^2) e_2^2 \\
&\quad - \left(\lambda_1 \gamma_a - \frac{c_1^2}{2} \right) r^2 - \left(\gamma_5 - \frac{\gamma_4^2}{2} \right) \tanh^2(e_f) + \frac{\zeta_0^2 \|x\|^2}{4\lambda_1 \gamma_b}.
\end{aligned} \tag{3-25}$$

Provided the sufficient gain conditions in (3-17) are satisfied, (3-15) and the definition of z can be used to show

$$\dot{V}_L \stackrel{a.e.}{\leq} - \left(\lambda - \frac{\zeta_0^2}{4\lambda_1 \gamma_b} \right) \tanh^2(\|z\|) \leq -c \tanh^2(\|z\|), \tag{3-26}$$

where $c \in \mathbb{R}$ is a positive constant. From the inequalities in (3-19) and (3-26), $V_L \in \mathcal{L}_\infty$; therefore, e_1, e_2, r , and $\tanh(e_f) \in \mathcal{L}_\infty$. Equations (3-2) and (3-3) can be used to show that \dot{e}_1 and $\dot{e}_2 \in \mathcal{L}_\infty$. From (3-8), $\delta \in \mathcal{L}_\infty$. Since $e_2, r \in \mathcal{L}_\infty$, it can be concluded from (3-15) that $x \in \mathcal{L}_\infty$. Equations (3-10) and (3-14) can be used to show that $\dot{r} \in \mathcal{L}_\infty$. Since $e_2 \in \mathcal{L}_\infty$, (3-4) can be used to show that $\cosh^{-2}(e_f) \dot{e}_f \in \mathcal{L}_\infty$. Since

$\dot{e}_1, \dot{e}_2, \dot{r}, \cosh^{-2}(e_f) \dot{e}_f \in \mathcal{L}_\infty$, the definition of z can be used to show that $\dot{z} \in \mathcal{L}_\infty$, and hence, z is uniformly continuous (UC). Since z is UC, the function $-c \tanh^2(\|z\|)$ is UC. Based on (3–26), Corollary 1 from [56] can be used to prove that $\tanh(\|z\|) \rightarrow 0$ as $t \rightarrow \infty$. From the definition of z it can be concluded that $e_1 \rightarrow 0$ as $t \rightarrow \infty$. \square

3.4 Simulation Results

A numerical simulation is presented to illustrate the performance of the developed controller and to provide a comparison with the controller in Chapter 2.

The model parameters for the simulation are shown in Table 3-1 and (3–27). The open-loop system was simulated with the following initial conditions: $h(0) = 0$ m, $\dot{h}(0) = 0$ m/s, $\alpha(0) = 11.5$ deg, and $\dot{\alpha}(0) = 0$ deg/s. It is evident from Figure (3-1) that the open-loop system, under the above initial conditions and no exogenous disturbances, experiences LCO behavior.

Table 3-1. Aeroelastic Model Parameters

Parameter	Parameter	Parameter	Parameter
m_w	4.0 kg	I_s	0.0050 kg·m ²
m_s	4.0 kg	c_{h_1}	2.743x10 ¹ kg/s
r_x	0.0	c_α	0.036 kg·m ² /s
r_h	0.0	k_h	2.200x10 ³ N/m
a	-0.6	ρ	1.225 kg/m ³
a_h	0.0	U	1.50x10 ¹ m/s
b	0.14 m	S	1.0 m
s_x	0.098	C_{l_α}	6.8 1/rad
s_h	1.4	C_{l_δ}	9.3x10 ¹ N/rad
I_w	0.043 kg·m ²	C_{m_δ}	2.3 N·m/rad

$$k_\alpha(q) = 0.5 - 11.05\alpha + 657.75\alpha^2 - 4290\alpha^3 + 8644.85\alpha^4. \quad (3-27)$$

The control objective in the subsequent numerical simulations is to regulate the AoA to zero degrees. In addition, an external disturbance, selected as $d(t) = \begin{bmatrix} 0 & 0.25 \sin(t) \end{bmatrix}^T$, was added to the numerical simulation and a zero-mean noise signal uniformly distributed over an interval was added to each measurement. For the

vertical displacement and velocity, the interval was $\pm 2.5 \times 10^{-3}$ m and $\pm 2.5 \times 10^{-3}$ m/s, respectively. For the AoA and AoA rate, the interval was $\pm 4.5 \times 10^{-2}$ rad and $\pm 1 \times 10^{-2}$ rad/s. Based on the identification performance of the NN, the NN feedforward parameters for the controller developed in Chapter 2 were selected as $n_2 = 25$, $\Gamma_1 = 10I_{26}$, and $\Gamma_2 = 10I_7$, where I_m denotes an $m \times m$ identity matrix. The RISE feedback control gains for the controller developed in Chapter 2 were determined through a 1500 sample Monte Carlo simulation in which the RISE feedback control gains for each sample were selected at random from within a specified interval. The gains used in the comparison study were selected as those that returned the minimum value for the following cost function

$$J = \sqrt{\frac{1}{n} \left(\sum_{i=1}^n \alpha^2(t_i) \right)}, \quad (3-28)$$

where n is the total number of time steps in the numerical simulation. The set of control gains that produced the smallest AoA RMS error were $\alpha_2 = 3.9513$, $k_s = 2.6112$, and $\beta_1 = 0.9966$. Figures (3-2) and (3-3) depict the performance of the unsaturated RISE controller developed in Chapter 2 and that same RISE controller with an *ad hoc* saturation applied to the commanded control. While the unsaturated controller suppressed the LCO behavior, the commanded control effort breached the actuator limit several times. When the *ad hoc* saturation was applied to the controller, the LCO behavior could not be suppressed and the system returned to an LCO state. This highlights the unpredictable response that can occur when applying an *ad hoc* saturation without considering the stability of the resulting closed-loop system.

The developed control strategy was applied to the system with the following gains: $\gamma_1 = 0.8375$, $\gamma_2 = 17.7604$, $\gamma_3 = 33.9025$, $\gamma_4 = 0.1745$, $\gamma_5 = 15.4652$, and $\beta = 5.5539$. Note that γ_4 represents the actuator limit in radians, which was taken to be ± 10 deg. The control gains for the developed controller were determined by applying the same Monte Carlo approach used to select the gains for the controller in Chapter 2.

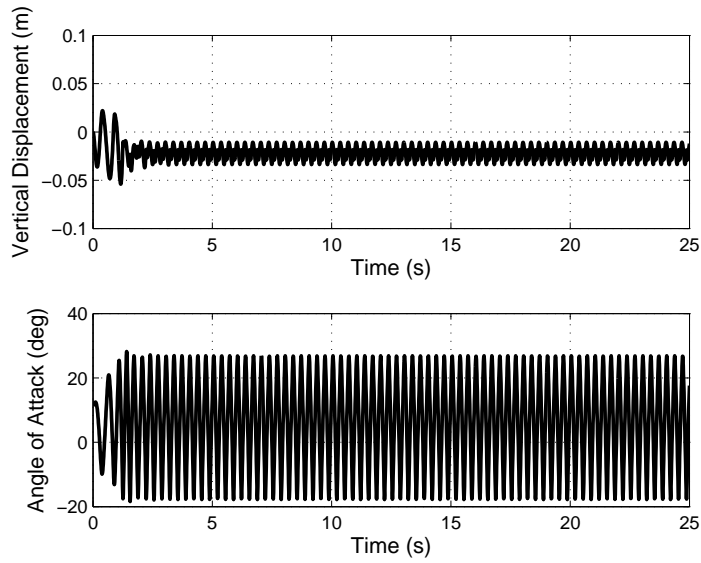


Figure 3-1. Aeroelastic system open-loop response without disturbances

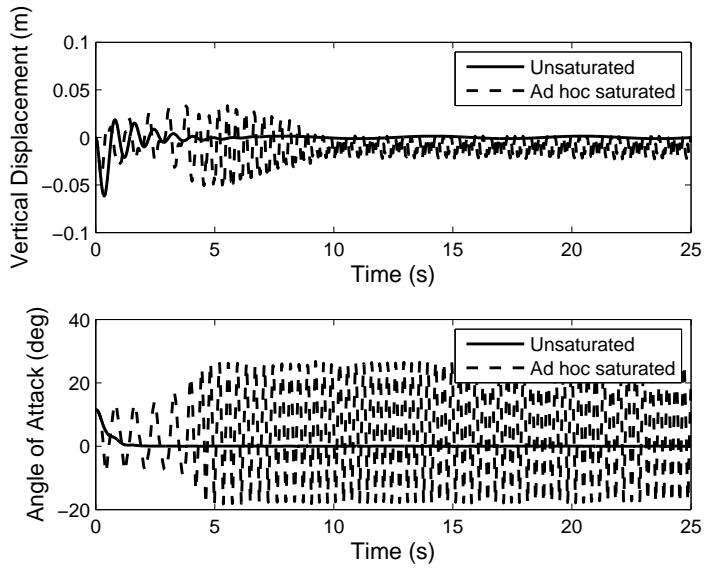


Figure 3-2. State trajectories of the controller developed in [2] with and without an *ad hoc* saturation.

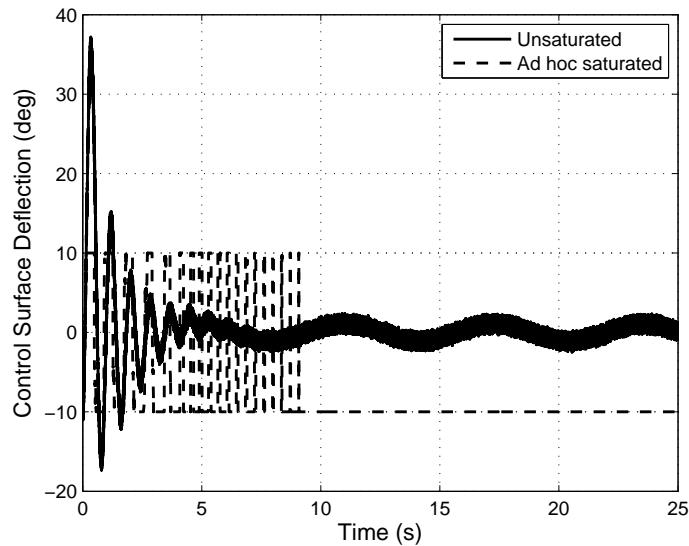


Figure 3-3. Commanded control effort for the controller developed in [2] with and without an *ad hoc* saturation.

The states and control surface deflection of the *ad hoc* saturated controller and the developed saturated controller are shown in Figures (3-4) and (3-5), respectively. While different gain selections will alter the performance, Figures (3-4) and (3-5) illustrate that the developed control strategy is capable of suppressing LCO behavior in the presence of actuator limits. The benefit of the developed method is that the saturation limit is included in the stability analysis guaranteeing asymptotic tracking, versus the *ad hoc* saturation which yields an unpredictable response.

A 1500 sample Monte Carlo simulation was also performed to demonstrate the robustness of the developed saturated controller to plant uncertainties and measurement noise. The model parameters were varied uniformly over a range that extended from 95% to 105% of the parameter values listed in Table 3-1. While the developed saturated controller successfully regulated the AoA for all 1500 samples, the transient performance varied significantly between samples.

The average trajectory and 3σ confidence bounds for the angle of attack, vertical position, and control surface deflection of the Monte Carlo samples are shown in

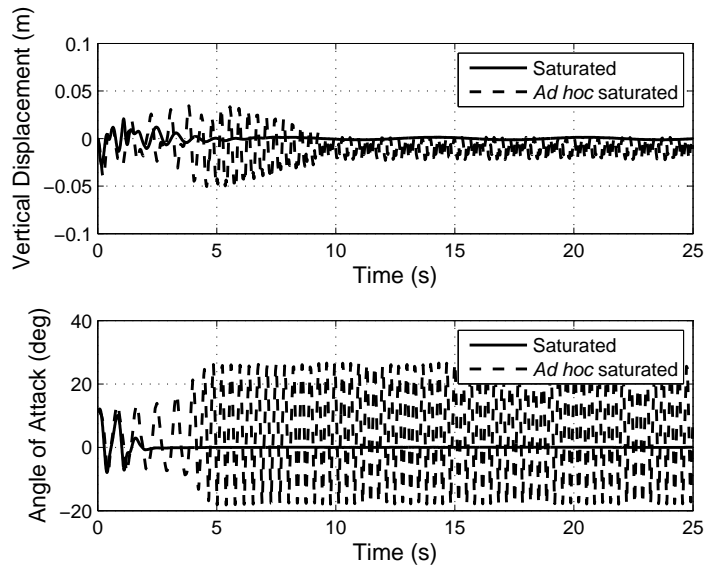


Figure 3-4. Comparison of the closed-loop aeroelastic system response of the controller in [2] with an *ad hoc* saturation and the developed saturated controller.

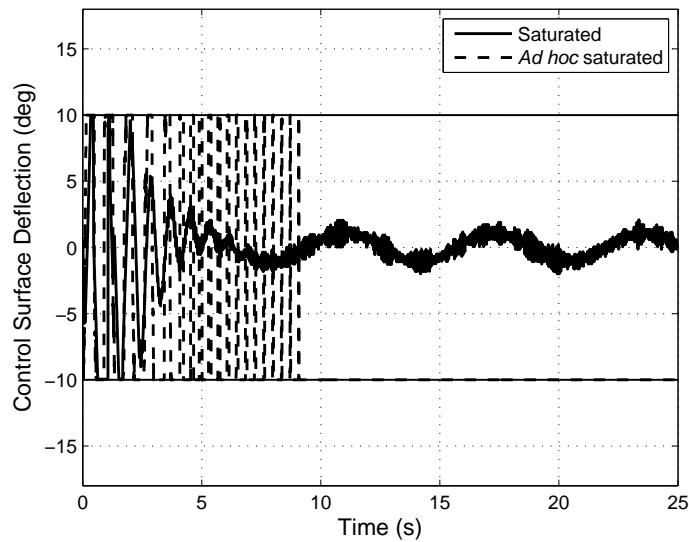


Figure 3-5. Comparison of the control surface deflections for the developed saturated controller and *ad hoc* saturated controller from [2]

Table 3-2. Monte Carlo Simulation Results

	Mean	Standard Deviation
Maximum Tracking Error	1.272×10^1 deg	3.04 deg
RMS Tracking Error	2.13 deg	2.53 deg

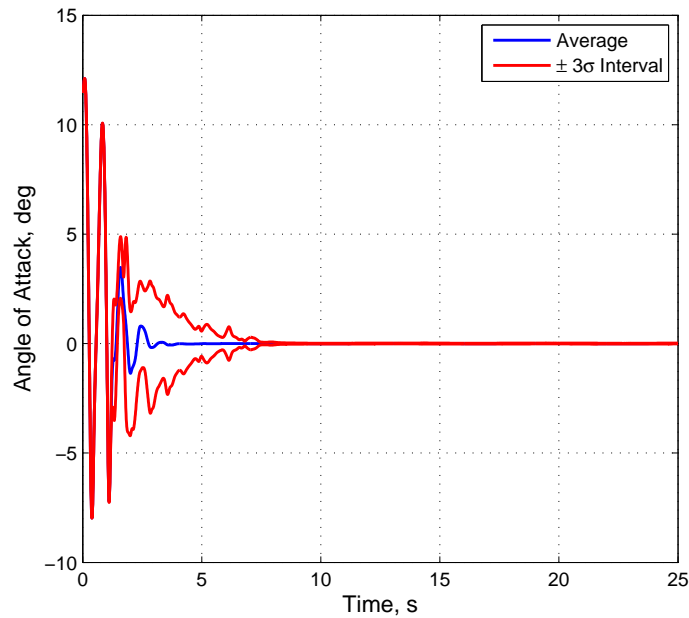


Figure 3-6. AoA trajectories for all 1500 Monte Carlo samples. The developed saturated controller suppressed the LCO behavior in all samples and the majority of the samples exhibit similar transient performance.

Figures (3-6) - (3-8). Figure (3-6) indicates that the AoA for all samples converge to zero after approximately 7 seconds, however the considered range of model uncertainties does impact the transient performance of the controller. The sensitivity in transient performance can be attributed to the saturation on the commanded control effort. As noted previously, under certain conditions the severity of the LCO can become more than the saturated controller can suppress and the system will return to an LCO state.

3.5 Summary

A saturated control strategy is developed to suppress store-induced LCO behavior of an aeroelastic system. The control strategy uses a saturated RISE controller to asymptotically track a desired AoA trajectory without exceeding actuator limits. A Lyapunov-based stability analysis guarantees asymptotic tracking in the presence of actuator constraints, exogenous disturbances, and modeling uncertainties. Simulations results are presented to illustrate the performance of the developed control strategy.

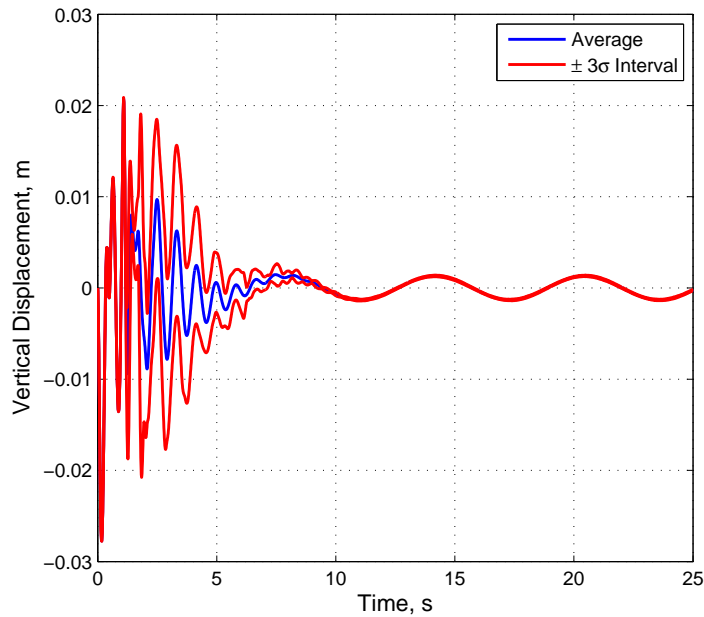


Figure 3-7. Vertical position trajectories of all 1500 Monte Carlo samples. The vertical position remained bounded for all samples despite being an uncontrolled state.

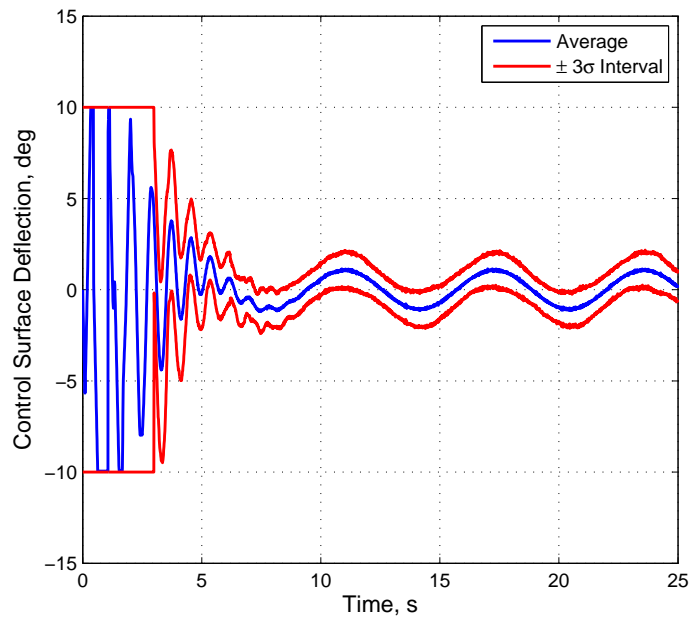


Figure 3-8. Control surface deflection for all 1500 Monte Carlo samples. The control effort for all samples remain within the actuation limit and demonstrate similar steady state performance.

A numerical simulation was presented that demonstrated the unpredictable closed-loop system response when an *ad hoc* saturation strategy is applied to the controller in Chapter 2. A comparison study revealed that the saturated controller developed in this paper achieved asymptotic tracking of the desired AoA trajectory while the *ad hoc* saturation strategy was unable to suppress the LCO behavior. A 1500 sample Monte Carlo simulation was presented to demonstrate the robustness of the developed controller to variations in the model parameters. A potential drawback of the developed control strategy is that under certain conditions, the severity of the produced LCO may result in sufficient gain conditions that can't be satisfied. That is, if the disturbances to the system are large enough, then the system could be destabilized. This is a direct result of the actuator limit; increasing the actuator limit relaxes the sufficient gain conditions and allows for larger disturbances. Furthermore, an adaptive feedforward term could potentially be included to compensate for the uncertain dynamics, thereby relaxing the sufficient gain conditions. However, for any controller that has restricted control authority, it is possible for some disturbance to dominate the controller's ability to yield a desired or even stable performance.

CHAPTER 4
BOUNDARY CONTROL OF LIMIT CYCLE OSCILLATIONS IN A FLEXIBLE AIRCRAFT
WING

The focus of this chapter is to develop a boundary control strategy for suppressing LCO motion in an aircraft wing whose dynamics are described by a system of linear partial differential equations (PDEs). A PDE backstepping method guarantees exponential regulation of the wing twist dynamics while a Lyapunov-based stability analysis is used to show boundedness of the wing bending dynamics.

4.1 Aircraft Wing Model

Consider a flexible wing of length $l \in \mathbb{R}$, mass per unit length of $\rho \in \mathbb{R}$, moment of inertia per unit length of $I_w \in \mathbb{R}$, and bending and torsional stiffnesses of $EI \in \mathbb{R}$ and $GJ \in \mathbb{R}$, respectively, with a store of mass $m_s \in \mathbb{R}$ and moment of inertia $J_s \in \mathbb{R}$ attached at the wing tip. The bending and twisting dynamics of the flexible wing are described by the following PDE system¹

$$\rho\omega_{tt} + EI\omega_{yyyy} + \eta_\omega EI\omega_{tyyyy} = L_w, \quad (4-1)$$

$$I_w\phi_{tt} - GJ\phi_{yy} - \eta_\phi GJ\phi_{tyy} = M_w, \quad (4-2)$$

where $\omega(y, t) \in \mathbb{R}$ and $\phi(y, t) \in \mathbb{R}$ denote the bending and twisting displacements, respectively, $y \in [0, l]$ denotes spanwise location on the wing, $\eta_\omega \in \mathbb{R}$ and $\eta_\phi \in \mathbb{R}$ denote Kelvin-Voigt damping coefficients in the bending and twisting states, respectively, and $L_w = \bar{L}_w\phi \in \mathbb{R}$ and $M_w = \bar{M}_w\phi \in \mathbb{R}$ denote the aerodynamic lift and moment on the wing, respectively, where \bar{L}_w and $\bar{M}_w \in \mathbb{R}$ denote aerodynamic lift and moment coefficients, respectively. In (4-1) and (4-2), the subscripts t and y denote partial derivatives. The boundary conditions for tip-based control are $\omega(0, t) = \omega_y(0, t) =$

¹ See Appendix F for details regarding the derivation of the dynamics.

$\omega_{yy}(l, t) = \phi(0, t) = 0$ and

$$EI\omega_{yyy}(l, t) + \eta_w EI\omega_{tyyy}(l, t) = m_s \omega_{tt}(l, t) - L_{tip}, \quad (4-3)$$

$$GJ\phi_y(l, t) + \eta_\phi GJ\phi_{ty}(l, t) = -J_s \phi_{tt}(l, t) + M_{tip}, \quad (4-4)$$

where $L_{tip} \in \mathbb{R}$ and $M_{tip} \in \mathbb{R}$ denote the aerodynamic lift and moment at the wing tip which can be implemented through flaps located at the wing tip [44]. It is assumed in (4-1) and (4-2) that the center of mass and shear center are coincident and all model parameters are constant.

4.2 Boundary Control of Wing Twist

The control objective is to ensure that the wing twist is regulated in the sense that $\phi(y, t) \rightarrow 0, \forall y \in [0, l]$ as $t \rightarrow \infty$ via boundary control at the wing tip. A PDE backstepping method will be used to transform the system in (4-2) into an exponentially stable target system using an invertible Volterra integral transformation [35]. The state transformation is defined as

$$\Phi(y, t) \triangleq \phi(y, t) - \int_0^y k(y, x) \phi(x, t) dx, \quad (4-5)$$

where the function $k(x, y) \in \mathbb{R}$ denotes the gain kernel. The exponentially stable target system is selected as

$$I_w \Phi_{tt} - GJ\Phi_{yy} - \eta_\phi GJ\Phi_{tyy} + (cGJ - \bar{M}_w) \Phi + \eta_\phi cGJ\Phi_t = 0, \quad (4-6)$$

where $c \in \mathbb{R}$ is a positive constant selected to satisfy the inequality, $c > \frac{\bar{M}_w}{GJ} - \frac{\pi^2}{4l^2}$, and the boundary conditions are $\Phi(0, t) = 0$ and $GJ\Phi_y(l, t) + \eta_\phi GJ\Phi_{ty}(l, t) = 0^2$. Due to the fact that the state transformation is invertible, stability of the target system in (4-6) translates to stability of the system in (4-2) with the boundary control in (4-13) [35]. The task

² See Appendix G

is now to find the gain kernel $k(y, x)$ that satisfies (4-6) and its boundary conditions. A linear PDE and associated boundary conditions that describe the gain kernel are obtained by substituting the state transformation in (4-5) into (4-6). Substituting the state transformation into the first term in (4-6) yields

$$\begin{aligned}
I_w \Phi_{tt} &= I_w \phi_{tt} - I_w \int_0^y k(y, x) \phi_{tt}(x, t) dx \\
&= \bar{M}_w \phi(y, t) + GJ \phi_{yy}(y, t) + \eta_\phi GJ \phi_{tyy}(y, t) \\
&\quad - \int_0^y k(y, x) (\bar{M}_w \phi(x, t) + GJ \phi_{xx}(x, t) + \eta_\phi GJ \phi_{txx}(x, t)) dx. \quad (4-7)
\end{aligned}$$

After integrating the last two terms by parts, (4-7) can be expressed as

$$\begin{aligned}
I_w \Phi_{tt} &= \bar{M}_w \phi(y, t) + GJ \phi_{yy}(y, t) + \eta_\phi GJ \phi_{tyy}(y, t) - GJk(y, y) \phi_y(y, t) \\
&\quad + GJk(y, 0) \phi_y(0, t) + GJk_x(y, y) \phi(y, t) - \eta_\phi GJk(y, y) \phi_{ty}(y, t) \\
&\quad + \eta_\phi GJk(y, 0) \phi_{ty}(0, t) + \eta_\phi GJk_x(y, y) \phi_t(y, t) \\
&\quad - \int_0^y [k(y, x) \bar{M}_w + GJk_{xx}(y, x)] \phi(x, t) dx \\
&\quad - \eta_\phi GJ \int_0^y k_{xx}(y, x) \phi_t(x, t) dx, \quad (4-8)
\end{aligned}$$

where $k_x(y, y) \triangleq \frac{\partial}{\partial x} k(y, x) |_{x=y}$. Similarly, expressions for the second and third terms in (4-6) can be obtained as

$$\begin{aligned}
GJ \Phi_{yy} &= GJ \phi_{yy}(y, t) - GJ \frac{d}{dy} (k(y, y)) \phi(y, t) - GJk(y, y) \phi_y(y, t) \\
&\quad - GJk_y(y, y) \phi(y, t) - GJ \int_0^y k_{yy}(y, x) \phi(x, t) dx, \quad (4-9)
\end{aligned}$$

$$\begin{aligned}
\eta_\phi GJ \Phi_{tyy} &= \eta_\phi GJ \phi_{tyy}(y, t) - \eta_\phi GJ \frac{d}{dy} (k(y, y)) \phi_t(y, t) - \eta_\phi GJk(y, y) \phi_{ty}(y, t) \\
&\quad - \eta_\phi GJk_y(y, y) \phi_t(y, t) - \eta_\phi GJ \int_0^y k_{yy}(y, x) \phi_t(x, t) dx, \quad (4-10)
\end{aligned}$$

where $\frac{d}{dy} (k(y, y)) \triangleq \frac{\partial}{\partial x} k(y, x) |_{x=y} + \frac{\partial}{\partial y} k(y, x) |_{x=y}$ and $k_y(y, y) \triangleq \frac{\partial}{\partial y} k(y, x) |_{x=y}$.

Substituting the state transformation in (4-5) into the last two terms in (4-6) and utilizing

the expressions in (4–8)-(4–10) yields

$$\begin{aligned}
& \left(2GJ \frac{d}{dy} (k(y, y)) + cGJ \right) \phi(y, t) + GJk(y, 0) \phi_y(0, t) \\
& + \eta_\phi GJk(y, 0) \phi_{ty}(0, t) + \eta_\phi \left(2GJ \frac{d}{dy} (k(y, y)) + cGJ \right) \phi_t(y, t) \\
& + \int_0^y (GJk_{yy}(y, x) - GJk_{xx}(y, x) - cGJk(y, x)) \phi(x, t) dx \\
& + \eta_\phi \int_0^y (GJk_{yy}(y, x) - GJk_{xx}(y, x) - cGJk(y, x)) \phi_t(x, t) dx = 0.
\end{aligned}$$

For the non-trivial solution of $\phi(y, t)$, the gain kernel $k(y, x)$ must satisfy the following PDE

$$k_{yy}(y, x) - k_{xx}(y, x) = ck(y, x), \quad (4-11)$$

with the boundary conditions $k(y, 0) = 0$ and $2 \frac{d}{dy} k(y, y) = -c$. Integration of the second boundary condition yields $k(y, y) = -\frac{c}{2}y$. The solution to the gain kernel PDE in (4–11) can be obtained by converting the PDE into an integral equation and applying the method of successive approximations [35]. The solution to (4–11) is

$$k(y, x) = -cx \frac{I_1 \left(\sqrt{c(y^2 - x^2)} \right)}{\sqrt{c(y^2 - x^2)}},$$

where $I_\varepsilon(\mu) \in \mathbb{R}$ denotes a modified Bessel function defined as

$$I_\varepsilon(\mu) \triangleq \sum_{\tau=0}^{\infty} \frac{\left(\frac{\mu}{2}\right)^{\varepsilon+2\tau}}{\tau! (\tau + \varepsilon)!}.$$

The boundary condition at $y = l$ can then be expressed as

$$\begin{aligned}
GJ\Phi_y(l, t) + \eta_\phi GJ\Phi_{ty}(l, t) &= GJ\phi_y(l, t) + \eta_\phi GJ\phi_{ty}(l, t) \\
&- (GJ\phi(l, t) + \eta_\phi GJ\phi_t(l, t)) k(l, l) \\
&- GJ \int_0^l k_y(l, x) (\phi(x, t) + \eta_\phi \phi_t(x, t)) dx, \quad (4-12)
\end{aligned}$$

where $k(l, l) = -\frac{c}{2}l$ and

$$k_y(l, x) = \frac{-clxI_2\left(\sqrt{c(l^2 - x^2)}\right)}{(l^2 - x^2)}.$$

From the boundary condition of the target system, $GJ\Phi_y(l, t) + \eta_\phi GJ\Phi_{ty}(l, t) = 0$, the left-hand side of (4-12) is equal to zero. From (4-4), the first two terms on the right-hand side of (4-12) can be replaced with $-J_s\phi_{tt}(l, t) + M_{tip}$ yielding

$$0 = M_{tip} - J_s\phi_{tt}(l, t) - (GJ\phi(l, t) + \eta_\phi GJ\phi_t(l, t))k(l, l) - GJ \int_0^l k_y(l, x) (\phi(x, t) + \eta_\phi\phi_t(x, t)) dx,$$

which can be solved for the boundary control at the wing tip

$$M_{tip} = J_s\phi_{tt}(l, t) + (GJ\phi(l, t) + \eta_\phi GJ\phi_t(l, t))k(l, l) + GJ \int_0^l k_y(l, x) (\phi(x, t) + \eta_\phi\phi_t(x, t)) dx. \quad (4-13)$$

Due to the fact that the state transformation is invertible, stability of the target system in (4-6) translates to stability of the system in (4-2) with the boundary control in (4-13).

Remark 4.1. The modified Bessel function used in the solution for $k(x, y)$ is an infinite sum, which for implementation purposes must be approximated using a finite sum.

It can be shown using the ratio test [59] that $I_\varepsilon(\mu)$ converges for any ε and $\mu \in \mathbb{R}$.

Since $I_\varepsilon(\mu)$ converges, for any small arbitrary number $\Delta > 0$, there exists T such that $|I_\varepsilon(\mu; \tau_0) - I_\varepsilon(\mu)| \leq \Delta$ for all $\tau_0 \geq T$ and $\mu \in \mathbb{R}$, where $I_\varepsilon(\mu; \tau_0) \triangleq \sum_{\tau=0}^{\tau_0} \frac{(\frac{\mu}{2})^{\varepsilon+2\tau}}{\tau!(\tau+\varepsilon)!}$. For the particular system used in the subsequent simulation section, the input $\mu \in [0, \sqrt{5}]$ and for $T = 10$, $\Delta = 6.7 \times 10^{-16}$. Figure (4-1) shows a plot of $I_1(\mu; 10)$ and $I_1(\mu)$.

4.3 Boundary Control of Wing Bending

The control objective is to ensure the wing bending state $\omega(y, t)$ remains bounded and achieves a steady state profile. Based on the system dynamics and boundary conditions given in (4-1) and (4-3) along with the subsequent stability analysis, the

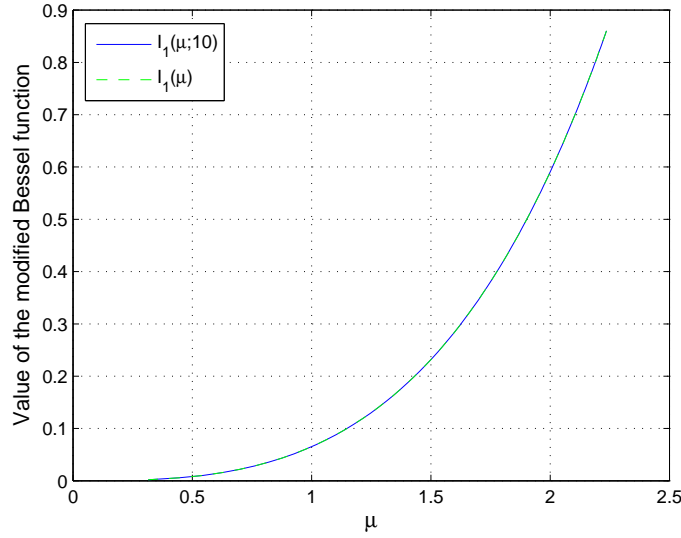


Figure 4-1. Approximation of the modified Bessel function used in the subsequent simulation section.

boundary control L_{tip} is designed as

$$L_{tip} = -\omega(l, t) - K\omega_t(l, t), \quad (4-14)$$

where $K \in \mathbb{R}$ is a positive constant control gain.

Theorem 4.1. *The boundary controllers given in (4-13) and (4-14) ensure that $\omega(y, t) \in \mathcal{L}_\infty$ and $\omega_t(y, t) \rightarrow 0$ as $t \rightarrow \infty$.*

Proof. To facilitate the subsequent stability analysis, let $c_1 \in \mathbb{R}$ be defined as $c_1 \triangleq$

$\sup_{y \in [0, l]} |\phi(y, 0)|$ and let $V_L(\sigma) : \mathbb{R}^4 \rightarrow \mathbb{R}$ be a positive-definite, continuously differentiable function defined as

$$V_L = \frac{1}{c_1^2 l} \left(\frac{1}{2} \int_0^l (\rho \omega_t^2 + EI \omega_{yy}^2) dy + \frac{1}{2} \omega^2(l, t) + \frac{m_s}{2} \omega_t^2(l, t) \right), \quad (4-15)$$

where $\sigma \in \mathbb{R}^4$ is defined as $\sigma \triangleq \left[\left(\int_0^l \omega_t^2 dy \right)^{1/2} \quad \left(\int_0^l \omega_{yy}^2 dy \right)^{1/2} \quad \omega(l, t) \quad \omega_t(l, t) \right]^T$. The

upper and lower bounds on V_L can be expressed as $\lambda_1 \|\sigma\|^2 \leq V_L \leq \lambda_2 \|\sigma\|^2$, where

$\lambda_1 \triangleq \min \left\{ \frac{\rho}{2c_1^2 l}, \frac{EI}{2c_1^2 l}, \frac{1}{2c_1^2 l}, \frac{m_s}{2c_1^2 l} \right\} \in \mathbb{R}$ and $\lambda_2 \triangleq \max \left\{ \frac{\rho}{2c_1^2 l}, \frac{EI}{2c_1^2 l}, \frac{1}{2c_1^2 l}, \frac{m_s}{2c_1^2 l} \right\} \in \mathbb{R}$. Taking the time

derivative of (4–15) yields

$$\dot{V}_L = \frac{1}{c_1^2 l} \left(\int_0^l \rho \omega_{tt} \omega_t dy + \int_0^l EI \omega_{yy} \omega_{t yy} dy + \omega(l, t) \omega_t(l, t) + \omega_t(l, t) m_s \omega_{tt}(l, t) \right). \quad (4-16)$$

Substituting the bending dynamics from (4–1) into the first integral of (4–16) results in

$$\begin{aligned} \dot{V}_L = & \frac{1}{c_1^2 l} \left(\int_0^l \omega_t (L_w \phi - EI \omega_{yyyy}) dy - \int_0^l \eta_\omega EI \omega_t \omega_{t yyy} dy + \int_0^l EI \omega_{yy} \omega_{t yy} dy \right) \\ & + \frac{1}{c_1^2 l} (\omega(l, t) \omega_t(l, t) + \omega_t(l, t) m_s \omega_{tt}(l, t)). \end{aligned}$$

Evaluating the second and third integral using integration by parts and applying the bending boundary conditions yields

$$- \int_0^l \eta_\omega EI \omega_t \omega_{t yyy} dy = -\eta_\omega EI \omega_t(l, t) \omega_{t yyy}(l, t) - \int_0^l \eta_\omega EI \omega_{t yy}^2 dy \quad (4-17)$$

$$\int_0^l EI \omega_{yy} \omega_{t yy} dy = -EI \omega_t(l, t) \omega_{yyy}(l, t) + \int_0^l EI \omega_t \omega_{yyy} dy. \quad (4-18)$$

After substituting (4–17) and (4–18) into (4–16) and canceling like terms, \dot{V}_L can be expressed as

$$\begin{aligned} \dot{V}_L = & \frac{1}{c_1^2 l} \left(\int_0^l \omega_t L_w \phi dy - \int_0^l \eta_\omega EI \omega_{t yy}^2 dy \right) \\ & + \frac{\omega_t(l, t)}{c_1^2 l} (\omega(l, t) + m_s \omega_{tt}(l, t) - \eta_\omega EI \omega_{t yy}(l, t) - EI \omega_{yyy}(l, t)). \end{aligned} \quad (4-19)$$

Using Lemmas A.12 and A.13 of [36], the two integrals in (4–19) can be bounded as

$$\int_0^l \omega_t L_w \phi dy \leq \frac{1}{\kappa} \int_0^l \omega_t^2 dy + \kappa \int_0^l L_w^2 \phi^2 dy, \quad (4-20)$$

$$- \int_0^l \eta_\omega EI \omega_{t yy}^2 dy \leq - \int_0^l \frac{\eta_\omega EI}{l^4} \omega_t^2 dy, \quad (4-21)$$

where $\delta \in \mathbb{R}$ is a positive constant. Substituting the boundary condition in (4–3), the inequalities in (4–20) and (4–21), and the control law in (4–14) into (4–19) yields

$$\dot{V}_L \leq -\frac{K}{c_1^2 l} \omega_t^2(l, t) - \frac{1}{c_1^2 l} \left(\frac{\eta_\omega EI}{l^4} - \frac{1}{\kappa} \right) \int_0^l \omega_t^2 dy + \frac{\kappa L_w^2}{c_1^2 l} \int_0^l \phi^2 dy. \quad (4-22)$$

To facilitate the stability analysis, let $z \triangleq \left[\omega_t(l, t) \left(\int_0^l \omega_t^2 dy \right)^{1/2} \right]^T \in \mathbb{R}^2$. The expression in (4–22) can be written as

$$\dot{V}_L \leq -\gamma(\|z\|) + \gamma(\zeta) \varphi(t), \quad (4-23)$$

where $\gamma(\|z\|) = \lambda_3 \|z\|^2$, $\lambda_3 \triangleq \min \left\{ \frac{K}{c_1^2 l}, \frac{1}{c_1^2 l} \left(\frac{\eta_\omega EI}{l^4} - \frac{1}{\kappa} \right) \right\}$, $\zeta = \sqrt{\frac{\kappa L_w^2}{\lambda_3}}$, and $\varphi(t) = \frac{1}{c_1^2 l} \int_0^l \phi^2 dy$. Since ϕ is exponentially stable, the function $\varphi \in \mathcal{L}_1$. Due to the selection of the constant c_1 , $|\varphi| \leq 1$. Corollary 2.18 from [60] can be applied to conclude that $\|\sigma\| \in \mathcal{L}_\infty$ and $\|z\| \rightarrow 0$ as $t \rightarrow \infty$; hence $|\omega(y, t)| \in \mathcal{L}_\infty$ and $|\omega_t(y, t)| \rightarrow 0$ as $t \rightarrow \infty$. \square

4.4 Numerical Simulation

A numerical simulation is presented to illustrate the performance of the developed controller. The simulations are performed using a Galerkin-based method to approximate the PDE system with a finite number of ODEs. It should be noted that the control design does not use the approximation, therefore the issue of spillover instabilities is avoided. The twisting and bending deflections are represented as a weighted sum of basis functions

$$\begin{aligned} \phi(y, t) &= a_0(t) h_0(y) + \sum_{i=1}^n a_i(t) h_i(y), \\ \omega(y, t) &= b_0(t) g_0(y) + \sum_{i=1}^p b_i(t) g_i(y), \end{aligned}$$

where n and $p \in \mathbb{R}$ denote the number of basis functions used in the approximations of the wing twisting deflection and bending deflection, respectively, and $h_0(y)$, $h_i(y)$, $g_0(y)$, and $g_i(y) \in \mathbb{R}$ are basis functions selected to satisfy the boundary conditions

$$\begin{aligned} h_0(0) = h_i(0) = 0, \quad h_{y_0}(l) = 1, \quad h_{y_i}(l) = 0, \\ g_0(0) = g_i(0) = 0, \quad g_{y_0}(0) = g_{y_i}(0) = 0, \\ g_{yy_0}(l) = g_{yy_i}(l) = 0, \quad g_{yyy_0}(l) = 1, \quad g_{yyy_i}(l) = 0. \end{aligned}$$

Substituting the approximations of the system states, the PDE system in (4-1) and (4-2) can be expressed as

$$\begin{aligned} & \rho \left(b_{tt_0}(t) g_0(y) + \sum_{i=1}^p b_{tt_i}(t) g_i(y) \right) + EI \left(b_0(t) g_{yyyy_0}(y) + \sum_{i=1}^p b_i(t) g_{yyyy_i}(y) \right) \\ & + \eta_w EI \left(b_{t_0}(t) g_{yyyy_0}(y) + \sum_{i=1}^p b_{t_i}(t) g_{yyyy_i}(y) \right) = \bar{L}_w \left(a_0(t) h_0(y) + \sum_{i=1}^n a_i(t) h_i(y) \right), \end{aligned} \quad (4-24)$$

$$\begin{aligned} & I_w \left(a_{tt_0}(t) h_0(y) + \sum_{i=1}^n a_{tt_i}(t) h_i(y) \right) - GJ \left(a_0(t) h_{yy_0}(y) + \sum_{i=1}^n a_i(t) h_{yy_i}(y) \right) \\ & - \eta_\phi GJ \left(a_{t_0}(t) h_{yy_0}(y) + \sum_{i=1}^n a_{t_i}(t) h_{yy_i}(y) \right) = \bar{M}_w \left(a_0(t) h_0(y) + \sum_{i=1}^n a_i(t) h_i(y) \right). \end{aligned} \quad (4-25)$$

Using Galerkin's method, (4-24) and (4-25) are converted to a set of ODEs as

$$B_1 \ddot{b}(t) + \eta_w B_2 \dot{b}(t) + B_2 b(t) - B_3 a(t) = 0, \quad (4-26)$$

$$I_w T_1 \ddot{a}(t) - \eta_\phi T_2 \dot{a}(t) - (T_2 + \bar{M}_w T_1) a(t) = 0, \quad (4-27)$$

where $b(t) \triangleq \begin{bmatrix} b_0(t) & b_1(t) & \dots & b_p(t) \end{bmatrix}^T$, $a(t) \triangleq \begin{bmatrix} a_0(t) & a_1(t) & \dots & a_n(t) \end{bmatrix}^T$, $B_1 \triangleq \rho \int_0^l g(y) g^T(y) dy$, $B_2 \triangleq EI \int_0^l g(y) g_{yyyy}^T(y) dy$, $B_3 \triangleq \bar{L}_w \int_0^l g(y) h^T(y) dy$, $T_1 \triangleq \int_0^l h(y) h^T(y) dy$, $T_2 \triangleq GJ \int_0^l h(y) h_{yy}^T(y) dy$, $g(y) \triangleq \begin{bmatrix} g_0(y) & g_1(y) & \dots & g_p(y) \end{bmatrix}^T$, and $h(y) \triangleq \begin{bmatrix} h_0(y) & h_1(y) & \dots & h_n(y) \end{bmatrix}^T$. The expressions in (4-26) and (4-27) are simulated to approximate the response of the PDE system.

The open-loop system was simulated with the following initial conditions: $\omega(y, 0) = 0$ m and $\phi(y, 0) = \frac{y^2}{2l^2}$ rad. It is evident from Figures (4-2) - (4-4) that the open-loop system, under the above initial conditions, experiences LCO behavior.

The control objective for the closed-loop system is to regulate the twisting and bending deformations of the flexible wing. Based on the transient performance of the

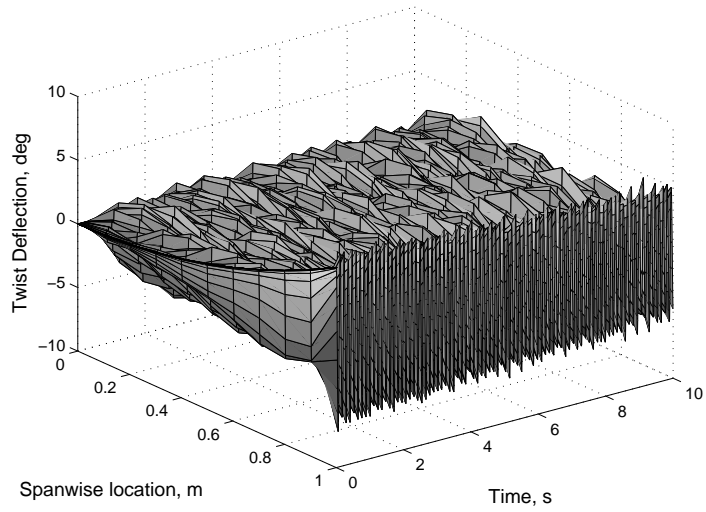


Figure 4-2. Open-loop twist deflection of the flexible aircraft wing.

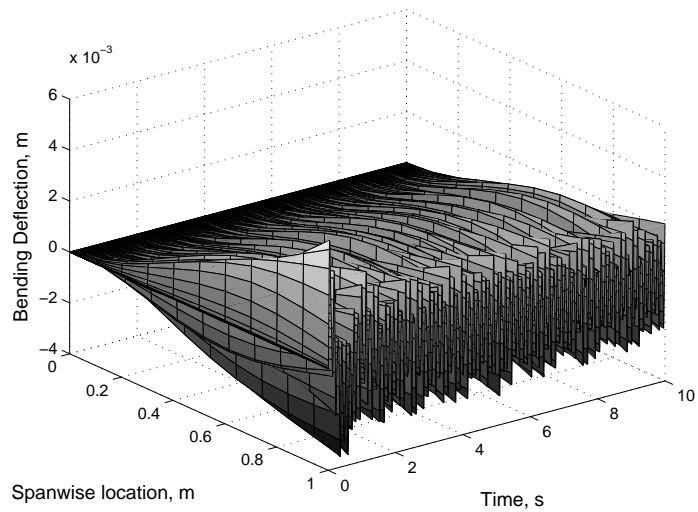


Figure 4-3. Open-loop bending deflection of the flexible aircraft wing.

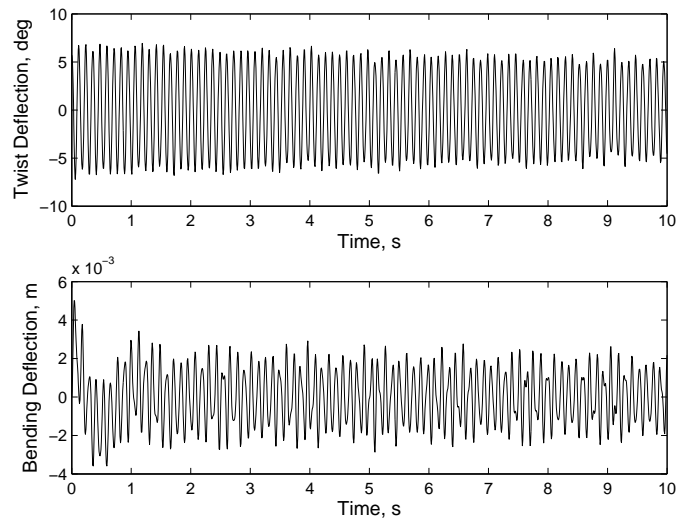


Figure 4-4. Open-loop response at the wing tip of the flexible aircraft wing.

closed-loop system, the control gains were selected as $c = 5$ and $k = 10$. The flexible state trajectories are shown in Figures (4-5) - (4-7). It is evident that the developed control strategy is capable of suppressing LCO behavior in the flexible aircraft wing. Figure (4-8) shows the force and moment commanded by the developed control strategy.

4.5 Summary

This chapter presents the construction of a boundary control strategy for suppressing LCO behavior in a flexible aircraft wing. The control design is separated into two parts: a backstepping-based control strategy used to design the aerodynamic moment at the wing tip and a Lyapunov-based controller for the aerodynamic lift at the wing tip. The developed control strategy ensures exponential regulation of the wing twist and asymptotic regulation of the wing bending to a steady-state profile. Numerical simulations illustrate the performance of the developed backstepping-based control design. One drawback of the developed controller is that it relies on the assumption that the distances from the wing elastic axis to the wing center of gravity and store center of gravity are zero. If this assumption is dropped, the PDE describing the dynamics of the

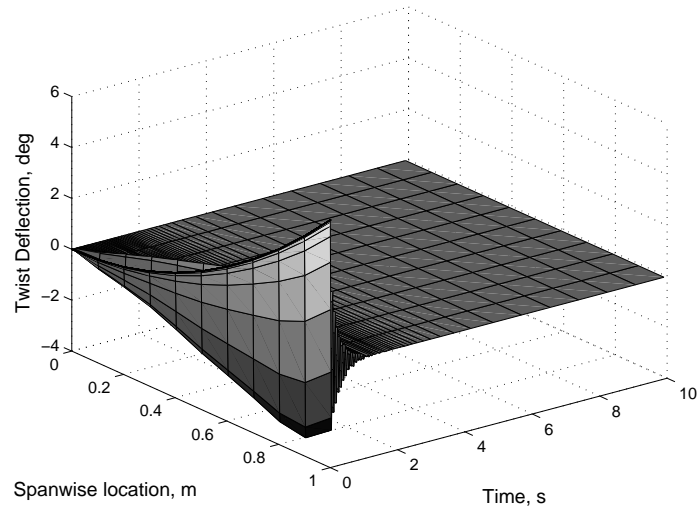


Figure 4-5. Closed-loop twist deflection of the flexible aircraft wing.

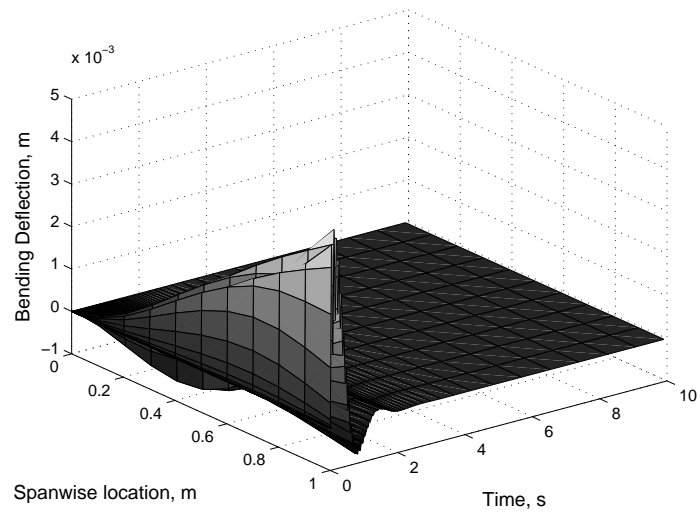


Figure 4-6. Closed-loop bending deflection of the flexible aircraft wing.

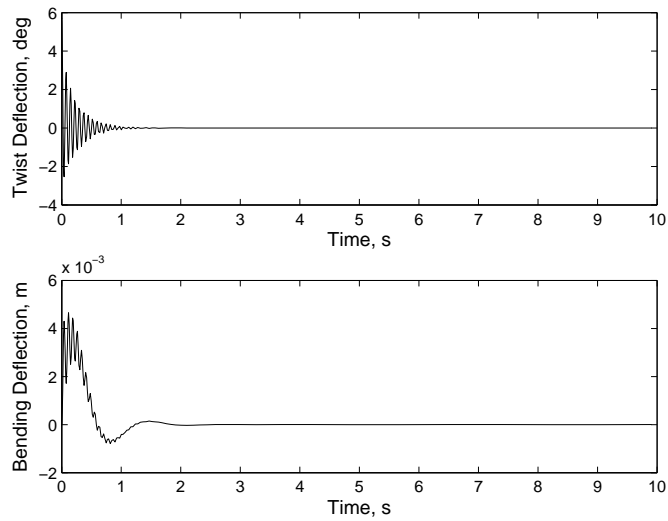


Figure 4-7. Closed-loop response at the wing tip of the flexible aircraft wing.

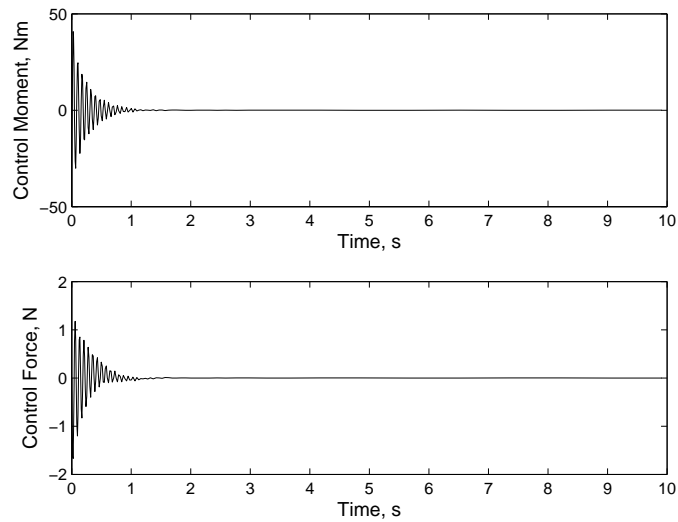


Figure 4-8. Lift and Moment commanded at the wing tip.

wing deformations becomes nonlinear which becomes a challenge for the backstepping strategy employed in this chapter. Instead, an approach similar to that of [36, 37], in which a Lyapunov-based analysis proves that the energy in the system decays to zero, could be used to generate the aerodynamic lift and moment at the wing tip. This strategy is considered in Chapter 5.

CHAPTER 5
ADAPTIVE BOUNDARY CONTROL OF LIMIT CYCLE OSCILLATIONS IN A FLEXIBLE
AIRCRAFT WING

The focus of this chapter is to develop an adaptive boundary control strategy for suppressing LCO motion in an aircraft wing whose dynamics are described by a system of nonlinear partial differential equations (PDEs). A Lyapunov-based stability analysis guarantees asymptotic regulation of the wing twist and bending dynamics.

5.1 Aircraft Wing Model

Consider a flexible wing of length $l \in \mathbb{R}$, mass per unit span of $\rho \in \mathbb{R}$, moment of inertia per unit length of $I_w \in \mathbb{R}$, and bending and torsional stiffnesses of $EI \in \mathbb{R}$ and $GJ \in \mathbb{R}$, respectively, with a store of mass $m_s \in \mathbb{R}$ and moment of inertia $J_s \in \mathbb{R}$ attached at the wing tip. The bending and twisting dynamics of the flexible wing are described by the following PDE system¹

$$\rho\omega_{tt} - \rho x_c c \sin(\phi) \phi_t^2 + \rho x_c c \cos(\phi) \phi_{tt} + EI\omega_{yyyy} = L_w, \quad (5-1)$$

$$(I_w + \rho x_c^2 c^2) \phi_{tt} + \rho x_c c \cos(\phi) \omega_{tt} - GJ\phi_{yy} = M_w, \quad (5-2)$$

where $\omega(y, t) \in \mathbb{R}$ and $\phi(y, t) \in \mathbb{R}$ denote the bending and twisting displacements, respectively, $y \in [0, l]$ denotes spanwise location on the wing, $x_c c \in \mathbb{R}$ represents the distance from the wing elastic axis to the wing center of gravity, and $L_w = \bar{L}_w \phi \in \mathbb{R}$ and $M_w = \bar{M}_w \phi \in \mathbb{R}$ denote the aerodynamic lift and moment on the wing, respectively, where \bar{L}_w and $\bar{M}_w \in \mathbb{R}$ denote aerodynamic lift and moment coefficients, respectively. In (5-1) and (5-2), the subscripts t and y denote partial derivatives. The boundary conditions for tip-based control are $\omega(0, t) = \omega_y(0, t) = \omega_{yy}(l, t) = \phi(0, t) = 0$ and

$$L_{tip} = m_s \omega_{tt}(l, t) - m_s x_s c \sin(\phi(l, t)) \phi_t^2(l, t) + m_s x_s c \cos(\phi(l, t)) \phi_{tt}(l, t)$$

¹ See Appendix F for details regarding the derivation of the dynamics.

$$-EI\omega_{yyy}(l, t), \quad (5-3)$$

$$M_{tip} = (m_s x_s^2 c^2 + J_s) \phi_{tt}(l, t) + m_s x_s c \cos(\phi(l, t)) \omega_{tt}(l, t) + GJ\phi_y(l, t), \quad (5-4)$$

where $L_{tip} \in \mathbb{R}$ and $M_{tip} \in \mathbb{R}$ denote the aerodynamic lift and moment at the wing tip and $x_s c \in \mathbb{R}$ represents the distance from the wing elastic axis to the store center of gravity.

It is assumed, based on Remark 5.1 in [36], that the system has the following properties

Property 1. If the potential energy of the system, $E_P \triangleq \frac{1}{2} \int_0^l (EI\omega_{yy}^2 + GJ\phi_y^2) dy \in \mathcal{L}_\infty$

$\forall t \in [0, \infty)$, then $\frac{\partial^n}{\partial y^n} \omega(y, t) \in \mathcal{L}_\infty$ and $\frac{\partial^m}{\partial y^m} \phi(y, t) \in \mathcal{L}_\infty$ for $n = 2, 3, 4$ and $m = 1, 2$

$\forall t \in [0, \infty)$ and $\forall y \in [0, l]$.

Property 2. If the kinetic energy of the system,

$$E_K \triangleq \frac{1}{2} \int_0^l (\rho\omega_t^2 + 2\rho x_s c \cos(\phi) \phi_t \omega_t + (I_w + \rho x_s^2 c^2) \phi_t^2) dy + \frac{1}{2} m_s \omega_t^2(l, t) + \frac{1}{2} J_s \phi_t^2(l, t),$$

is bounded $\forall t \in [0, \infty)$, then $\frac{\partial^q}{\partial t^q} \omega(y, t) \in \mathcal{L}_\infty$ and $\frac{\partial^q}{\partial t^q} \phi(y, t) \in \mathcal{L}_\infty$ for $q = 1, 2, 3$

$\forall t \in [0, \infty)$ and $\forall y \in [0, l]$.

5.2 Boundary Control Development

The control objective is to ensure the wing bending and twisting deformations are regulated in the sense that $\omega(y, t) \rightarrow 0$ and $\phi(y, t) \rightarrow 0$, $\forall y \in [0, l]$ as $t \rightarrow \infty$ via boundary control at the wing tip. To facilitate the subsequent stability analysis, let the auxiliary signal $e(t) \in \mathbb{R}^2$ and $\bar{M} \in \mathbb{R}^{2 \times 2}$ be defined as

$$e \triangleq \begin{bmatrix} \omega_t(l, t) - \omega_{yyy}(l, t) & \phi_t(l, t) + \phi_y(l, t) \end{bmatrix}^T, \quad (5-5)$$

$$\bar{M} \triangleq \begin{bmatrix} m_s & m_s x_s c \cos(\phi(l, t)) \\ m_s x_s c \cos(\phi(l, t)) & m_s x_s^2 c^2 + J_s \end{bmatrix}.$$

The open-loop dynamics of the auxiliary signal are obtained by multiplying the time derivative of e by \bar{M} to yield

$$\bar{M}\dot{e} = \begin{bmatrix} m_s\omega_{tt}(l, t) + m_s x_s c \cos(\phi(l, t)) \phi_{tt}(l, t) \\ m_s x_s c \cos(\phi(l, t)) \omega_{tt}(l, t) + (m_s x_s^2 c^2 + J_s) \phi_{tt}(l, t) \end{bmatrix} + \begin{bmatrix} m_s x_s c \cos(\phi(l, t)) \phi_{ty}(l, t) - m_s \omega_{tyyy}(l, t) \\ (m_s x_s^2 c^2 + J_s) \phi_{ty}(l, t) - m_s x_s c \cos(\phi(l, t)) \omega_{tyyy}(l, t) \end{bmatrix}. \quad (5-6)$$

Substituting the boundary conditions in (5-3) and (5-4) into (5-6) yields

$$\bar{M}\dot{e} = \begin{bmatrix} L_{tip} \\ M_{tip} \end{bmatrix} + \begin{bmatrix} m_s x_s c \sin(\phi(l, t)) \phi_t^2(l, t) + EI\omega_{yyy}(l, t) \\ (m_s x_s^2 c^2 + J_s) \phi_{ty}(l, t) - m_s x_s c \cos(\phi(l, t)) \omega_{tyyy}(l, t) \end{bmatrix} + \begin{bmatrix} -m_s \omega_{tyyy}(l, t) + m_s x_s c \cos(\phi(l, t)) \phi_{ty}(l, t) \\ -GJ\phi_y(l, t) \end{bmatrix}. \quad (5-7)$$

After some algebraic manipulation, (5-7) can be expressed as

$$\bar{M}\dot{e} = U - \frac{1}{2}\dot{\bar{M}}e + Y\theta, \quad (5-8)$$

where $U \triangleq \begin{bmatrix} L & M \end{bmatrix}^T \in \mathbb{R}^2$, $\theta \in \mathbb{R}^5$ is a vector of unknown parameters, and $Y \in \mathbb{R}^{2 \times 5}$ is a regression matrix of known quantities. Specifically, θ and Y are defined as

$$\theta \triangleq \begin{bmatrix} m_s x_s c & EI & m_s & GJ & (m_s x_s^2 c^2 + J_s) \end{bmatrix}^T, \quad Y \triangleq \begin{bmatrix} \frac{1}{2} \sin(\phi(l, t)) (\phi_t^2(l, t) - \phi_t(l, t) \phi_y(l, t)) + \cos(\phi(l, t)) \phi_{ty}(l, t) & \omega_{yyy}(l, t) \\ \frac{1}{2} \sin(\phi(l, t)) \phi_t(l, t) (\omega_{yyy}(l, t) - \omega_t(l, t)) - \cos(\phi(l, t)) \omega_{tyyy}(l, t) & 0 \\ -\omega_{tyyy}(l, t) & 0 & 0 \\ 0 & \phi_y(l, t) & \phi_{ty}(l, t) \end{bmatrix}.$$

Based on the open-loop dynamics in (5–8), the boundary control is designed as

$$U = -Ke - Y\hat{\theta}, \quad (5-9)$$

where $K \in \mathbb{R}$ is a positive constant control gain and $\hat{\theta} \in \mathbb{R}^5$ is a vector of estimates of the uncertain parameters in θ . The vector of parameter estimates $\hat{\theta}$ is updated according to the gradient update law defined as

$$\dot{\hat{\theta}} = \Gamma Y^T e, \quad (5-10)$$

where $\Gamma \in \mathbb{R}^{5 \times 5}$ is a positive constant control gain. Substituting (5–9) into (5–8) yields the following closed-loop dynamics

$$\bar{M}\dot{e} = -\frac{1}{2}\dot{M}e - Ke + Y\tilde{\theta}, \quad (5-11)$$

where $\tilde{\theta} \triangleq \theta - \hat{\theta}$.

5.3 Stability Analysis

To facilitate the subsequent stability analysis, let the auxiliary terms $E_T \in \mathbb{R}$ and $E_c \in \mathbb{R}$ be defined as

$$\begin{aligned} E_T \triangleq & \frac{1}{2} \int_0^l (\rho\omega_t^2 + 2\rho x_c c \cos(\phi) \phi_t \omega_t + (I_w + \rho x_c^2 c^2) \phi_t^2) dy \\ & + \frac{1}{2} \int_0^l (EI\omega_{yy}^2 + GJ\phi_y^2) dy, \end{aligned} \quad (5-12)$$

$$\begin{aligned} E_c \triangleq & \beta_1 \int_0^l \rho\omega_y y (\omega_t + x_c c \cos(\phi) \phi_t) dy \\ & + \beta_1 \int_0^l \phi_y y ((I_w + \rho x_c^2 c^2) \phi_t + \rho x_c c \cos(\phi) \omega_t) dy, \end{aligned} \quad (5-13)$$

where $\beta_1 \in \mathbb{R}$ is a positive weighting constant. The auxiliary term E_T is analogous to the energy in the wing, and E_c contains cross terms used to facilitate the stability analysis.

Using Young's Inequality, an upper bound on E_T can be expressed as

$$E_T \leq \frac{1}{2} \int_0^l ((\rho + \rho |x_c c|) \omega_t^2 + (I_w + \rho x_c^2 c^2 + \rho |x_c c|) \phi_t^2 + EI\omega_{yy}^2 + GJ\phi_y^2) dy$$

$$\leq \frac{1}{2} \max \{(\rho + \rho |x_c c|), (I_w + \rho x_c^2 c^2 + \rho |x_c c|), EI, GJ\} E_b,$$

where $E_b \in \mathbb{R}$ is defined as

$$E_b \triangleq \int_0^l (\omega_t^2 + \omega_{yy}^2 + \phi_t^2 + \phi_y^2) dy. \quad (5-14)$$

In a similar manner, E_T can be lower bounded as

$$E_T \geq \frac{1}{2} \min \{(\rho - \rho |x_c c|), (I_w + \rho x_c^2 c^2 - \rho |x_c c|), EI, GJ\} E_b. \quad (5-15)$$

Provided that $|x_c c| < 1$ and $I_w > \rho x_c^2 c^2 - \rho |x_c c|$, E_T will be non-negative.

Remark 5.1. The conditions $|x_c c| < 1$ and $I_w > \rho x_c^2 c^2 - \rho |x_c c|$ are engineering design considerations that ensure the store is mounted sufficiently close to the wing center of mass.

After using Young's Inequality, the cross term E_c can be upper bounded as

$$\begin{aligned} |E_c| &\leq \beta_1 \rho l (1 + |x_c c|) \int_0^l \omega_t^2 dy + \beta_1 \rho l (1 + |x_c c|) \int_0^l \omega_y^2 dy \\ &\quad + \beta_1 l (I_w + \rho x_c^2 c^2 + \rho |x_c c|) \int_0^l (\phi_t^2 + \phi_y^2) dy. \end{aligned} \quad (5-16)$$

Lemma A.12 in [36] can be applied to the second integral in (5-16) to yield

$$\begin{aligned} |E_c| &\leq \beta_1 \rho l (1 + |x_c c|) \int_0^l \omega_t^2 dy + \beta_1 \rho l^3 (1 + |x_c c|) \int_0^l \omega_{yy}^2 dy \\ &\quad + \beta_1 l (I_w + \rho x_c^2 c^2 + \rho |x_c c|) \int_0^l (\phi_t^2 + \phi_y^2) dy \\ &\leq \beta_1 l \max \{(\rho + \rho |x_c c|), l^2 (\rho + \rho |x_c c|), (I_w + \rho x_c^2 c^2 + \rho |x_c c|)\} E_b. \end{aligned} \quad (5-17)$$

From (5-17), E_c can be lower bounded as

$$E_c \geq -\beta_1 l \max \{(\rho + \rho |x_c c|), l^2 (\rho + \rho |x_c c|), (I_w + \rho x_c^2 c^2 + \rho |x_c c|)\} E_b. \quad (5-18)$$

From (5-15) and (5-18), if β_1 is selected as

$$\beta_1 < \frac{\min \{(\rho - \rho |x_c c|), (I_w + \rho x_c^2 c^2 - \rho |x_c c|), EI, GJ\}}{2l \max \{(\rho + \rho |x_c c|), l^2 (\rho + \rho |x_c c|), (I_w + \rho x_c^2 c^2 + \rho |x_c c|)\}},$$

then

$$\zeta_1 E_b \leq E_T + E_c \leq \zeta_2 E_b \quad (5-19)$$

where the constants ζ_1 and ζ_2 are defined as

$$\begin{aligned} \zeta_1 &\triangleq \frac{1}{2} \min \{ (\rho - \rho |x_c c|), (I_w + \rho x_c^2 c^2 - \rho |x_c c|), EI, GJ \} \\ &\quad - \beta_1 l \max \{ (\rho + \rho |x_c c|), l^2 (\rho + \rho |x_c c|), (I_w + \rho x_c^2 c^2 + \rho |x_c c|) \}, \\ \zeta_2 &\triangleq \frac{1}{2} \min \{ (\rho + \rho |x_c c|), (I_w + \rho x_c^2 c^2 + \rho |x_c c|), EI, GJ \} \\ &\quad + \beta_1 l \max \{ (\rho + \rho |x_c c|), l^2 (\rho + \rho |x_c c|), (I_w + \rho x_c^2 c^2 + \rho |x_c c|) \}. \end{aligned}$$

Remark 5.2. β_1 will be positive provided that the store is mounted sufficiently close to the wing center of mass, as mentioned in Remark 5.1. If β_1 is positive, then the constants ζ_1 and ζ_2 will also be positive.

Theorem 5.1. *The boundary control law in (5-9) along with the adaptive update law in (5-10) ensure the system states $\omega(y, t) \rightarrow 0$ and $\phi(y, t) \rightarrow 0$ as $t \rightarrow \infty$ provided the following sufficient gain conditions are satisfied:*

$$K > \frac{1}{2} \max \{ EI + \beta_1 EIl \}, \quad \beta_1 < 1, \quad \beta_1 \rho - \beta_1 \rho x_c c - \bar{L}_w > 0, \quad (5-20)$$

$$\frac{3EI}{2} - \frac{\bar{L}_w l^3}{2} > 0, \quad \beta_1 (I_w + \rho x_c^2 c^2) - \beta_1 \rho x_c c - \bar{M}_w > 0, \quad (5-21)$$

$$\beta_1 GJ - \beta_1 \bar{M}_w l^3 - \beta_1 \bar{M}_w l - \beta_1 \bar{L}_w l^3 - (\bar{M}_w + \bar{L}_w) l^2 > 0, \quad (5-22)$$

$$\beta_1 EIl + EI - \beta_1 \rho - \beta_1 \rho x_c c l > 0, \quad GJ - \beta_1 l (I_w + \rho x_c^2 c^2) - \beta_1 \rho x_c c l > 0. \quad (5-23)$$

Remark 5.3. The sufficient gain conditions in (5-20)-(5-23) can be satisfied by a combination of gain selection and engineering design consideration. Selection of the wing aerodynamic properties can be done to satisfy aircraft performance criteria (e.g., minimum takeoff distance, maximum range, etc.). The structural properties of the wing can then be selected to satisfy the sufficient conditions above. Increasing the stiffness and mass of the wing or mounting the store closer to the wing center of gravity will satisfy the sufficient conditions.

Proof. Let V_L be a positive-definite, continuously differentiable function defined as

$$V_L \triangleq E_T + E_c + \frac{1}{2}e^T \bar{M}e + \frac{1}{2}\tilde{\theta}^T \Gamma^{-1} \tilde{\theta}. \quad (5-24)$$

Based on (5-24) and the inequalities in (5-19), V_L can be bounded as

$$\zeta_1 E_b + \frac{\lambda_{\min}(\bar{M})}{2} \|e\|^2 + \frac{\lambda_{\min}(\Gamma^{-1})}{2} \|\tilde{\theta}\|^2 \leq V_L \leq \zeta_2 E_b + \frac{\lambda_{\max}(\bar{M})}{2} \|e\|^2 + \frac{\lambda_{\max}(\Gamma^{-1})}{2} \|\tilde{\theta}\|^2, \quad (5-25)$$

where $\lambda_{\min}(\xi)$ and $\lambda_{\max}(\xi)$ denote the minimum and maximum eigenvalue of ξ , respectively.

Differentiating (5-24) and substituting (5-10) and (5-11) into the resulting expression yields

$$\dot{V}_L = \dot{E}_T + \dot{E}_c - e^T K e. \quad (5-26)$$

In (5-26), \dot{E}_T is determined by differentiating (5-12) with respect to time to obtain

$$\begin{aligned} \dot{E}_T &= \int_0^l \omega_t (\rho \omega_{tt} + \rho x_c c \cos(\phi) \phi_{tt} - \rho x_c c \sin(\phi) \phi_t^2) dy + \int_0^l (EI \omega_{yy} \omega_{tyy} + GJ \phi_y \phi_{ty}) dy \\ &+ \int_0^l \phi_t ((I_w + \rho x_c^2 c^2) \phi_{tt} + \rho x_c c \cos(\phi) \omega_{tt}) dy. \end{aligned} \quad (5-27)$$

Substituting (5-1) and (5-2) into the first and third integrals of (5-27) yields

$$\begin{aligned} \dot{E}_T &= \int_0^l (\bar{L}_w \phi \omega_t + \bar{M}_w \phi \phi_t) dy - \int_0^l EI \omega_t \omega_{yyyy} dy + \int_0^l EI \omega_{yy} \omega_{tyy} dy + \int_0^l GJ \phi_t \phi_{yy} dy \\ &+ \int_0^l GJ \phi_y \phi_{ty} dy. \end{aligned} \quad (5-28)$$

Integrating by parts the third and fifth integrals in (5-28) and applying the boundary conditions of the PDE system results in

$$\int_0^l EI \omega_{yy} \omega_{tyy} dy = -EI \omega_{yyy}(l, t) \omega_t(l, t) + \int_0^l EI \omega_t \omega_{yyyy} dy, \quad (5-29)$$

$$\int_0^l GJ \phi_y \phi_{ty} dy = GJ \phi_y(l, t) \phi_t(l, t) - \int_0^l GJ \phi_t \phi_{yy} dy. \quad (5-30)$$

Using the expressions in (5–29) and (5–30), (5–28) can be rewritten as

$$\dot{E}_T = \int_0^l (\bar{L}_w \phi \omega_t + \bar{M}_w \phi \phi_t) dy - EI \omega_{yyy}(l, t) \omega_t(l, t) + GJ \phi_y(l, t) \phi_t(l, t). \quad (5-31)$$

Using the auxiliary signal definition in (5–5), (5–31) can be expressed as

$$\begin{aligned} \dot{E}_T = & \int_0^l (\bar{L}_w \phi \omega_t + \bar{M}_w \phi \phi_t) dy + e^T \begin{bmatrix} \frac{EI}{2} & 0 \\ 0 & \frac{GJ}{2} \end{bmatrix} e - \frac{EI}{2} \omega_t^2(l, t) - \frac{EI}{2} \omega_{yyy}^2(l, t) \\ & - \frac{GJ}{2} \phi_y^2(l, t) - \frac{GJ}{2} \phi_t^2(l, t). \end{aligned}$$

In (5–26), \dot{E}_c is determined by differentiating (5–13) with respect to time to yield

$$\begin{aligned} \dot{E}_c = & \beta_1 \int_0^l \omega_y y (\rho \omega_{tt} + \rho x_c c \cos(\phi) \phi_{tt} - \rho x_c c \sin(\phi) \phi_t^2) dy \\ & + \beta_1 \int_0^l \rho x_c c \cos(\phi) \phi_t \omega_{ty} y dy + \beta_1 \int_0^l \rho \omega_t \omega_{ty} y dy \\ & + \beta_1 \int_0^l \phi_y y ((I_w + \rho x_c^2 c^2) \phi_{tt} + \rho x_c c \cos(\phi) \omega_{tt} - \rho x_c c \sin(\phi) \phi_t \omega_t) dy \\ & + \beta_1 \int_0^l \phi_{ty} y ((I_w + \rho x_c^2 c^2) \phi_t + \rho x_c c \cos(\phi) \omega_t) dy. \end{aligned} \quad (5-32)$$

The expression for \dot{E}_c can be simplified by integrating the second integral as

$$\begin{aligned} \beta_1 \int_0^l \rho x_c c \cos(\phi) \phi_t \omega_{ty} y dy = & \beta_1 \rho x_c c l \cos(\phi(l, t)) \phi_t(l, t) \omega_t(l, t) \\ & - \beta_1 \int_0^l \rho x_c c \cos(\phi) \phi_t \omega_t dy \\ & + \beta_1 \int_0^l \rho x_c c \sin(\phi) \phi_y \phi_t \omega_t y dy \\ & - \beta_1 \int_0^l \rho x_c c \cos(\phi) \phi_{ty} \omega_t y dy. \end{aligned} \quad (5-33)$$

Substituting the expression in (5–33) and the system dynamics in (5–1) and (5–2) into (5–32) yields

$$\begin{aligned} \dot{E}_c = & \beta_1 \int_0^l (\bar{L}_w \phi - EI \omega_{yyy}) \omega_y y dy + \beta_1 \int_0^l \rho \omega_t \omega_{ty} y dy \\ & + \beta_1 \rho x_c c l \cos(\phi(l, t)) \phi_t(l, t) \omega_t(l, t) \end{aligned}$$

$$\begin{aligned}
& -\beta_1 \int_0^l \rho x_c c \cos(\phi) \phi_t \omega_t dy + \beta_1 \int_0^l (\bar{M}_w \phi + GJ \phi_{yy}) \phi_y dy \\
& + \beta_1 \int_0^l (I_w + \rho x_c^2 c^2) \phi_t \phi_{ty} dy. \tag{5-34}
\end{aligned}$$

After integrating by parts the terms $-\beta_1 \int_0^l EI \omega_{yyy} \omega_y dy$, $\beta_1 \int_0^l \rho \omega_t \omega_{ty} dy$,

$\beta_1 \int_0^l GJ \phi_{yy} \phi_y dy$, and $\beta_1 \int_0^l (I_w + \rho x_c^2 c^2) \phi_t \phi_{ty} dy$ from (5-34)², \dot{E}_c can be expressed as

$$\begin{aligned}
\dot{E}_c = & \beta_1 \int_0^l (\bar{L}_w \phi \omega_y + \bar{M}_w \phi \phi_y) dy - \beta_1 EI l \omega_{yyy}(l, t) \omega_y(l, t) - \frac{3}{2} \beta_1 EI \int_0^l \omega_{yy}^2 dy \\
& + \frac{1}{2} \beta_1 \rho \omega_t^2(l, t) - \frac{1}{2} \beta_1 \rho \int_0^l \omega_t^2 dy - \beta_1 \rho x_c c \int_0^l \cos(\phi) \phi_t \omega_t dy \\
& + \beta_1 \rho x_c c l \cos(\phi(l, t)) \phi_t(l, t) \omega_t(l, t) + \frac{1}{2} \beta_1 GJ \phi_y^2(l, t) \\
& - \frac{1}{2} \beta_1 GJ \int_0^l \phi_y^2 dy + \frac{1}{2} \beta_1 l (I_w + \rho x_c^2 c^2) \phi_t^2(l, t) - \frac{1}{2} \beta_1 (I_w + \rho x_c^2 c^2) \int_0^l \phi_t^2 dy.
\end{aligned}$$

Using Young's Inequality and Lemma A.12 from [36], \dot{E}_c can be upper bounded as

$$\begin{aligned}
\dot{E}_c \leq & -(1 - x_c c) \frac{\beta_1 \rho}{2} \int_0^l \omega_t^2 dy - \left(\frac{3EI}{2} - \frac{\bar{L}_w l^3}{2} \right) \beta_1 \int_0^l \omega_{yy}^2 dy \\
& - ((I_w + \rho x_c^2 c^2) - \rho x_c c) \frac{\beta_1}{2} \int_0^l \phi_t^2 dy + \frac{1}{2} \beta_1 \rho \omega_t^2(l, t) \\
& - (GJ - \bar{M}_w l^3 - \bar{M}_w l - \bar{L}_w l^3) \frac{\beta_1}{2} \int_0^l \phi_y^2 dy - \beta_1 EI l \omega_{yyy}(l, t) \omega_y(l, t) \\
& + \beta_1 \rho x_c c l \phi_t(l, t) \omega_t(l, t) + \frac{1}{2} \beta_1 GJ \phi_y^2(l, t) + \frac{1}{2} \beta_1 l (I_w + \rho x_c^2 c^2) \phi_t^2(l, t). \tag{5-35}
\end{aligned}$$

Using (5-5), $-\beta_1 EI l \omega_{yyy}(l, t) \omega_y(l, t)$ can be expressed as

$$-\beta_1 EI l \omega_{yyy}(l, t) \omega_y(l, t) = -\frac{\beta_1 EI l}{2} \omega_{yyy}^2(l, t) - \frac{\beta_1 EI l}{2} \omega_t^2(l, t) + \frac{\beta_1 EI l}{2} e_1^2, \tag{5-36}$$

where e_1 denotes the first element of the vector e , (i.e., $e_1 \triangleq \omega_t(l, t) - \omega_{yyy}(l, t)$). Using

(5-36), (5-35) can be rewritten as

$$\dot{E}_c \leq -(1 - x_c c) \frac{\beta_1 \rho}{2} \int_0^l \omega_t^2 dy - \left(\frac{3EI}{2} - \frac{\bar{L}_w l^3}{2} \right) \beta_1 \int_0^l \omega_{yy}^2 dy$$

² See Appendix H

$$\begin{aligned}
& - \left((I_w + \rho x_c^2 c^2) - \rho x_c c \right) \frac{\beta_1}{2} \int_0^l \phi_t^2 dy + \frac{\beta_1 EI l}{2} e_1^2 + \frac{1}{2} \beta_1 l (I_w + \rho x_c^2 c^2) \phi_t^2(l, t) \\
& - (GJ - \bar{M}_w l^3 - \bar{M}_w l - \bar{L}_w l^3) \frac{\beta_1}{2} \int_0^l \phi_y^2 dy - \frac{\beta_1 EI l}{2} \omega_{yyy}^2(l, t) - \frac{\beta_1 EI l}{2} \omega_y^2(l, t) \\
& + \frac{1}{2} \beta_1 \rho \omega_t^2(l, t) + \beta_1 \rho x_c c l \phi_t(l, t) \omega_t(l, t) + \frac{1}{2} \beta_1 GJ \phi_y^2(l, t). \tag{5-37}
\end{aligned}$$

Inserting (5-31) and (5-37) into (5-26) and using Young's inequality yields

$$\begin{aligned}
\dot{V}_L \leq & -\frac{1}{2} (\beta_1 \rho - \beta_1 \rho x_c c - \bar{L}_w) \int_0^l \omega_t^2 dy - \left(\frac{3EI}{2} - \frac{\bar{L}_w l^3}{2} \right) \beta_1 \int_0^l \omega_{yy}^2 dy \\
& - \frac{1}{2} (\beta_1 (I_w + \rho x_c^2 c^2) - \beta_1 \rho x_c c - \bar{M}_w) \int_0^l \phi_t^2 dy \\
& - \frac{1}{2} (\beta_1 GJ - \beta_1 \bar{M}_w l^3 - \beta_1 \bar{M}_w l - \beta_1 \bar{L}_w l^3 - (\bar{M}_w + \bar{L}_w) l^2) \int_0^l \phi_y^2 dy \\
& - \frac{1}{2} (\beta_1 EI l + EI - \beta_1 \rho - \beta_1 \rho x_c c l) \omega_t^2(l, t) \\
& - \frac{1}{2} (GJ - \beta_1 l (I_w + \rho x_c^2 c^2) - \beta_1 \rho x_c c l) \phi_t^2(l, t) - \frac{1}{2} (\beta_1 EI l + EI) \omega_{yyy}^2(l, t) \\
& - \frac{1}{2} (GJ - \beta_1 GJ) \phi_y^2(l, t) - \left(K - \frac{1}{2} \max \{ EI + \beta_1 EI l, GJ \} \right) \|e\|^2. \tag{5-38}
\end{aligned}$$

Provided the sufficient conditions in (5-20)-(5-23) are satisfied, (5-38) can be expressed as

$$\dot{V}_L \leq -\lambda_1 E_b(t) - \lambda_2 e^2(t), \tag{5-39}$$

where $\lambda_1 \in \mathbb{R}$ and $\lambda_2 \in \mathbb{R}$ are positive constants defined as

$$\begin{aligned}
\lambda_1 & \triangleq \frac{1}{2} \min \left\{ \beta_1 \rho - \beta_1 \rho x_c c - \bar{L}_w, \frac{3EI}{2} - \frac{\bar{L}_w l^3}{2}, \beta_1 (I_w + \rho x_c^2 c^2) - \beta_1 \rho x_c c - \bar{M}_w \right. \\
& \quad \left. \beta_1 GJ - \beta_1 \bar{M}_w l^3 - \beta_1 \bar{M}_w l - \beta_1 \bar{L}_w l^3 - (\bar{M}_w + \bar{L}_w) l^2 \right\}, \\
\lambda_2 & \triangleq K - \frac{1}{2} \max \{ EI + \beta_1 EI l, GJ \}.
\end{aligned}$$

It can be concluded from (5-24) and (5-39) that $V_L \in \mathcal{L}_\infty$; hence $E_b \in \mathcal{L}_\infty$, $e \in \mathcal{L}_\infty$, and $\tilde{\theta} \in \mathcal{L}_\infty$. Since $E_b \in \mathcal{L}_\infty$, it can be concluded that $\int_0^l \omega_{yy}^2 dy \in \mathcal{L}_\infty$ and $\int_0^l \phi_y^2 dy \in \mathcal{L}_\infty$; hence the elastic potential energy in the wing $E_P \in \mathcal{L}_\infty$ and by Property 1 $\omega_{yyy}(l, t) \in \mathcal{L}_\infty$ and $\phi_y(l, t) \in \mathcal{L}_\infty$. Since $e \in \mathcal{L}_\infty$, $\omega_{yyy}(l, t) \in \mathcal{L}_\infty$, and $\phi_y(l, t) \in \mathcal{L}_\infty$, (5-5) can be

used to show $\omega_t(l, t) \in \mathcal{L}_\infty$ and $\phi_t(l, t) \in \mathcal{L}_\infty$. Since $\omega_t(l, t) \in \mathcal{L}_\infty$, $\phi_t(l, t) \in \mathcal{L}_\infty$, and $E_b \in \mathcal{L}_\infty$, the kinetic energy of the system $E_K \in \mathcal{L}_\infty$ and by Property 2, $\frac{\partial^q}{\partial t^q} \omega(y, t) \in \mathcal{L}_\infty$ and $\frac{\partial^q}{\partial t^q} \phi(y, t) \in \mathcal{L}_\infty$ for $q = 1, 2, 3$. Equations (5–3) and (5–4) can be used to show that the boundary control input, $U \in \mathcal{L}_\infty$. Differentiating $g(t)$ from (5–39) with respect to time yields

$$\dot{g} = \lambda_1 \dot{E}_b + 2\lambda_2 e \dot{e}, \quad (5-40)$$

where

$$\dot{E}_b = 2 \int_0^l (\omega_t \omega_{tt} + \omega_{yy} \omega_{t yy} + \phi_t \phi_{tt} + \phi_{ty} \phi_y) dy. \quad (5-41)$$

After integrating by parts the second and fourth terms in (5–41), \dot{E}_b can be expressed as

$$\dot{E}_b = 2 \int_0^l (\omega_t (\omega_{tt} + \omega_{yyyy}) + \phi_t (\phi_{tt} - \phi_{yy})) dy - 2\omega_t(l, t) \omega_{yyy}(l, t) + 2\phi_t(l, t) \phi_y(l, t). \quad (5-42)$$

Since $\omega_t(y, t)$, $\omega_{tt}(y, t)$, $\omega_{yyyy}(y, t)$, $\phi_t(y, t)$, $\phi_{tt}(y, t)$, $\phi_{yy}(y, t)$, $\omega_t(l, t)$, $\omega_{yyy}(l, t)$, $\phi_t(l, t)$, and $\phi_y(l, t) \in \mathcal{L}_\infty$ (from Properties 1 and 2), (5–42) can be used to conclude that $\dot{E}_b \in \mathcal{L}_\infty$. Equations (5–11) and (5–40) can be used to show that $\dot{g} \in \mathcal{L}_\infty$. Lemma A.6 from [36] can be applied to (5–39) to conclude $\lim_{t \rightarrow \infty} g(t) = 0$ and hence

$$\lim_{t \rightarrow \infty} E_b(t), e(t) = 0.$$

Using (5–14) and Lemma A.12 in [36] the following inequalities can be developed

$$E_b \geq \int_0^l \omega_{yy}^2 dy \geq \frac{1}{l^3} \omega^2(y, t) \geq 0, \quad (5-43)$$

$$E_b \geq \int_0^l \phi_y^2 dy \geq \frac{1}{l} \phi^2(y, t) \geq 0. \quad (5-44)$$

Since $E_b \rightarrow 0$ as $t \rightarrow \infty$, it can be concluded from (5–43) and (5–44) that $\omega(y, t) \rightarrow 0$ and $\phi(y, t) \rightarrow 0$ as $t \rightarrow \infty$. □

5.4 Summary

This chapter presents the construction of a boundary control strategy for suppressing LCO behavior in an uncertain flexible aircraft wing. The boundary control strategy retains the full PDE system, thereby avoiding potential spillover instabilities, and ensures asymptotic regulation of the distributed states in the presence of parametric uncertainties. A potential drawback to the developed method is the need for measurements of high-order spatial derivatives of the distributed states (e.g., $\omega_{yyy}(l, t)$).

CHAPTER 6 CONCLUSION AND FUTURE WORK

6.1 Dissertation Summary

The focus of this work is to develop control methods for the suppression of limit cycle oscillations (LCO) in aircraft systems. The driving mechanism behind LCO behavior remains unknown; however, the behavior is prevalent on the current generation of fighter aircraft and is expected to persist on next generation aircraft. The major concerns associated with LCO behavior are its impact on the safe release of ordnance and the ability of the pilot to perform necessary mission-related tasks.

Chapter 2 focuses on the development of an adaptive control strategy to suppress LCO behavior in an uncertain two degree of freedom airfoil section. The developed controller features a neural network (NN) feedforward term to compensate for uncertainties in the airfoil dynamics and a robust integral of the sign of the error (RISE) feedback term to ensure asymptotic tracking of the airfoil angle of attack. The simulation results of Chapter 2, as seen in previous RISE-based control strategies, indicate that the RISE-based controller can demand a large control effort in response to large initial offsets or large disturbances. In Chapter 3, a saturated RISE-based controller is developed in which the RISE control structure is embedded in smooth hyperbolic functions to ensure actuator constraints are not breached while maintaining asymptotic tracking with a continuous controller. The actuator limit is known *a priori* and can be adjusted via changing the control gains.

Chapters 4 and 5 focus on the development of partial differential equation (PDE)-based boundary control methods for the suppression of LCO behavior in a flexible aircraft wing. Chapter 4 uses a PDE-based backstepping method to transform a linear PDE system describing the dynamics of the distributed states to an exponentially stable linear PDE system. Chapter 5 develops a boundary control strategy that uses a gradient-based adaptive update law to compensate for linear-in-the-parameters (LP)

uncertainties and a Lyapunov-based analysis to show that the energy in the system remains bounded and asymptotically decays to zero. The differences between the two PDE-based control strategies are the type of system used in the design and the required measurements for implementation. The strategy in Chapter 4 is designed for a linear PDE model of the flexible aircraft wing and uses measurements of the flexible states across the entire wing span. The controller in Chapter 5 is designed for a nonlinear PDE model and requires measurements of the higher spatial derivatives of the flexible states at the actuator location (e.g., $\omega_{yyy}(l, t)$).

6.2 Limitations and Future Work

The work in this dissertation develops new robust and adaptive controllers for the suppression of LCO behavior in aircraft systems. In this section, open problems related to the work in this dissertation are discussed.

From Chapter 2:

1. A practical limitation in the developed RISE-based control strategy is that as the severity of the LCO behavior increases, the developed controller can demand a large control surface deflection. Additionally, the Monte Carlo simulation results indicated that the maximum control effort is sensitive to variations in the parameter uncertainties, which could lead to unexpected actuator saturation. This limitation is addressed in Chapter 3.

From Chapter 3:

1. A potential drawback of the saturated RISE-based control strategy is that under certain conditions, the LCO produced could be too severe resulting in sufficient gain conditions that can't be satisfied. This is a direct result of the actuator limit; increasing the actuator limit relaxes the sufficient gain conditions. Furthermore, an adaptive feedforward term could potentially be included to compensate for the uncertain dynamics, thereby relaxing the sufficient gain conditions. However, for any controller that has restricted control authority, it is possible for some

disturbance to dominate the controller's ability to yield a desired or even stable performance.

From Chapter 4:

1. One drawback of the developed PDE-based backstepping controller is that it relies on the assumption that the distances from the wing elastic axis to the wing center of gravity and store center of gravity are zero. Without this assumption, the PDE describing the dynamics of the wing deformations becomes nonlinear which does not facilitate the use of the backstepping strategy employed in this chapter. Instead, an approach similar to that of [36,37], in which a Lyapunov-based analysis proves that the energy in the system decays to zero, could be used to generate the aerodynamic lift and moment at the wing tip. Chapter 5 addresses this limitation.
2. Due to the lack of clarity amongst researchers as to the driving mechanism behind LCO, a common practice in literature, and in the work of Chapters 2 and 3, is to replicate the symptoms of LCO behavior by including nonlinearities in the wing structure. In most cases, this is a nonlinear torsional stiffness. The control strategies in Chapters 2 and 3 provide a framework that can be readily adapted to compensate for the driving mechanism as it becomes better understood. However, due to the structure of the PDE-based backstepping method, if the driving mechanism is nonlinear, its incorporation into the developed control structure may not be feasible, and a method similar to [36, 37] must be employed.

From Chapter 5:

1. Since the controller in Chapter 5 was developed for a nonlinear PDE, it can be adapted more readily to compensate for the inclusion of the driving mechanism behind LCO behavior. The control structure will require small changes, mostly to the sufficient gain conditions to include the influence of the uncertainties associated with the driving mechanism; however, more complex systems typically require more complex candidate Lyapunov functions (i.e., the definition for E_c

will change to account for cross-terms associated with the model of the driving mechanism).

2. A potential drawback to the developed method is the need for measurements of high-order spatial derivatives of the distributed states (e.g., $\omega_{yyy}(l, t)$). A shear sensor attached at the wingtip can be used to measure $\omega_{yyy}(l, t)$ and torque measurements at the wingtip can be used to determine $\phi_y(l, t)$. Future efforts are focused on developing PDE-based output feedback boundary control strategies that would eliminate the need for high-order spatial derivative measurements.

APPENDIX A
PROOF THAT M IS INVERTIBLE (CH 3)

Lemma A.1. M , given by the expressions in (2-2) and (2-4)-(2-6), is invertible.

To show that M is invertible, it is necessary to show that $\det(M) \neq 0$. The $\det(M)$ can be expressed as $\det(M) = m_1 m_4 - m_2^2$ where $m_1, m_2, m_4 \in \mathbb{R}$ are defined in (2-4)-(2-6). Since $\det(M)$ appears in g , which is used in the Lyapunov function, the following condition is desirable

$$m_1 m_4 - |m_2|^2 > 0. \quad (\text{A-1})$$

From (2-5), m_2 can be written as $m_2 = p \cos(\alpha) - l \sin(\alpha)$, where $p = (r_x - a) m_w b + (s_x - a) m_s b \in \mathbb{R}$ and $l = (s_h - a_h) m_s b + (r_h - a_h) m_w b \in \mathbb{R}$. The maximum value of m_2 can be expressed as $|m_2| \leq \sqrt{p^2 + l^2}$. Substituting for the values of p and l , $|m_2|^2$ can be expressed as

$$\begin{aligned} |m_2|^2 &\leq (r_x - a)^2 b^2 m_w^2 + 2(r_x - a)(s_x - a) b^2 m_s m_w \\ &\quad + 2(s_h - a_h)(r_h - a_h) b^2 m_w m_s + (r_h - a_h)^2 b^2 m_w^2 \\ &\quad + (s_x - a)^2 b^2 m_s^2 + (s_h - a_h)^2 b^2 m_s^2. \end{aligned} \quad (\text{A-2})$$

Using (2-4) and (2-6), $m_1 m_4$ can be expressed as

$$\begin{aligned} m_1 m_4 &= (r_x - a)^2 b^2 m_w^2 + (r_x - a)^2 b^2 m_w m_s \\ &\quad + (r_h - a_h)^2 b^2 m_w^2 + (r_h - a_h)^2 b^2 m_w m_s \\ &\quad + (s_x - a)^2 b^2 m_s m_w + (s_h - a_h)^2 b^2 m_s m_w \\ &\quad + (s_x - a)^2 b^2 m_s^2 + (s_h - a_h)^2 b^2 m_s^2 \\ &\quad + (I_w + I_s)(m_w + m_s). \end{aligned} \quad (\text{A-3})$$

Evaluating the $\det(M)$ using (A-2) and (A-3) yields

$$\begin{aligned} \det(M) &\geq [(r_x - a)^2 - 2(r_x - a)(s_x - a)] b^2 m_w m_s \\ &\quad + [(s_h - a_h)^2 + (s_x - a)^2] b^2 m_w m_s \end{aligned}$$

$$\begin{aligned}
& + [(r_h - a_h)^2 - 2(r_h - a_h)(s_h - a_h)] b^2 m_w m_s \\
& + (I_w + I_s)(m_s + m_w). \tag{A-4}
\end{aligned}$$

After some algebraic manipulation, the expression in (A-4) can be rewritten as

$$\begin{aligned}
\det(M) & \geq [(r_x - a) - (s_x - a)]^2 b^2 m_w m_s \\
& + [(r_h - a_h) - (s_h - a_h)]^2 b^2 m_w m_s \\
& + (I_w + I_s)(m_s + m_w). \tag{A-5}
\end{aligned}$$

Since the first two terms in (A-5) and the mass and moment of inertia of the wing and store are always positive, $\det(M) > 0$; hence M^{-1} is invertible.

APPENDIX B
PROOF OF $g > 0$ (CH 3)

Lemma B.1. *Given the expression in (2–16), $g > 0$ if the following condition is satisfied*

$$\frac{m_1 C_{m_\delta}}{C_{l_\delta}} > \varsigma \quad (\text{B-1})$$

To prove that g must be strictly greater than zero, (2–16) is used to write g as $g = \frac{1}{\det(M)} [m_2 C_{l_\delta} + m_1 C_{m_\delta}]$. Using the results of Appendix A, $\frac{1}{\det(M)} > 0$. Therefore, for $g > 0$, the term $[m_2 C_{l_\delta} + m_1 C_{m_\delta}]$ must be positive. From (2–5), m_2 is sign indefinite so for $[m_2 C_{l_\delta} + m_1 C_{m_\delta}]$ to remain positive, $m_1 C_{m_\delta} > m_2 C_{l_\delta}$. From (2–5), m_2 can be upper bounded as $|m_2| \leq \varsigma$, where $\varsigma \in \mathbb{R}$ is a known positive constant. From (2–16) and the upper bound on m_2 , $g > 0$ provided that $\frac{m_1 C_{m_\delta}}{C_{l_\delta}} > \varsigma$. This sufficient condition can be satisfied by adjusting the geometry of the wing-store system. For example, the left-hand side can be increased by increasing the control surface effectiveness ratio $\frac{C_{m_\delta}}{C_{l_\delta}}$, which can be done by changing the wing airfoil. The constant ς can be made smaller by decreasing the distance between the wing elastic axis and the store center of gravity.

APPENDIX C
GROUPING OF TERMS IN $\dot{\chi}_1$ AND $\dot{\chi}_2$ (CH 3)

From (2-17), the auxiliary function $\chi \in \mathbb{R}$ is defined as

$$\chi \triangleq \frac{1}{g}f - \frac{1}{g_d}f_d = \chi_1 + \chi_2,$$

where $\chi_1 \in \mathbb{R}$ contains all terms in χ whose time derivative is bounded by the norm of the states and $\chi_2 \in \mathbb{R}$ contains all terms whose time derivative is bounded by a constant. The auxiliary functions χ_1 and χ_2 are explicitly defined as

$$\begin{aligned} \chi_1 &= \frac{\det(M)}{(m_1 C_{m_\delta} + m_2 C_{l_\delta})} (\gamma_1 \dot{e}_1 + \gamma_2 e_2) \\ \chi_2 &= \frac{m_2 \left(\tilde{C}_{11} \dot{h} + \tilde{C}_{12} \dot{\alpha} + \tilde{K}_{11} h + \tilde{K}_{12} \alpha \right)}{(m_1 C_{m_\delta} + m_2 C_{l_\delta})} - \frac{m_1 \left(\tilde{C}_{21} \dot{h} + \tilde{C}_{22} \dot{\alpha} + \tilde{K}_{22} \alpha \right)}{(m_1 C_{m_\delta} + m_2 C_{l_\delta})} \\ &\quad - \frac{\det(M) \ddot{\alpha}_d}{(m_1 C_{m_\delta} + m_2 C_{l_\delta})}. \end{aligned}$$

APPENDIX D
DEVELOPMENT OF THE BOUND ON \tilde{N} (CH 3)

Recall from (2–32), the auxiliary function \tilde{N} is defined as

$$\begin{aligned} \tilde{N} \triangleq & -\frac{1}{2} \frac{d}{dt} \left(\frac{1}{g} \right) r + \dot{\chi}_1 + e_2 - \text{proj} \left(\Gamma_1 \hat{\sigma}' \hat{V}^T \dot{x}_d e_2 \right)^T \hat{\sigma} \\ & - \hat{W}^T \hat{\sigma}' \text{proj} \left(\Gamma_2 \dot{x}_d \left(\hat{\sigma}'^T \hat{W} e_2 \right)^T \right)^T x_d. \end{aligned} \quad (\text{D-1})$$

From the assumption on the desired trajectories and (2–23) and (2–24), the last two terms in \tilde{N} can be upper bounded as

$$\begin{aligned} \left| \text{proj} \left(\Gamma_1 \hat{\sigma}' \hat{V}^T \dot{x}_d e_2 \right)^T \hat{\sigma} \right| & \leq c_1 |e_2| \leq c_1 \|z\| \\ \left| \hat{W}^T \hat{\sigma}' \text{proj} \left(\Gamma_2 \dot{x}_d \left(\hat{\sigma}'^T \hat{W} e_2 \right)^T \right)^T x_d \right| & \leq c_2 |e_2| \leq c_2 \|z\|, \end{aligned}$$

where $c_1, c_2 \in \mathbb{R}$ are known positive constants. Taking the time derivative of χ_1 , defined in Appendix C, yields

$$\begin{aligned} \dot{\chi}_1 = & \left(\frac{\frac{d}{dt} (\det(M))}{(m_1 C_{m_\delta} + m_2 C_{l_\delta})} - \frac{\det(M) (\dot{m}_2 C_{l_\delta})}{(m_1 C_{m_\delta} + m_2 C_{l_\delta})^2} \right) (\gamma_1 \dot{e}_1 + \gamma_2 e_2) \\ & + \frac{\det(M)}{(m_1 C_{m_\delta} + m_2 C_{l_\delta})} (\gamma_1 \ddot{e}_1 + \gamma_2 \dot{e}_2). \end{aligned}$$

From Appendix B and the expression for $\det(M)$ in Appendix A, the terms $(m_1 C_{m_\delta} + m_2 C_{l_\delta})$ and $(m_1 C_{m_\delta} + m_2 C_{l_\delta})^2$ are bounded below by a constant while $\det(M)$ is upper bounded by a constant. Taking the time derivative of $\det(M)$ yields

$$\begin{aligned} \frac{d}{dt} (\det(M)) & = -2m_2 \dot{m}_2 \\ & = 2m_2 m_w b \dot{\alpha} (r_h - a_h) \cos(\alpha) + 2m_2 m_w b \dot{\alpha} (r_x - a) \sin(\alpha) \\ & \quad + 2m_2 m_s b \dot{\alpha} (s_h - a_h) \cos(\alpha) + 2m_2 m_s b \dot{\alpha} (s_h - a) \sin(\alpha). \end{aligned}$$

Since $\|\dot{q}\| \leq \kappa_2$ and using the result in Appendix B, $\frac{d}{dt} (\det(M)) \leq c_3$, where $c_3 \in \mathbb{R}$ is a known positive constant.

The upper bound on $\dot{\chi}_1$ can be expressed as

$$|\dot{\chi}_1| \leq \left| \left(\frac{\frac{d}{dt}(\det(M))}{(m_1 C_{m_\delta} + m_2 C_{l_\delta})} - \frac{\det(M) (\dot{m}_2 C_{l_\delta})}{(m_1 C_{m_\delta} + m_2 C_{l_\delta})^2} \right) |(\gamma_1 \dot{e}_1 + \gamma_2 \dot{e}_2)| \right. \\ \left. + \left| \frac{\det(M)}{(m_1 C_{m_\delta} + m_2 C_{l_\delta})} (\gamma_1 \ddot{e}_1 + \gamma_2 \ddot{e}_2) \right| \right.$$

Using the upper bounds on $\frac{d}{dt}(\det(M))$, \dot{m}_2 , and the expressions in (2-12) and (2-13), the upper bound on $\dot{\chi}_1$ can be rewritten as

$$|\dot{\chi}_1| \leq c_4 |e_1| + c_5 |e_2| + c_6 |r| \leq c'_1 \|z\|,$$

where $c_4, c_5, c_6, c'_1 \in \mathbb{R}$ are known positive constants.

The first term in (D-1) can be expressed as

$$-\frac{1}{2} \frac{d}{dt} \left(\frac{1}{g} \right) r = \frac{r}{2g^2} \left(\frac{(-2m_2 \dot{m}_2) (m_1 C_{m_\delta} + m_2 C_{l_\delta})}{\det(M)^2} \right) + \frac{r \dot{m}_2 C_{l_\delta}}{2g^2 \det(M)}. \quad (\text{D-2})$$

Using the upper bounds on \dot{m}_2 and m_2 and the lower bounds on g and $\det(M)$, the expression in (D-2) can be upper bounded as

$$\left| \frac{1}{2} \frac{d}{dt} \left(\frac{1}{g} \right) r \right| \leq c'_2 |r| \leq c'_2 \|z\|.$$

The upper bound on \tilde{N} can then be expressed as

$$|\tilde{N}| \leq \left| \frac{1}{2} \frac{d}{dt} \left(\frac{1}{g} \right) r \right| + |\dot{\chi}_1| + |e_2| + \left| \text{proj} \left(\Gamma_1 \hat{\sigma}' \hat{V}^T \dot{x}_d e_2 \right)^T \hat{\sigma} \right| \\ + \left| \hat{W}^T \hat{\sigma}' \text{proj} \left(\Gamma_2 \dot{x}_d \left(\hat{\sigma}'^T \hat{W} e_2 \right)^T \right)^T x_d \right|.$$

Therefore, using the developed upper bounds on the individual terms,

$$|\tilde{N}| \leq (c'_1 + c'_2 + 1 + c_1 + c_2) \|z\| \leq \eta \|z\|,$$

where $\eta \in \mathbb{R}$ is a known positive constant.

APPENDIX E
DETAILS ON THE DEVELOPMENT OF THE CONSTANTS c_{m_1} , c_{m_2} , AND c_{m_3} (CH 4)

Using the results of Appendix B, $g > \varepsilon_1$ where $\varepsilon_1 \in \mathbb{R}$ is a known positive constant.

Since $m_2^2 \geq 0$, $|\det(M)| \leq m_1 m_4$ and $\left| \frac{\det(M)}{g} \right| \leq \frac{m_1 m_4}{g} < c_{m_1}$.

Taking the time derivative of $\det(M)$ yields

$$\begin{aligned} \frac{d}{dt}(\det(M)) &= -2m_2 \dot{m}_2 \\ &= 2m_2 m_w b \dot{\alpha} (r_h - a_h) \cos(\alpha) + 2m_2 m_w b \dot{\alpha} (r_x - a) \sin(\alpha) \\ &\quad + 2m_2 m_s b \dot{\alpha} (s_h - a_h) \cos(\alpha) + 2m_2 m_s b \dot{\alpha} (s_x - a) \sin(\alpha). \end{aligned}$$

Since $\|\dot{q}\| \leq \kappa_2$ and using the result in Appendix B, the time derivative of $\det(M)$ can be upper bounded as $\frac{d}{dt}(\det(M)) < \varepsilon_2$ where $\varepsilon_2 \in \mathbb{R}$ is a known positive constant. Since $g > \varepsilon_1$, $\frac{\frac{d}{dt}(\det(M))}{g}$ can be upper bounded as

$$\left| \frac{\frac{d}{dt}(\det(M))}{g} \right| \leq \frac{\varepsilon_2}{\varepsilon_1} = c_{m_2}.$$

Using the result in Appendix B and the upper bound on $\frac{d}{dt}(\det(M))$, \dot{m}_2 can be upper bounded as $\dot{m}_2 \leq \varepsilon_3$ where $\varepsilon_3 \in \mathbb{R}$ is a known positive constant. Using the result in Appendix A, the term $\frac{\dot{m}_2 C_{l_\delta} \det(M)}{g^2}$ can be upper bounded as

$$\frac{\dot{m}_2 C_{l_\delta} \det(M)}{g^2} \leq \frac{\varepsilon_3 C_{l_\delta} \varepsilon_4}{\varepsilon_1^2} < c_{m_3},$$

where $\varepsilon_4 > |\det(M)|$.

APPENDIX F
DERIVATION OF THE BENDING AND TWISTING DYNAMICS OF A FLEXIBLE WING
(CH 5/6)

Consider a flexible wing with a store attached at the wing tip and uniform cross section undergoing bending and twisting motions. The wing has span $l \in \mathbb{R}$, chord length $c \in \mathbb{R}$, mass per unit length of $\rho \in \mathbb{R}$, polar moment of inertia per unit length of $I_w \in \mathbb{R}$, bending rigidity $EI \in \mathbb{R}$, and torsional rigidity $GJ \in \mathbb{R}$. The attached store has mass $m_s \in \mathbb{R}$ and moment of inertia $J_s \in \mathbb{R}$. Define a right-hand coordinate system as follows: the origin is on the shear center at the root of the wing, the x axis points out the rear of the wing, and the y axis extends to the wing tip. Let $\omega \triangleq \omega(y, t) \in \mathbb{R}$ denote the bending deflection and $\phi \triangleq \phi(y, t) \in \mathbb{R}$ denote the twisting deformation at the spanwise location $y \in [0, l]$. Furthermore, it is assumed that the center of gravity and aerodynamic center of the wing cross section and the center of gravity of the store are not colinear with the elastic axis of the wing. Let $x_{cC} \in \mathbb{R}$ and $x_{sC} \in \mathbb{R}$ represent the distances from the wing elastic axis to the wing center of gravity and store center of gravity, respectively. Let the vectors $p(y, t) \in \mathbb{R}^3$ and $p_l(t) \in \mathbb{R}^3$ denote the position of the center of gravity of an arbitrary wing cross section and the position of the center of gravity of the store, respectively. These vectors are expressed as

$$p(y, t) \triangleq \begin{bmatrix} x_{cC} \cos(\phi(y, t)) & y & \omega(y, t) + x_{cC} \sin(\phi(y, t)) \end{bmatrix}^T,$$

$$p_l(t) \triangleq \begin{bmatrix} x_{sC} \cos(\phi(l, t)) & l & \omega(l, t) + x_{sC} \sin(\phi(l, t)) \end{bmatrix}^T.$$

The kinetic energy of the wing and store can be expressed as

$$\begin{aligned} T_{wing} &= \frac{\rho}{2} \int_0^l p_t^T(y, t) p_t(y, t) dy + \frac{I_w}{2} \int_0^l \phi_t^2(y, t) dy \\ &= \frac{1}{2} \int_0^l \rho (\omega_t^2(y, t) + 2x_{cC} \cos(\phi(y, t)) \omega_t(y, t) \phi_t(y, t) + x_{cC}^2 \phi_t^2(y, t)) dy \\ &\quad + \frac{1}{2} \int_0^l I_w \phi_t^2(y, t) dy, \\ T_{store} &= \frac{m_s}{2} p_{l_t}^T(t) p_{l_t}(t) + \frac{J_s}{2} \phi_t^2(l) \end{aligned}$$

$$= \frac{m_s}{2} (\omega_t^2(l) + 2x_s c \cos(\phi(l)) \omega_t(l) \phi_t(l) + x_s^2 c^2 \phi_t^2(l)) + \frac{J_s}{2} \phi_t^2(l),$$

where the subscript t denotes the partial derivative with respect to t , $\omega(l) \triangleq \omega(l, t)$, and $\phi(l) \triangleq \phi(l, t)$. The potential energy in the wing can be written as

$$U = \frac{1}{2} \int_0^l (EI \omega_{yy}^2 + GJ \phi_y^2) dy,$$

where the subscript y denotes the partial derivative with respect to y . The Lagrangian for the wing-store system is defined as

$$\begin{aligned} \mathcal{L} &\triangleq T_{wing} + T_{store} - U \\ &= \frac{1}{2} \int_0^l (\rho \omega_t^2 + 2\rho x_s c \cos(\phi) \omega_t \phi_t + (\rho x_s^2 c^2 + I_w) \phi_t^2 - EI \omega_{yy}^2 - GJ \phi_y^2) dy \\ &\quad + \frac{m_s}{2} \omega_t^2(l) + m_s x_s c \cos(\phi(l)) \omega_t(l) \phi_t(l) + \left(\frac{m_s}{2} x_s^2 c^2 + \frac{J_s}{2} \right) \phi_t^2(l). \end{aligned}$$

Hamilton's principle is given as

$$\int_{t_1}^{t_2} (\delta W + \delta \mathcal{L}) dt = 0,$$

where $\delta \mathcal{L}$ denotes the variation in the Lagrangian and δW denotes the virtual work expressed as

$$\delta W = \int_0^l (L_w \delta \omega + M_w \delta \phi - \eta_w EI \omega_{t yy} \delta \omega_{yy} - \eta_\phi GJ \phi_{t y} \delta \phi_y) dy + L_{tip} \delta \omega(l) + M_{tip} \delta \phi(l),$$

where $L_w \in \mathbb{R}$ and $M_w \in \mathbb{R}$ represent the aerodynamic lift and moment per unit length, respectively, $L_{tip} \in \mathbb{R}$ and $M_{tip} \in \mathbb{R}$ denote the aerodynamic lift and moment at the wing tip, respectively, and $\eta_w \in \mathbb{R}$ and $\eta_\phi \in \mathbb{R}$ denote Kelvin-Voigt damping coefficients. The variation in the Lagrangian can be written as

$$\begin{aligned} \delta \mathcal{L} &= \frac{\partial \mathcal{L}}{\partial \omega_t} \delta \omega_t + \frac{\partial \mathcal{L}}{\partial \omega_{yy}} \delta \omega_{yy} + \frac{\partial \mathcal{L}}{\partial \phi} \delta \phi + \frac{\partial \mathcal{L}}{\partial \phi_t} \delta \phi_t + \frac{\partial \mathcal{L}}{\partial \phi_y} \delta \phi_y \\ &\quad + \frac{\partial \mathcal{L}}{\partial \omega_t(l)} \delta \omega_t(l) + \frac{\partial \mathcal{L}}{\partial \phi(l)} \delta \phi(l) + \frac{\partial \mathcal{L}}{\partial \phi_t(l)} \delta \phi_t(l), \end{aligned}$$

where the partial derivatives are evaluated as

$$\begin{aligned}
\frac{\partial \mathcal{L}}{\partial \omega_t} &= \int_0^l (\rho \omega_t + \rho x_c c \cos(\phi) \phi_t) dy, \\
\frac{\partial \mathcal{L}}{\partial \omega_{yy}} &= - \int_0^l EI \omega_{yy} dy, \\
\frac{\partial \mathcal{L}}{\partial \phi} &= - \rho x_c c \int_0^l \sin(\phi) \phi_t \omega_t dy, \\
\frac{\partial \mathcal{L}}{\partial \phi_t} &= \int_0^l (\rho x_c c \cos(\phi) \omega_t + (\rho x_c^2 c^2 + I_w) \phi_t) dy, \\
\frac{\partial \mathcal{L}}{\partial \phi_y} &= - \int_0^l GJ \phi_y dy, \\
\frac{\partial \mathcal{L}}{\partial \omega_t(l)} &= m_s \omega_t(l) + m_s x_s c \cos(\phi(l)) \phi_t(l), \\
\frac{\partial \mathcal{L}}{\partial \phi(l)} &= - m_s x_s c \sin(\phi(l)) \phi_t(l) \omega_t(l), \\
\frac{\partial \mathcal{L}}{\partial \phi_t(l)} &= m_s x_s c \cos(\phi(l)) \omega_t(l) + (m_s x_s^2 c^2 + J_s) \phi_t(l).
\end{aligned}$$

Substituting the expressions for δW and $\delta \mathcal{L}$ into Hamilton's principle yields

$$\begin{aligned}
& - \int_{t_1}^{t_2} \int_0^l EI \omega_{yy} \delta \omega_{yy} dy dt + \int_{t_1}^{t_2} \int_0^l (\rho \omega_t + \rho x_c c \cos(\phi) \phi_t) \delta \omega_t dy dt \\
& - \int_{t_1}^{t_2} \int_0^l GJ \phi_y \delta \phi_y dy dt + \int_{t_1}^{t_2} \int_0^l (\rho x_c c \cos(\phi) \omega_t + (\rho x_c^2 c^2 + I_w) \phi_t) \delta \phi_t dy dt \\
& - \eta_w \int_{t_1}^{t_2} \int_0^l EI \omega_{tyy} \delta \omega_{yy} dy dt - \eta_\phi \int_{t_1}^{t_2} \int_0^l GJ \phi_{ty} \delta \phi_y dy dt \\
& + \int_{t_1}^{t_2} (m_s \omega_t(l) + m_s x_s c \cos(\phi(l)) \phi_t(l)) \delta \omega_t(l) dt \\
& + \int_{t_1}^{t_2} (m_s x_s c \cos(\phi(l)) \omega_t(l) + (m_s x_s^2 c^2 + J_s) \phi_t(l)) \delta \phi_t(l) dt \\
& - m_s x_s c \int_{t_1}^{t_2} \sin(\phi(l)) \phi_t(l) \omega_t(l) \delta \phi(l) dt + \int_{t_1}^{t_2} \int_0^l (L_w \delta \omega + M_w \delta \phi) dy dt \\
& - \rho x_c c \int_{t_1}^{t_2} \int_0^l \sin(\phi) \phi_t \omega_t \delta \phi dy dt + \int_{t_1}^{t_2} (L_{tip} \delta \omega(l) + M_{tip} \delta \phi(l)) dt = 0. \quad (\text{F-1})
\end{aligned}$$

The equations of motion and boundary conditions for the wing-store system are obtained by integrating by parts select terms from (F-1). Integrating by parts the first eight

integrals in (F-1) and recalling that the variations at $t = t_1$ and $t = t_2$ are zero yields

$$\begin{aligned}
-\int_{t_1}^{t_2} \int_0^l EI\omega_{yy}\delta\omega_{yy}dydt &= -\int_{t_1}^{t_2} EI\omega_{yy}(l)\delta\omega_y(l)dt + \int_{t_1}^{t_2} EI\omega_{yy}(0)\delta\omega_y(0)dt \\
&+ \int_{t_1}^{t_2} \frac{\partial}{\partial y}(EI\omega_{yy}(l))\delta\omega(l)dt - \int_{t_1}^{t_2} \frac{\partial}{\partial y}(EI\omega_{yy}(0))\delta\omega(0)dt \\
&- \int_{t_1}^{t_2} \int_0^l \frac{\partial^2}{\partial y^2}(EI\omega_{yy})\delta\omega dydt, \tag{F-2}
\end{aligned}$$

$$\begin{aligned}
-\int_{t_1}^{t_2} \int_0^l GJ\phi_y\delta\phi_ydydt &= -\int_{t_1}^{t_2} GJ\phi_y(l)\delta\phi(l)dt + \int_{t_1}^{t_2} GJ\phi_y(0)\delta\phi(0)dt \\
&+ \int_{t_1}^{t_2} \int_0^l \frac{\partial}{\partial y}(GJ\phi_y)\delta\phi dydt, \tag{F-3}
\end{aligned}$$

$$\begin{aligned}
\int_{t_1}^{t_2} \int_0^l (\rho\omega_t + \rho x_c c \cos(\phi)\phi_t)\delta\omega_t dydt &= -\int_{t_1}^{t_2} \int_0^l (\rho\omega_{tt} - \rho x_c c \sin(\phi)\phi_t^2)\delta\omega dydt \\
&- \int_{t_1}^{t_2} \int_0^l \rho x_c c \cos(\phi)\phi_{tt}\delta\omega dydt \tag{F-4}
\end{aligned}$$

$$\begin{aligned}
&\int_{t_1}^{t_2} \int_0^l \rho x_c c \cos(\phi)\omega_t\delta\phi_t dydt \\
+ \int_{t_1}^{t_2} \int_0^l (\rho x_c^2 c^2 + I_w)\phi_t\delta\phi_t dydt &= \int_{t_1}^{t_2} \int_0^l \rho x_c c \sin(\phi)\omega_t\phi_t\delta\phi dydt \\
&- \int_{t_1}^{t_2} \int_0^l \rho x_c c \cos(\phi)\omega_{tt}\delta\phi dydt, \\
&- \int_{t_1}^{t_2} \int_0^l (\rho x_c^2 c^2 + I_w)\phi_{tt}\delta\phi dydt \tag{F-5}
\end{aligned}$$

$$\begin{aligned}
-\eta_w \int_{t_1}^{t_2} \int_0^l EI\omega_{t yy}\delta\omega_{yy}dydt &= -\eta_w \int_{t_1}^{t_2} EI\omega_{t yy}(l)\delta\omega_y(l)dt \\
&+ \eta_w \int_{t_1}^{t_2} EI\omega_{t yy}(0)\delta\omega_y(0)dt \\
&+ \eta_w \int_{t_1}^{t_2} \frac{\partial}{\partial y}(EI\omega_{t yy}(l))\delta\omega(l)dt \\
&- \eta_w \int_{t_1}^{t_2} \frac{\partial}{\partial y}(EI\omega_{t yy}(0))\delta\omega(0)dt
\end{aligned}$$

$$-\eta_w \int_{t_1}^{t_2} \int_0^l \frac{\partial^2}{\partial y^2} (EI\omega_{tyy}) \delta\omega dy dt, \quad (\text{F-6})$$

$$\begin{aligned} -\eta_\phi \int_{t_1}^{t_2} \int_0^l GJ\phi_{ty} \delta\phi_y dy dt &= -\eta_\phi \int_{t_1}^{t_2} GJ\phi_{ty}(l) \delta\phi(l) dt \\ &+ \eta_\phi \int_{t_1}^{t_2} GJ\phi_{ty}(0) \delta\phi(0) dt \\ &+ \eta_\phi \int_{t_1}^{t_2} \int_0^l \frac{\partial}{\partial y} (GJ\phi_{ty}) \delta\phi dy dt, \end{aligned} \quad (\text{F-7})$$

$$\begin{aligned} \int_{t_1}^{t_2} m_s \omega_t(l) \delta\omega_t(l) dt &= \int_{t_1}^{t_2} m_s x_s c \sin(\phi(l)) \phi_t^2(l) \delta\omega(l) dt \\ + \int_{t_1}^{t_2} m_s x_s c \cos(\phi(l)) \phi_t(l) \delta\omega_t(l) dt &= - \int_{t_1}^{t_2} m_s x_s c \cos(\phi(l)) \phi_{tt}(l) \delta\omega(l) dt \\ &- \int_{t_1}^{t_2} m_s \omega_{tt}(l) \delta\omega(l) dt, \end{aligned} \quad (\text{F-8})$$

$$\begin{aligned} \int_{t_1}^{t_2} m_s x_s c \cos(\phi(l)) \omega_t(l) \delta\phi_t(l) dt \\ + \int_{t_1}^{t_2} (m_s x_s^2 c^2 + J_s) \phi_t(l) \delta\phi_t(l) dt &= \int_{t_1}^{t_2} m_s x_s c \sin(\phi(l)) \omega_t(l) \phi_t(l) \delta\phi(l) dt \\ &- \int_{t_1}^{t_2} m_s x_s c \cos(\phi(l)) \omega_{tt}(l) \delta\phi(l) dt \\ &- \int_{t_1}^{t_2} (m_s x_s^2 c^2 + J_s) \phi_{tt}(l) \delta\phi(l) dt, \end{aligned} \quad (\text{F-9})$$

Substituting (F-2)-(F-9) into (F-1) yields the following PDE system and boundary conditions

$$\begin{aligned} L_w &= \rho\omega_{tt} - \rho x_c c \sin(\phi) \phi_t^2 + \rho x_c c \cos(\phi) \phi_{tt} + \frac{\partial^2}{\partial y^2} (EI\omega_{yy}) \\ &+ \eta_w \frac{\partial^2}{\partial y^2} (EI\omega_{tyy}), \end{aligned} \quad (\text{F-10})$$

$$\begin{aligned} M_w &= (I_w + \rho x_c^2 c^2) \phi_{tt} + \rho x_c c \cos(\phi) \omega_{tt} - \frac{\partial}{\partial y} (GJ\phi_y) \\ &- \eta_\phi \frac{\partial}{\partial y} (GJ\phi_{ty}), \end{aligned} \quad (\text{F-11})$$

$$\omega(0) = \omega_y(0) = \omega_{yy}(l) = \phi(0) = 0, \quad (\text{F-12})$$

$$L_{tip} = m_s \omega_{tt}(l) - m_s x_s c \sin(\phi(l)) \phi_t^2(l) + m_s x_s c \cos(\phi(l)) \phi_{tt}(l) - \frac{\partial}{\partial y} (EI \omega_{yy}(l) - \eta_w EI \omega_{tyy}(l)), \quad (\text{F-13})$$

$$M_{tip} = (m_s x_s^2 c^2 + J_s) \phi_{tt}(l) + m_s x_s c \cos(\phi(l)) \omega_{tt}(l) + GJ \phi_y(l) + \eta_\phi GJ \phi_{ty}(l) \quad (\text{F-14})$$

The development in Chapter 4 is based on the assumptions that EI and GJ are constants and $x_c = x_s = 0$. Under these assumptions, (F-10), (F-11), (F-13), and (F-14) become

$$L_w = \rho \omega_{tt} + EI \omega_{yyyy} + \eta_w EI \omega_{tyyy}, \quad (\text{F-15})$$

$$M_w = I_w \phi_{tt} - GJ \phi_{yy} - \eta_\phi GJ \phi_{ty}, \quad (\text{F-16})$$

$$EI \omega_{yyy}(l) + \eta_w EI \omega_{tyyy}(l) = m_s \omega_{tt}(l) - L_{tip},$$

$$GJ \phi_y(l) + \eta_\phi GJ \phi_{ty}(l) = -J_s \phi_{tt}(l) + M_{tip}.$$

The development in Chapter 5 is based on the assumptions that EI and GJ are constants and the Kelvin-Voigt damping coefficients are zero. Under these assumptions, (F-10), (F-11), (F-13), and (F-14) become

$$L_w = \rho \omega_{tt} - \rho x_c c \sin(\phi) \phi_t^2 + \rho x_c c \cos(\phi) \phi_{tt} + EI \omega_{yyyy}, \quad (\text{F-17})$$

$$M_w = (I_w + \rho x_c^2 c^2) \phi_{tt} + \rho x_c c \cos(\phi) \omega_{tt} - GJ \phi_{yy} \quad (\text{F-18})$$

$$L_{tip} = m_s \omega_{tt}(l) - m_s x_s c \sin(\phi(l)) \phi_t^2(l) + m_s x_s c \cos(\phi(l)) \phi_{tt}(l) - EI \omega_{yyy}(l),$$

$$M_{tip} = (m_s x_s^2 c^2 + J_s) \phi_{tt}(l) + m_s x_s c \cos(\phi(l)) \omega_{tt}(l) + GJ \phi_y(l)$$

APPENDIX G
EXPONENTIAL STABILITY OF THE TARGET SYSTEM (CH 5)

The target system in Chapter 5 is given as

$$I_w \Phi_{tt} - GJ\Phi_{yy} - \eta_\phi GJ\Phi_{tyy} + (cGJ - \bar{M}_w) \Phi + \eta_\phi cGJ\Phi_t = 0, \quad (\text{G-1})$$

where $c \in \mathbb{R}$ is a constant control gain and the boundary conditions are $\Phi(0, t) = 0$ and $GJ\Phi_y(l, t) + \eta_\phi GJ\Phi_{ty}(l, t) = 0$. Since (G-1) is a linear PDE, its solution is assumed to be of the form $\Phi(y, t) = g(t)h(y)$. Substituting the assumed solution into (G-1) yields

$$I_w h(y) g_{tt}(t) - GJg(t) h_{yy}(y) - \eta_\phi GJg_t(t) h_{yy}(y) + (cGJ - \bar{M}_w) g(t) h(y) + \eta_\phi cGJg_t(t) h(y) = 0.$$

Gathering the like terms on opposite sides of the equation results in

$$\frac{I_w g_{tt}(t) + (cGJ - \bar{M}_w) g(t) + \eta_\phi cGJg_t(t)}{-GJg(t) - \eta_\phi GJg_t(t)} = -\frac{h_{yy}(y)}{h(y)}. \quad (\text{G-2})$$

The equality in (G-2) can only hold if the right-hand side and left-hand side are equal to a constant σ . Examining the right-hand side of (G-2) results in the following ordinary differential equation for $h(y)$

$$h_{yy}(y) + \sigma h(y) = 0 \quad (\text{G-3})$$

with the boundary conditions $h(0) = 0$ and $h_y(l) = 0$. The cases where $\sigma < 0$ and $\sigma = 0$ lead directly to the trivial solution (i.e., $h(y) = 0$). A non-trivial solution to the case where $\sigma > 0$ exists and is expressed as $h(y) = a_1 \cos(\sqrt{\sigma}x) + a_2 \sin(\sqrt{\sigma}x)$ where a_1 and $a_2 \in \mathbb{R}$ are constants determined through the application of the boundary conditions. Applying the boundary conditions yields $a_1 = 0$ and $\sqrt{\sigma}l = \frac{(2n+1)}{2}\pi$, where $n = 0, 1, 2, \dots$. The general solution to (G-3) can be written as

$$h(y) = \sum_{n=0}^{\infty} A_n \sin\left(\frac{(2n+1)\pi}{2l}x\right),$$

where $A_n \in \mathbb{R}$ is a constant associated with the n th particular solution.

Examining the left-hand side of (G–2) yields

$$I_w g_{tt}(t) + \eta_\phi GJ(c + \sigma) g_t(t) + ((c + \sigma)GJ - \bar{M}_w) g(t) = 0,$$

whose n th pair of eigenvalues ξ_n satisfy the following quadratic expression

$$I_w \xi_n^2 + \eta_\phi GJ(c + \sigma_n) \xi_n + (c + \sigma_n)GJ - \bar{M}_w = 0,$$

where $\sigma_n = \frac{(2n+1)^2 \pi^2}{4l^2}$. The n th pair of eigenvalues can be expressed as

$$\xi_n = \frac{-\eta_\phi GJ(c + \sigma_n) \pm \sqrt{\eta_\phi^2 GJ^2 (c + \sigma_n)^2 + 4I_w \bar{M}_w - 4I_w GJ(c + \sigma_n)}}{2I_w}. \quad (\text{G–4})$$

For the case in which $\eta_\phi^2 GJ^2 (c + \sigma_n)^2 + 4I_w \bar{M}_w - 4I_w GJ(c + \sigma_n) = 0$, the resulting eigenvalues are $\xi_n = -\frac{\eta_\phi GJ(c + \sigma_n)}{2I_w}$. In the case where $\eta_\phi^2 GJ^2 (c + \sigma_n)^2 + 4I_w \bar{M}_w - 4I_w GJ(c + \sigma_n) < 0$, the eigenvalues will be complex with $Re(\xi_n) = -\frac{\eta_\phi GJ(c + \sigma_n)}{2I_w}$, where $Re(\xi_n)$ denotes the real part of ξ_n . Lastly, when $\eta_\phi^2 GJ^2 (c + \sigma_n)^2 + 4I_w \bar{M}_w - 4I_w GJ(c + \sigma_n) > 0$, the resulting eigenvalues will be real and distinct. Since the square root term in (G–4) is positive, both real eigenvalues will be negative if the following inequality is satisfied,

$$-\eta_\phi GJ(c + \sigma_n) + \sqrt{\eta_\phi^2 GJ^2 (c + \sigma_n)^2 + 4I_w \bar{M}_w - 4I_w GJ(c + \sigma_n)} < 0.$$

After some algebraic manipulation and recalling that $\sigma_n = \frac{(2n+1)^2 \pi^2}{4l^2}$, the sufficient condition above can be expressed as

$$c > \frac{\bar{M}_w}{GJ} - \frac{(2n+1)^2 \pi^2}{4l^2}. \quad (\text{G–5})$$

As $n \rightarrow \infty$, the right-hand side of (G–5) gets smaller; hence, if the inequality is satisfied for $n = 0$, it will be satisfied for all n . Substituting $n = 0$ into (G–5) yields the following sufficient condition

$$c > \frac{\bar{M}_w}{GJ} - \frac{\pi^2}{4l^2}.$$

Since all eigenvalues have negative real parts, the target system in (G-1) is exponentially stable.

APPENDIX H
INTEGRATION BY PARTS OF SELECT TERMS IN \dot{E}_C (CH 6)

The development of an upper bound for \dot{E}_c relies on the integration by parts of the terms

$-\beta_1 \int_0^l EI\omega_{yyyy}\omega_y y dy$, $\beta_1 \int_0^l \rho\omega_t\omega_{ty} y dy$, $\beta_1 \int_0^l GJ\phi_{yy}\phi_y y dy$, and $\beta_1 \int_0^l (I_w + \rho x_c^2 c^2) \phi_t\phi_{ty} y dy$ from (5–34). Integration of the first term,

$-\beta_1 \int_0^l EI\omega_{yyyy}\omega_y y dy$ yields

$$\begin{aligned} -\beta_1 \int_0^l EI\omega_{yyyy}\omega_y y dy &= -\beta_1 EI l \omega_{yyy}(l, t) \omega_y(l, t) + \beta_1 EI \int_0^l \omega_{yyy}\omega_y dy \\ &\quad + \beta_1 EI \int_0^l \omega_{yyy}\omega_{yy} y dy, \\ -\beta_1 \int_0^l EI\omega_{yyyy}\omega_y y dy &= -\beta_1 EI l \omega_{yyy}(l, t) \omega_y(l, t) - \beta_1 EI \int_0^l \omega_{yy}^2 dy \\ &\quad + \beta_1 EI \int_0^l \omega_{yyy}\omega_{yy} y dy, \end{aligned} \quad (\text{H-1})$$

$$\begin{aligned} -\beta_1 \int_0^l EI\omega_{yyyy}\omega_y y dy &= -\beta_1 EI l \omega_{yyy}(l, t) \omega_y(l, t) - 2\beta_1 EI \int_0^l \omega_{yy}^2 dy \\ &\quad - \beta_1 EI \int_0^l \omega_{yyy}\omega_{yy} y dy. \end{aligned} \quad (\text{H-2})$$

After adding (H-1) to (H-2) and combining like terms, $-\beta_1 \int_0^l EI\omega_{yyyy}\omega_y y dy$ can be expressed as

$$-\beta_1 \int_0^l EI\omega_{yyyy}\omega_y y dy = -\beta_1 EI l \omega_{yyy}(l, t) \omega_y(l, t) - \frac{3}{2}\beta_1 EI \int_0^l \omega_{yy}^2 dy. \quad (\text{H-3})$$

The terms $\beta_1 \int_0^l \rho\omega_t\omega_{ty} y dy$, $\beta_1 \int_0^l GJ\phi_{yy}\phi_y y dy$, and $\beta_1 \int_0^l (I_w + \rho x_c^2 c^2) \phi_t\phi_{ty} y dy$ are evaluated as

$$\begin{aligned} \beta_1 \int_0^l \rho\omega_t\omega_{ty} y dy &= \beta_1 \rho l \omega_t^2(l, t) - \beta_1 \rho \int_0^l \omega_t^2 dy - \beta_1 \int_0^l \rho\omega_t\omega_{ty} y dy, \quad (\text{H-4}) \\ \beta_1 \int_0^l GJ\phi_{yy}\phi_y y dy &= \beta_1 GJ l \phi_y^2(l, t) - \beta_1 GJ \int_0^l \phi_y^2 dy \\ &\quad - \beta_1 \int_0^l GJ\phi_{yy}\phi_y y dy, \end{aligned} \quad (\text{H-5})$$

$$\beta_1 \int_0^l (I_w + \rho x_c^2 c^2) \phi_t\phi_{ty} y dy = \beta_1 (I_w + \rho x_c^2 c^2) l \phi_t^2(l, t) - \beta_1 (I_w + \rho x_c^2 c^2) \int_0^l \phi_t^2 dy$$

$$-\beta_1 \int_0^l (I_w + \rho x_c^2 c^2) \phi_t \phi_{ty} y dy, \quad (\text{H-6})$$

which after some algebraic manipulation are rewritten as

$$\beta_1 \int_0^l \rho \omega_t \omega_{ty} y dy = \frac{1}{2} \beta_1 \rho l \omega_t^2 (l, t) - \frac{1}{2} \beta_1 \rho \int_0^l \omega_t^2 dy, \quad (\text{H-7})$$

$$\beta_1 \int_0^l GJ \phi_{yy} \phi_y y dy = \frac{1}{2} \beta_1 GJ l \phi_y^2 (l, t) - \frac{1}{2} \beta_1 GJ \int_0^l \phi_y^2 dy, \quad (\text{H-8})$$

$$\begin{aligned} \beta_1 \int_0^l (I_w + \rho x_c^2 c^2) \phi_t \phi_{ty} y dy &= \frac{1}{2} \beta_1 (I_w + \rho x_c^2 c^2) l \phi_t^2 (l, t) \\ &\quad - \frac{1}{2} \beta_1 (I_w + \rho x_c^2 c^2) \int_0^l \phi_t^2 dy. \end{aligned} \quad (\text{H-9})$$

REFERENCES

- [1] D. E. Thompson Jr. and T. W. Strganac, "Nonlinear analysis of store-induced limit cycle oscillations," *Nonlinear Dynamics*, vol. 39, pp. 159–178, 2005.
- [2] B. J. Bialy, C. L. Pasilliao, H. T. Dinh, and W. E. Dixon, "Lyapunov-based tracking of store-induced limit cycle oscillations in an aeroelastic system," in *Proc. ASME Dyn. Syst. Control Conf.*, Fort Lauderdale, Florida, October 2012.
- [3] P. S. Beran, T. W. Strganac, K. Kim, and C. Nichkawde, "Studies of store-induced limit cycle oscillations using a model with full system nonlinearities," *Nonlinear Dynamics*, vol. 37, pp. 323–339, 2004.
- [4] R. W. Bunton and C. M. Denegri Jr., "Limit cycle oscillation characteristics of fighter aircraft," *J. Aircraft*, vol. 37, pp. 916–918, 2000.
- [5] C. M. Denegri Jr., "Limit cycle oscillation flight test results of a fighter with external stores," *J. Aircraft*, vol. 37, pp. 761–769, 2000.
- [6] J. J. Block and T. W. Strganac, "Applied active control for a nonlinear aeroelastic structure," *J. Guid. Contr. Dynam.*, vol. 21, pp. 838–845, 1999.
- [7] J. Ko, T. W. Strganac, and A. Kurdila, "Stability and control of a structurally nonlinear aeroelastic system," *J. Guid. Contr. Dynam.*, vol. 21, pp. 718–725, 1998.
- [8] W. Zhang and Z. Ye, "Control law design for transonic aeroservoelasticity," *Aerospace Science and Technology*, vol. 11, pp. 136–145, 2007.
- [9] B. P. Danowsky, P. M. Thompson, C. Farhat, T. Lieu, C. Harris, and J. Lechniak, "Incorporation of feedback control into a high-fidelity aeroservoelastic fighter aircraft model," *J. Aircraft*, vol. 47, pp. 1274–1282, 2010.
- [10] P. M. Thompson, B. P. Danowsky, C. Farhat, T. Lieu, J. Lechniak, and C. Harris, "High-fidelity aeroservoelastic predictive analysis capability incorporating rigid body dynamics," in *Proc. AIAA Atmospheric Flight Mechanics, AIAA 2011-6209*, 2011.
- [11] L. Cavagna, S. Ricci, and A. Scotti, "Active aeroelastic control over a four control surface wing model," *Aerospace Science and Technology*, vol. 13, pp. 374–382, 2009.
- [12] Z. Prime, B. Cazzolato, C. Doolan, and T. Strganac, "Linear-parameter-varying control of an improved three-degree-of-freedom aeroelastic model," *J. Guid. Contr. Dynam.*, vol. 33, pp. 615–618, 2010.
- [13] M. R. Elhami and M. F. Narab, "Comparison of SDRE and SMC control approaches for flutter suppression in a nonlinear wing section," in *Proc. Am. Control Conf.*, 2012, pp. 6148–6153.

- [14] J. Ko, T. W. Strganac, and A. Kurdila, "Adaptive feedback linearization for the control of a typical wing section with structural nonlinearity," *Nonlinear Dynamics*, vol. 18, pp. 289–301, 1999.
- [15] T. W. Strganac, J. Ko, D. E. Thompson, and A. Kurdila, "Identification and control of limit cycle oscillations in aeroelastic systems," *J. Guid. Contr. Dynam.*, vol. 23, pp. 1127–1133, 2000.
- [16] J. Ko, T. W. Strganac, J. L. Junkins, M. R. Akella, and A. Kurdila, "Structured model reference adaptive control for a wing section with structural nonlinearity," *J. Vib. Control*, vol. 8, pp. 553–573, 2002.
- [17] G. Platanitis and T. W. Strganac, "Control of a nonlinear wing section using leading- and trailing-edge surfaces," *J. Guid. Contr. Dynam.*, vol. 27, pp. 52–58, 2004.
- [18] N. Fischer, Z. Kan, R. Kamalapurkar, and W. E. Dixon, "Saturated RISE feedback control for a class of second-order nonlinear systems," *IEEE Trans. Automat. Control*, to appear.
- [19] D. H. Hodges and R. A. Ormiston, "Stability of elastic bending and torsion of uniform cantilever rotor blades in hover with variable structural coupling," National Aeronautics and Space Administration, Technical Note D-8192, 1976.
- [20] M. Y. Ziabari and B. Ghadiri, "Vibration analysis of elastic uniform cantilever rotor blades in unsteady aerodynamics modeling," *J. Aircraft*, vol. 47, no. 4, pp. 1430–1434, 2010.
- [21] D. H. Hodges and E. H. Dowell, "Nonlinear equations of motion for the elastic bending and torsion of twisted nonuniform rotor blades," National Aeronautics and Space Administration, Technical Note D-7818, 1974.
- [22] X. Zhang, W. Xu, S. S. Nair, and V. Chellaboina, "Pde modeling and control of a flexible two-link manipulator," *IEEE Trans. Contr. Syst. Tech.*, vol. 13, no. 2, pp. 301–312, 2005.
- [23] Y. Morita, F. Matsuno, Y. Kobayashi, M. Ikeda, H. Ukai, and H. Kando, "Lyapunov-based force control of a flexible arm considering bending and torsional deformation," in *Proc. of the 15th Triennial IFAC World Congress*, 2002.
- [24] J. Martins, Z. Mohamed, M. Tokhi, J. Sá da Costa, and M. Botto, "Approaches for dynamic modelling of flexible manipulator systems," *IEE Proc. Contr. Theor. Appl.*, vol. 150, no. 4, pp. 401–411, 2003.
- [25] P. D. Christofides and P. Daoutidis, "Finite-dimensional control of parabolic pde systems using approximate inertial manifolds," *J. Math. Anal. Appl.*, vol. 216, pp. 398–420, 1997.

- [26] A. Shawky, A. Ordys, and M. Grimble, "End-point control of a flexible-link manipulator using H_∞ nonlinear control via a state-dependent riccati equation," in *2002 IEEE International Conference on Control Applications*, 2002.
- [27] L. Meirovitch, *Analytical Methods in Vibrations*. New York, NY, USA: The Macmillan Company, 1967.
- [28] F. Bucci and I. Lasiecka, "Optimal boundary control with critical penalization for a PDE model of fluid-solid interactions," *Calc. Var.*, vol. 37, pp. 217–235, 2010.
- [29] C. I. Byrnes, I. G. Laukó, D. S. Gilliam, and V. I. Shubov, "Output regulation for linear distributed parameter systems," *IEEE Trans. Autom. Contr.*, vol. 45, pp. 2236–2252, 2000.
- [30] Z.-H. Luo, "Direct strain feedback control of flexible robot arms: New theoretical and experimental results," *IEEE Trans. Autom. Contr.*, vol. 38, pp. 1610–1622, 1993.
- [31] Z.-H. Luo and B. Guo, "Further theoretical results on direct strain feedback control of flexible robot arms," *IEEE Trans. Autom. Contr.*, vol. 40, pp. 747–751, 1995.
- [32] M. J. Balas, "Feedback control of flexible systems," *IEEE Trans. Autom. Contr.*, vol. AC-23, pp. 673–679, 1978.
- [33] L. Meirovitch and H. Baruh, "On the problem of observation spillover in self-adjoint distributed-parameter systems," *J. Optim. Theory App.*, vol. 39, pp. 269–291, 1983.
- [34] M. J. Balas, "Trends in large space structure control theory: Fondest hopes, wildest dreams," *IEEE Trans. Autom. Contr.*, vol. AC-27, pp. 522–35, 1982.
- [35] M. Krstic and A. Smyshlyaev, *Boundary control of PDEs: A course on Backstepping Designs*. SIAM, 2008.
- [36] M. S. de Queiroz, D. M. Dawson, S. P. Nagarkatti, and F. Zhang, *Lyapunov-Based Control of Mechanical Systems*. Birkhauser, 2000.
- [37] M. S. de Queiroz and C. D. Rahn, "Boundary control of vibration and noise in distributed parameter systems: An overview," *Mech. Syst. Signal Process.*, vol. 16, pp. 19–38, 2002.
- [38] R. Vazquez and M. Krstic, "A closed-form feedback controller for stabilization of the linearized 2-d navier-stokes poiseuille system," *IEEE Trans. Autom. Contr.*, vol. 52, pp. 2298–2312, 2007.
- [39] M. S. de Queiroz, D. M. Dawson, M. Agarwal, and F. Zhang, "Adaptive nonlinear boundary control of a flexible link robot arm," *IEEE Trans. Robot. Autom.*, vol. 15, pp. 779–787, 1999.

- [40] M. P. Fard and S. I. Sagatun, "Exponential stabilization of a transversely vibrating beam by boundary control via Lyapunov's direct method," *J. Dyn. Syst. Meas. Contr.*, vol. 123, pp. 195–200, 2001.
- [41] W. He, S. S. Ge, B. V. E. How, Y. S. Choo, and K.-S. Hong, "Robust adaptive boundary control of a flexible marine riser with vessel dynamics," *Automatica*, vol. 47, pp. 722–732, 2011.
- [42] A. A. Siranosian, M. Krstic, A. Smyshlyaev, and M. Bement, "Gain scheduling-inspired boundary control for nonlinear partial differential equations," *J. Dyn. Syst. Meas. Contr.*, vol. 133, p. 051007, 2011.
- [43] S. P. Nagarkatti, D. M. Dawson, M. S. de Queiroz, and B. Costic, "Boundary control of a two-dimensional flexible rotor," *Int. J. Adapt Control Signal Process.*, vol. 15, pp. 589–614, 2001.
- [44] A. A. Paranjape, J. Guan, S.-J. Chung, and M. Krstic, "Pde boundary control for flexible articulated wings on a robotic aircraft," *IEEE Transactions on Robotics*, vol. 29, no. 3, pp. 625–640, 2013.
- [45] P. M. Patre, W. MacKunis, K. Kaiser, and W. E. Dixon, "Asymptotic tracking for uncertain dynamic systems via a multilayer neural network feedforward and RISE feedback control structure," *IEEE Trans. Automat. Control*, vol. 53, no. 9, pp. 2180–2185, 2008.
- [46] P. Patre, W. Mackunis, K. Dupree, and W. E. Dixon, "Modular adaptive control of uncertain Euler-Lagrange systems with additive disturbances," *IEEE Trans. Automat. Control*, vol. 56, no. 1, pp. 155–160, 2011.
- [47] W. MacKunis, P. Patre, M. Kaiser, and W. E. Dixon, "Asymptotic tracking for aircraft via robust and adaptive dynamic inversion methods," *IEEE Trans. Control Syst. Technol.*, vol. 18, no. 6, pp. 1448–1456, 2010.
- [48] M. Krstic, P. V. Kokotovic, and I. Kanellakopoulos, *Nonlinear and Adaptive Control Design*. John Wiley & Sons, 1995.
- [49] J. P. Aubin and H. Frankowska, *Set-valued analysis*. Birkhäuser, 2008.
- [50] A. Filippov, "Differential equations with discontinuous right-hand side," *Am. Math. Soc. Transl.*, vol. 42 no. 2, pp. 199–231, 1964.
- [51] A. F. Filippov, *Differential Equations with Discontinuous Right-hand Sides*. Kluwer Academic Publishers, 1988.
- [52] G. V. Smirnov, *Introduction to the theory of differential inclusions*. American Mathematical Society, 2002.
- [53] D. Shevitz and B. Paden, "Lyapunov stability theory of nonsmooth systems," *IEEE Trans. Autom. Control*, vol. 39 no. 9, pp. 1910–1914, 1994.

- [54] B. Paden and S. Sastry, "A calculus for computing Filippov's differential inclusion with application to the variable structure control of robot manipulators," *IEEE Trans. Circuits Syst.*, vol. 34 no. 1, pp. 73–82, 1987.
- [55] R. Kamalapurkar, J. Klotz, R. Downey, and W. E. Dixon. (2013) Supporting lemmas for RISE-based control methods. arXiv:1306.3432v2.
- [56] N. Fischer, R. Kamalapurkar, and W. E. Dixon, "LaSalle-Yoshizawa corollaries for nonsmooth systems," *IEEE Trans. Automat. Control*, vol. 58, no. 9, pp. 2333–2338, 2013.
- [57] W. E. Dixon, M. S. de Queiroz, D. M. Dawson, and F. Zhang, "Tracking control of robot manipulators with bounded torque inputs," *Robotica*, vol. 17, pp. 121–129, 1999.
- [58] F. H. Clarke, *Optimization and nonsmooth analysis*. SIAM, 1990.
- [59] W. Rudin, *Principles of Mathematical Analysis*. McGraw-Hill, 1976.
- [60] Z. Qu, *Robust Control of Nonlinear Uncertain Systems*. Wiley Inc., New-York, 1998.

BIOGRAPHICAL SKETCH

Brendan Bialy was born in Binghamton, New York. He received a Bachelor of Science degree in aeronautical and mechanical engineering from Clarkson University in 2010. After completing his undergraduate degree, Brendan decided to pursue doctoral research under the advisement of Dr. Warren Dixon at the University of Florida. Brendan earned a Master of Science degree in December of 2012 and completed his Ph.D. in May of 2014, both in aerospace engineering and focused on nonlinear control of uncertain aircraft systems. Additionally, Brendan has worked as a student researcher at NASA Langley Research Center in Hampton, Virginia and at the Air Force Research Laboratory, Munitions Directorate at Eglin AFB, Florida.